

POLITECNICO DI TORINO

DEPARTMENT OF MECHANICAL AND AEROSPACE
ENGINEERING

Automotive Engineering
Class L-9 (DM270)

Bachelor's Degree Thesis

Optimisation of the Suspensions' Kinematics of an FSAE Vehicle



**Politecnico
di Torino**

Advisors

prof. Andrea Tonoli
eng. Stefano Favelli

Candidate

Gabriele Roccatani

ACADEMIC YEAR 2023-2024

Contents

List of Figures	III
1 Minimum Stiffness	1
1.1 Methodology	1
1.2 Telemetry Analysis	2
1.3 Load Cases and Stiffness	8
2 Critical Corners	15
2.1 Methodology	15
2.2 Trajectory Modelling	16
2.3 Vehicle Simulations	17
3 Working Conditions of the Tyres	21
3.1 Methodology	21
3.2 Vehicle Simulation	25
3.3 Tyres' Working Conditions Optimisation	28
4 Suspensions' Lower Parts Kinematics	36
4.1 Components of the Lower Part of the SC22's Suspensions	36
4.2 Hardpoints' Position Calculation Methods	37
4.3 Suspension Kinematics Parameters	38
4.3.1 Front View Swing Arm	40
4.3.2 Roll Centre	49
4.3.3 Front View Analysis of the Kingpin Axis	63
4.3.4 Side View Analysis of the Kingpin Axis	69
4.3.5 Side View Swing Arm	76
4.3.6 Anti-Features	78
4.3.7 Pitch Centre	80
4.3.8 Wishbones Aperture Angle	81
4.3.9 Ackermann Percentage	82
4.3.10 Bump Steer	87
4.4 Parametric Model	92

List of Figures

1.1	Low Pass Filter - Example	4
1.2	Aggressive Filtering - Example	4
1.3	Mild Filtering - Example	5
1.4	Different Filtering Strengths and Techniques	6
1.5	Linear Correlation Plots	6
1.6	Log Analysis Results - Table	8
2.1	Raw Data vs Smoothed Data of some corners	17
2.2	Track Map with Combined Traction and Brake Input	19
2.3	Track Map with Corner Numbers	19
2.4	Results of the Analysis	20
3.1	Tyres' Speed and Side-slip	22
3.2	Roll Gradient Components of the <i>SC22</i>	26
3.3	Roll Gradient Components of the <i>SC22</i> with Re-scaled Heave Stiffness	26
3.4	Correlation Between Simulation and Real Tests	28
3.5	Double Track Model	29
3.6	Lateral Force and Lateral Force Differential	33
3.7	KPI Interface - Front Left Tyre	34
4.1	Front Suspension SC22 lower part	37
4.2	Front View Instant Centre	39
4.3	Roll and Vertical Wheel Travel Relation	42
4.4	Camber Gain Sensitivity to fvsa	42
4.5	front view Instant Centre Effect	45
4.6	Fvsa sensitivity to upper wishbone length and inclination	48
4.7	Roll Centre Height	50
4.8	Simplified Model of the Front View of a Suspension	51
4.9	Lateral force potential of a tyre during cornering with 2g of lateral acceleration	54
4.10	Lateral Load Transfer Components in Non Steady State Cornering . .	58
4.11	Double Track Model of a Vehicle	60
4.12	Front View of a Vehicle Featuring a Centred Roll Centre	61
4.13	Front View of a Vehicle Featuring a Roll Centre Moved Towards the Internal Side of the Corner	62
4.14	Front View of a Vehicle Featuring a Roll Centre Moved Towards the External Side of the Corner	63
4.15	Kingpin Geometry	64
4.16	Model Used to Determine the Camber Variation Due to the Kingpin Inclination	65

4.17	Steering Wheel Angle to Camber Angle Curve Due to a Kingpin Inclination of 5.9 degrees	66
4.18	Wheel Centre Trajectory Around the Kingpin Axis	67
4.19	Steering Wheel Angle to Camber Angle Curve Due to a Caster Angle of 6.3 degrees	71
4.20	Wheel Centre Trajectory Around the Kingpin Axis - Camber Effect	71
4.21	Lateral Force and Moment on the Z-Axis Versus Side-slip Angle	73
4.22	Lateral Force and Self-aligning Moment Components Versus Side-slip Angle - Caster Trail = 10 [mm]	75
4.23	Upper View of a Simplified Wishbone	82
4.24	Ackermann Geometry	83
4.25	Ackermann Geometry	84
4.26	Ackermann Geometry Validation	86
4.27	Ackermann Geometry Validation	86
4.28	Two Limit Cases for the Bump Steer	88
4.29	Bump Steer Model	89
4.30	Bump Steer Model	90
4.31	Inner Hardpoints' Plane	93
4.32	Camber Related Parameters Effect - Front Axle	93
4.33	Camber Related Parameters Effect - Rear Axle	95
4.34	Lower Suspension Hardpoints - Front Axle	100
4.35	Front View of the Lower Part of the Suspension - Front Axle	101
4.36	Side View of the Lower Part of the Suspension - Front Axle	102
4.37	Inner Hardpoints Plane - Front Axle	102
4.38	Complete View of the Lower Part of the Suspension - Front Axle	103

Chapter 1

Minimum Stiffness

1.1 Methodology

The design of the kinematics of a suspension is an articulated process, which is made by a lot of different steps. In the analysis carried out in this paper, the choice of the minimum suspensions stiffness is the first of them.

Target

There are a number of ways to determine how stiff a suspension needs to be. For instance, the ideal combination of stiffness and damping for a given vehicle mass can be decided through a frequency analysis. Whilst this method can be useful for road cars as containing the noise, vibration and harshness (NVH) perceived by driver and passengers is one of the main targets, in racing cars other factors (such as the ride height optimisation) are far more crucial than suspension frequency when optimising the vehicle's performance. For instance, vehicles featuring significant aerodynamic characteristics tend to present higher roll stiffness and damping on the front axle than ones on the rear axle in order to maintain the front wing as parallel to the ground as possible hence optimising its performance. Given that this thesis treats the suspensions' kinematics of a racing oriented vehicle, the focus of this chapter will not be on suspensions' frequency; indeed, the suspension frequency will be a consequence of the minimum stiffness and the setup choices.

The primary target when designing an FSAE vehicle is neither performance nor safety as the car primarily has to be rule compliant. For this reason, the rules need to be taken into consideration when deciding the minimum suspension stiffness. In fact, the rule T 2.2.2 of the 2023 Formula Student Rule Book states that the aerodynamic devices should not touch the track surface. Therefore, the main focus of the calculation of the minimum suspension stiffness should be to limit the variation of the front and rear ride heights, in order to guarantee a minimum clearance between the aerodynamic components and the ground under any circumstance. In reality, the judges will deem as irregular only the vehicles that repeatedly and systematically touch the ground. This means that, if some surface irregularities in a zone of a track, such as bumps, make the car to briefly touch the tarmac, the vehicle will be considered rule compliant. Although this observation might seem like a finesse, it makes the study of the suspensions' minimum stiffness by far simpler as road irregularities are not a part of the equation and so the effect of damping on fast

suspension movements can be neglected.

Process

The process adopted for our case study can be divided in two steps. Firstly, there is an analysis of all the telemetry data recorded on track during the of the latest car produced and tested, which in this case is the *SC22*. From this analysis, the critical cases where the car's aerodynamic devices are most likely to touch the ground are identified. Secondly, the appropriate suspensions' stiffness are determined accordingly to the critical cases chosen.

1.2 Telemetry Analysis

The data gathered during the track testing of a racing vehicle are an invaluable resource when designing a new iteration of the vehicle. In particular, The parameters necessary to determine the minimum suspensions' stiffness are the lateral acceleration, the longitudinal acceleration and the speed of the vehicle. For any of these parameters, the extreme values need to be found to identify the critical cases above-mentioned.

Weakness of Telemetry Data

In order to determine the maximum and minimum values of the vehicle's accelerations and speeds in the stints, it is of paramount importance to clean the data from any kind of noise or disturbance, which can potentially make the peak values and the lowest value to respectively be much higher or much lower than what they really are. In our case study, the acceleration data present an high level of noise; therefore, these signals must be cleaned in order to perform a meaningful analysis.

Adopted Solution

Many smoothing techniques were tested, such as Gaussian regression, local linear and quadratic regression and Savitzky-Golay polynomial filter. Nevertheless, the two filtering techniques which have demonstrated to be the most effective are also the most widely adopted. They are the moving average and the low-pass filter.

Moving Average Filtering

The moving average is a smoothing process which can be used on discrete signals. This process consists in substituting each value of a signal with the average of a precise group of numbers near to the value replaced. In this case, a centred moving average is employed, which means that half of the numbers used to generate the average value are just before the value to be substituted, whereas the others are immediately after such value. By centering the moving average, phase shifts can be avoided in the filtered signal.

From a mathematical point of view, a centered moving average can be expressed

through the following two equations, which are respectively used for an even number of values employed to perform each average of the moving average and an odd number of values:

$$y(k) = \sum_{k-r/2+1}^{k+r/2} u(n) / r \quad (1.1)$$

$$y(k) = \sum_{k-r/2}^{k+r/2} u(n) / r \quad (1.2)$$

A brief description of the letters in these formulas follows:

- " u " = unfiltered signal
- " y " = filtered signal
- " r " = number of values employed in the moving average
- " k " = position of the new value in the filtered signal

Low Pass Filter

The data logged from the control unit of the vehicle are time series. Consequently, for each value of the recorded signal, there is a corresponding value of time. For the Fourier Theorem, the characteristics of a signal over time and can be approximated with a Fourier series, which is a series of sinusoidal waves with a range of frequencies, amplitudes and phases. This means to perform a frequency (or spectral) analysis of the signal.

A spectral analysis of a time series can be performed by categorising each wave signal in the Fourier series on a plot of the amplitude in decibels (dB) against the frequency (Hz). Additionally, also the phase (deg) can be displayed against the frequency (Hz); however, this analysis is not meaningful for the goal of signal cleaning.

By performing a spectral analysis of a logged signal, it can be often noticed that the bandwidth of the frequency analysis extends far beyond the logging frequency of the signal. In fact, this phenomenon is mostly related to the presence of noise in the signal, which is detrimental to the integrity of the signal itself.

A low pass filter reduces the amplitude of the parts of the Fourier series which are over a determined frequency. In this way, the noise can be drastically reduced as reported in *Figure 1.1*. However, despite the reduction of the amplitude of the higher frequency series can contain the effects of noise and disturbances, these cannot be totally eliminated as they affect also the lower frequency signals.

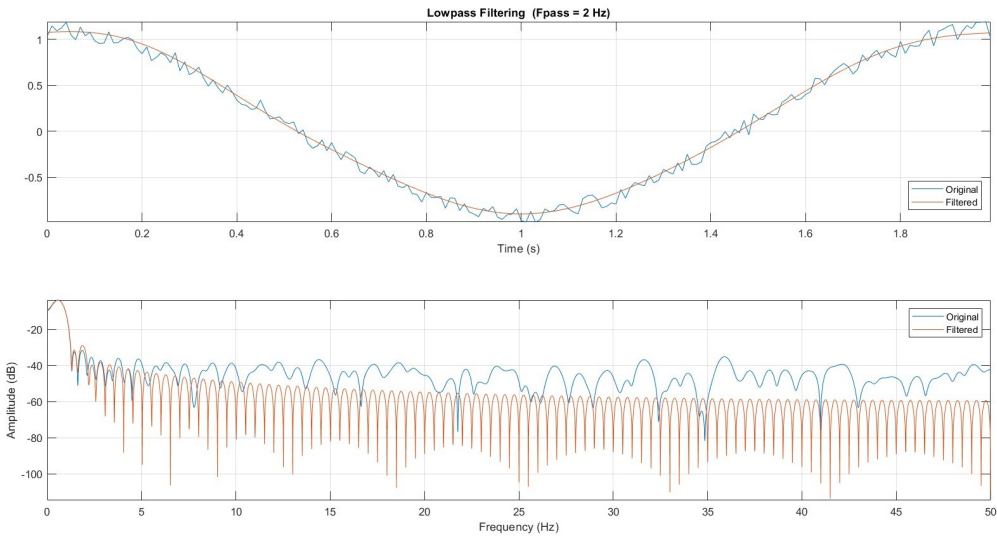


Figure 1.1: Low Pass Filter - Example

Filtering Parameters' Choice

The target of smoothing or filtering a signal is to reduce the noise without sacrificing the information contained in the signal itself. For instance, a too aggressive filtering could potentially flatten the signal or eliminate some trend present in the real signal as shown in *Figure 1.2*, whereas a mild filtering could not be enough to clear the trends introduced by the disturbances in the signal as displayed in *Figure 1.3*. For these reasons, the choice of the filtering parameters is of paramount importance.

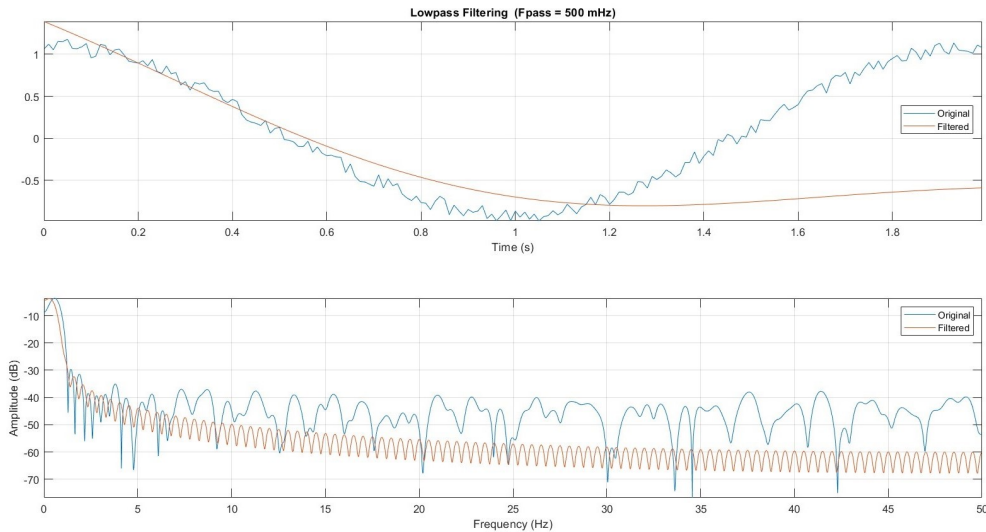


Figure 1.2: Aggressive Filtering - Example

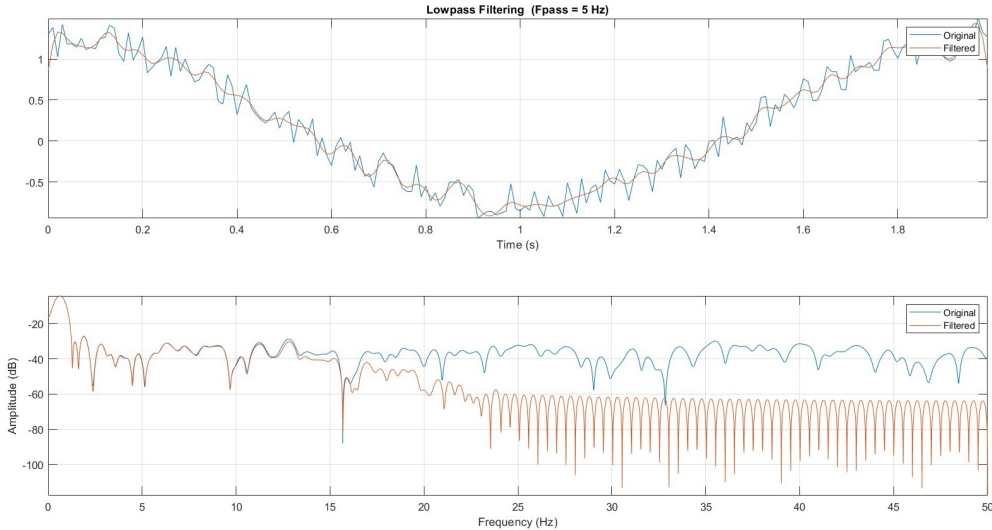


Figure 1.3: Mild Filtering - Example

The parameters to choose change depending on the kind of filtering technique employed. In particular, the parameters to fine-tune in a moving average are:

- the moving average interval length
- the number of elements in the interval after the value subjected to the average
- the number of elements in the interval before the value subjected to the average

While the values to be modified in a low pass filter are:

- the frequency where the filtering in amplitude starts
- the steepness of the filter

Starting from the moving average, the number of values belonging to the interval that are placed before or after the number subjected to average is not specified as the moving average used is centered. The important parameter in the smoothing of the signal through moving average is the interval length. In fact, as the interval gets larger the signal gets smoother, but also flatter. Consequently, large moving average intervals are likely to cause a loss of information.

In order to determine a way to understand at which level of smoothness (or filtering) the data in a signal start to degrade, a correlation with a clean signal has to be used. For instance, to clean the lateral acceleration data an estimation of side-slip angle on the four tyres and the vertical load on the four tyres could have been used in conjunction with the tyre data, which are employed to estimate the lateral force on the vehicle, and compare it with smoothed versions of the lateral acceleration to find the best match. Nevertheless, in our specific case, the yaw rate signal was subjected to the same inconsistencies present in the lateral acceleration as the *SC22* (the vehicle employed during testing) was equipped with only one inertial measurement unit. Furthermore, the tyre data at our disposal are not precise enough to make this kind of analysis. This is the reason why, in this paper, the lateral acceleration signal will be compared to the steering input.

In the *Figure 1.4* reported here below, the unfiltered lateral acceleration, some versions of the lateral acceleration smoothed by using a moving average with respectively 10, 20, 30, 80 and 200 elements, a smoothed version of the lateral acceleration obtained by applying a low pass filter and the steering angle are plotted against the sample number. It is possible to notice that the third row, which is the one containing the lateral acceleration filtered by a moving average using 20 elements, is the most similar to the steering input when only the moving averages signals are considered. In addition, a degradation of the signal can also be observed in the moving average performed using 200 elements.

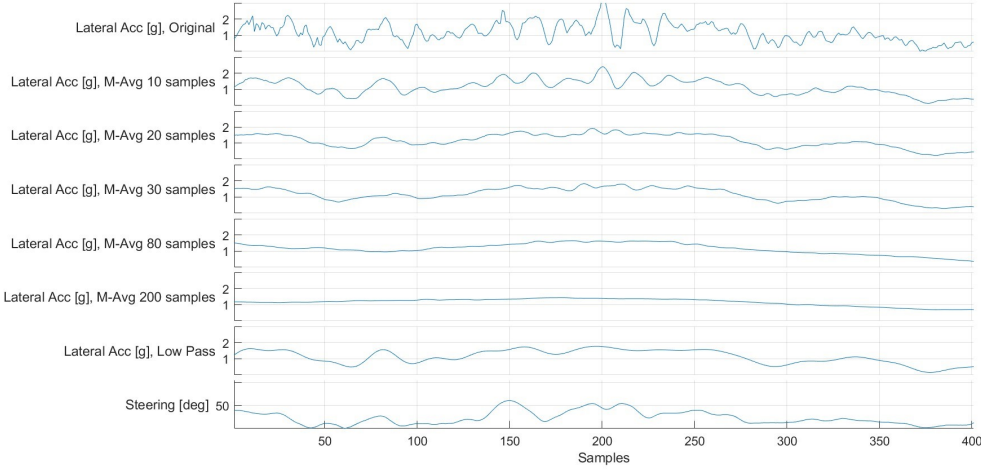


Figure 1.4: Different Filtering Strengths and Techniques

Despite a visual analysis can be a good starting point to determine which is the best moving average length, it is not enough. That being the case, a linear correlation analysis between steering and filtered acceleration can be carried out, which is what is described in *Figure 1.5*. In particular, the plots illustrate the steering angle against the lateral accelerations mentioned above, in the same order as previously reported.

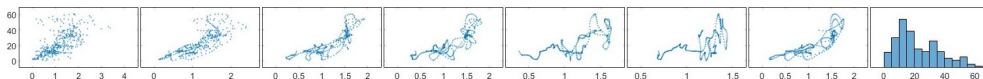


Figure 1.5: Linear Correlation Plots

From this analysis, the linear correlation factors, which indicate how well the plots in *Figure 1.5* fit a straight line, can be obtained as a percentage. The higher the percentage the better the correlation. In the following *Table 1.1* a precise corner has been taken to perform this analysis; nevertheless, the results obtained are highly reproducible. It is clear from the results that the 20 elements moving average is the best choice for this signal.

Lateral Acceleration Unfiltered	62.77%
Lateral Acceleration Moving Average - 10 elements	77.59%
Lateral Acceleration Moving Average - 20 elements	82.98%
Lateral Acceleration Moving Average - 30 elements	80.99%
Lateral Acceleration Moving Average - 80 elements	70.78%
Lateral Acceleration Moving Average - 200 elements	56.87%
Lateral Acceleration Low Pass Filter	83.04%

Table 1.1: Linear Correlation Factors

A similar analysis has been actuated to determine the best parameters for the low pass filter. In the end, a frequency of 4Hz and the highest steepness possible to implement in Matlab has shown the best results in terms of linear correlation as reported in *Table 1.1*. Whilst the moving average provides the best correlation and also a clean signal (*Figure 1.5*), the low pass filter requires an high computational time. In fact, from my tests, the low pass filter instead of a moving average can be up to 80 times slower than the moving average.

The values of smoothing parameters found above will be also used to filter the longitudinal acceleration as it is subjected to the same kind of disturbance degrading the lateral acceleration.

Significant Conditions

The combinations of lateral acceleration in " g ", longitudinal acceleration in " g " and speed in " m/s ", which are necessary to determine the load cases, need for the calculation of the minimum stiffness of the suspensions, will be obtained by requiring the **Critical Conditions**:

- Maximum Combined Acceleration (Max Combined)
- Maximum Lateral Acceleration (Max Lateral)
- Maximum Traction Acceleration (Max Traction)
- Maximum Braking Acceleration (Max Braking)

Where the combined accelerations are obtained as by applying the Pythagoras' theorem on the lateral acceleration and the longitudinal one.

For each condition, the respective lateral acceleration, longitudinal acceleration and speed will be found and filtered using either moving average or a low pass filter. After that, only the highest values are taken for the next analysis.

The process described above is carried out through Matlab scripting. The engineer who wants to use this script just needs to specify the script location, the log file's location, the name of the file and the kind of results that will appear on the final table (Max Lateral, Max Combined, Max Traction, Max Braking or All of them). The table containing the results will pop up as the code is executed. In this way, the whole process is completely automated.

	Parameters	Filtering	Max Lateral	Max Combined	Max Traction	Max Braking
1	Lateral Acc [g]	Moving Avg	2.3769	-2.3769	-0.7962	-0.5967
2	Longitudinal Acc [g]	Moving Avg	-0.4620	-0.4620	0.9213	-2.0033
3	Combined Acc [g]	Moving Avg	2.4227	2.4227	1.2683	2.1122
4	Speed [m/s]	Moving Avg	18.4578	18.4578	18.2058	23.0236
5	Lateral Acc [g]	Low Pass	2.5791	-2.5791	-0.7331	-0.3879
6	Longitudinal Acc [g]	Low Pass	-0.4821	-0.4821	0.9268	-2.2317
7	Combined Acc [g]	Low Pass	2.6085	2.6085	1.2597	2.1749
8	Speed [m/s]	Low Pass	18.2344	18.2344	18.7794	23.4488

Figure 1.6: Log Analysis Results - Table

1.3 Load Cases and Stiffness

The combinations of accelerations and speed, determined as explained in previous paragraph, will be needed to find the load cases, which are the vertical forces applied on the tyres. Once the load cases have been found, the stiffness that enables the vehicle's aerodynamic components to not touch the ground.

Input Data

There are 3 kind of data which are necessary to find the minimum stiffness. In particular, there are the data needed to determine the load transfer, the data regarding the aerodynamic components that are most likely to touch the tarmac and some additional data classifiable as safety factors or various stiffness. The data of the first type that need to be provided are:

- m_s = **sprung mass** [kg]
- m_u = **unsprung mass** [kg]
- m = **total mass of the moving vehicle** [kg]
- h_{CG} = **height from the ground of the centre of gravity of the total mass** [mm]
- h_{CP} = **height from the ground of the centre of pressure of the vehicle** [mm]
- wb = **wheelbase** [mm]
- w_f = **front weight repartition**
- a_f = **front aerodynamic repartition**
- b_f = **front braking repartition**
- t_f = **front traction repartition**
- C_z = **downforce coefficient** [m^2]
- C_x = **drag coefficient** [m^2]
- **antidive**
- **antilift**_{rear}
- **antisquat**
- **antilift**_{front}

The necessary data of the second kind are:

- hfw_{main} = height from the ground of the lowest part of the main element of the front wing [mm]
- hfw_{end} = height from the ground of the lowest part of the endplates of the front wing [mm]
- hsp_{front} = height from the ground of the front part of the sidepods [mm]
- hsp_{rear} = height from the ground of the rear part of the sidepods [mm]
- xfw_{main} = distance on the x axis of the most distant point the main element of the front wing [mm]
- xfw_{end} = distance on the x axis of the most distant point the endplate of the front wing [mm]
- xsp_{front} = distance on the x axis of the front part of the sidepods [mm]
- xsp_{rear} = distance on the x axis of the rear part of the sidepods [mm]
- xrd = distance on the x axis of the most distant part of the rear diffuser [mm]
- yfw_{end} = distance on the y axis of the endplates of the front wing [mm]
- ysp_{front} = distance on the y axis of the front part of the sidepods [mm]
- ysp_{rear} = distance on the y axis of the rear part of the sidepods [mm]

The additional data needed are:

- K_{tyre} = tyre vertical stiffness at 1psi [N/mm]
- K_{spring} = spring stiffness [N/mm]
- V_{max} = maximum speed that the vehicle can reach [m/s]
- g = gravitational acceleration [m/s²]
- ρ = air density at ambient temperature [kg/m³]
- $clearance$ = minimum margin from the ground of every part of the vehicle [mm]
- $corrcoef$ = corrective coefficient needed to consider that next year's car will be faster, and so the load cases should be increased

Performance Correction

The corrective coefficient " $corrcoef$ " can be taught as a safety factor. In fact, in the majority of cases, while the suspension is being designed, it is not possible to know how much the performance of the vehicle will evolve. For our case study, the corrective coefficient has been set at 10% due to the fact that the *SC22* has never been pushed to its full potential during testing. In order to determine the right value of $corrcoeff$ also a theoretical GGV plot could have been used; however, such method has shown to be too conservative, due to incorrect tyre performance scaling.

The corrective coefficient is applied to the accelerations, as they are multiplied for " $1 + corrcoef$ ". However, considering that the trajectory of the vehicle through a corner does not change significantly when the vehicle performances improve, then also the speed will change by a factor of " $\sqrt{1 + corrcoef}$ " as a consequence of the relation *Equation 1.3*.

$$a_c = V^2/R \quad (1.3)$$

Where:

- a_c = centripetal acceleration [m/s²]
- V = tangential speed [m/s]
- R = radius of curvature of the vehicle's trajectory [m]

The corrective coefficient is applied on all the load cases except the Max Traction, given that large improvements in traction performance can only be obtained through a marked reduction of the vehicle's mass or a crucial over hold of the launch control. Moreover, although the speed of the vehicle in Max Lateral, Max Combined and Max Braking is increased as explained, it cannot be higher than the maximum speed that the car can possibly reach.

Other Kinds of Correction

The input factor "*clearance*" is a margin that needs to be left from the ground when the car undergoes the critical conditions.

The clearance employed for this method should only be correlated with the minimum distance between the real car and ground. As a matter of facts, the ground clearance of a real vehicle is highly dynamic due to the continuous variation of its speed and accelerations. Therefore, the real dynamic right heights of a racing car has to be tuned by using different dampers setups.

Vertical Forces in Max Braking and Max Traction

The variation vertical load during any maneuver of the vehicle on a flat plane with no slopes is caused by three phenomena. The first one is the aerodynamic downforce, the second one is the aerodynamic drag, whereas the last one is the inertial force.

The aerodynamic forces can be found by considering the air density, the two aerodynamic coefficients and the speed of the vehicle (respectively for downforce and drag). The aerodynamic downforce " F_{az} " can be defined as in *Equation 1.4*, while the *Equation 1.8* describes the aerodynamic drag " F_{ax} ".

$$F_{az} = \frac{1}{2} * rho * C_z * V^2 \quad (1.4)$$

$$F_{ax} = \frac{1}{2} * rho * C_x * V^2 \quad (1.5)$$

Whilst F_{az} is distributed on the front and the rear axle depending on w_f (as reported in the *Equations 1.6* and *1.7*), the effects of F_{ax} on the vertical load on the tyres

needs to be calculated through the equilibrium of moments described in *Equation 1.8*.

$$Fa_{zf} = Fa_z * w_f \quad (1.6)$$

$$Fa_{zr} = Fa_z * (1 - w_f) \quad (1.7)$$

$$Fa_x * wb = Fa_f * h_{CP} = -Fa_r * h_{CP} \quad (1.8)$$

Where Fa_f and Fa_r are vertical forces applied respectively on the front axle and on the rear axle, which are due to the aerodynamic drag.

The effect of the inertia in Max Braking and Max Traction is mainly acting in the longitudinal direction. Therefore, the moment equilibrium for the inertia will be executed in the longitudinal direction. Moreover, the longitudinal forces create a vertical reaction on the car due to the suspension geometry, which oppose to the suspension movement when the vehicle is subjected to a load transfer. This effect is quantified in the anti-features, which will be taken into account in the final calculation. The topic of the anti-features will be thoroughly explained in *Chapter 4*.

At this point in the analysis this effect cannot be quantified as the suspension geometry has not been defined yet. Consequently, low values of the anti-features have been adopted, in order to have some margin when modifying the suspension geometry without risking that the car will touch the ground. Furthermore, two approximations are considered for this analysis. Firstly, the side view geometry of the suspension is considered to be equal on the front and on the rear. Secondly, the anti-features are non-dependent on the wheel travel. In this way the anti-features can be calculated as outlined in the *Equations 1.9, 1.10, 1.11* and *1.12*.

$$antidive = <Chosen\ Value> \quad (1.9)$$

$$antilift_{rear} = antidive * (1 - b_f) / b_f \quad (1.10)$$

$$antisquat = antidive \quad (1.11)$$

$$antilift_{front} = antisquat * (1 - t_f) / t_f \quad (1.12)$$

All in all, the vertical load caused by the inertia (Fi_f for the front and Fi_r for the rear) can be quantified as reported in the *Equations 1.14* and *1.15* for Max Braking,

$$F_x = m * a_x * g \quad (1.13)$$

$$Fi_f * wb = (F_x * h_{CG}) * (1 - antidive) \quad (1.14)$$

$$Fi_r * wb = -(F_x * h_{CG}) * (1 - antilift_{rear}) \quad (1.15)$$

and as presented in *Equations 1.16* and *1.17* for Max Traction (F_x is negative in this case).

$$Fi_f * wb = (F_x * h_{CG}) * (1 - antilift_{front}) \quad (1.16)$$

$$Fi_r * wb = -(F_x * h_{CG}) * (1 - antisquat) \quad (1.17)$$

The three effects described need to be summed in order to obtain the total load transfer on the front axle and on the rear axle, then the results need to be halved to determine the variation in vertical load on one of the tyres of each axle. Consequently, the load transfer on one of the front tyre will be calculated as expressed in

Equation 1.18, whilst the load transfer on one of the front tyre will be determined as in *Equation 1.19*.

$$Fd_f = (Fa_{zf} + Fa_f + Fi_f)/2 \quad (1.18)$$

$$Fd_r = (Fa_{zr} + Fa_r + Fi_r)/2 \quad (1.19)$$

Minimum Heave Stiffness

To determine the minimum heave stiffness of the suspensions, may well be a rather difficult task if the right assumptions are not taken. Therefore, the process performed here will be quite simplified. In fact, the heave stiffness will be considered constant and it will be the same for the front and for the rear suspensions. Moreover, the load cases are considered as steady state forces which acts on the vehicle; therefore the effect of dampers is neglected and this leads to a conservative result. However these simplifications, the value obtained in this analysis can still be useful as input values for more complex models, which will be employed in further analysis.

The minimum heave stiffness is calculated by considering the load transfer determined as explained in the previous paragraphs. In particular, the load transfer in traction is employed to determine the stiffness that makes the rear diffuser have a distance to the ground that is equal to the clearance specified in the input data. This procedure is represented by *Equation 1.20*, where the minimum heave stiffness of each wheel " Kg " is the unknown.

$$hrd - \text{clearance} = (Fd_r/\mathbf{Kg} - Fd_f/\mathbf{Kg}) * xrd/wb + Fd_f/\mathbf{Kg} \quad (1.20)$$

Whereas the minimum heave stiffness for the braking load cases can be limited by either the main element or the endplate of the front wing to get nearer to the ground than the clearance. These two occurrences are respectively represented by the *Equations 1.21* and *1.22*, in both of them the unknown is the minimum heave stiffness " Kg ".

$$hfw_{main} - \text{clearance} = (Fd_f/\mathbf{Kg} - Fd_r/\mathbf{Kg}) * (wb - xfw_{main})/wb + Fd_r/\mathbf{Kg} \quad (1.21)$$

$$hfw_{end} - \text{clearance} = (Fd_f/\mathbf{Kg} - Fd_r/\mathbf{Kg}) * (wb - xfw_{end})/wb + Fd_r/\mathbf{Kg} \quad (1.22)$$

After these 3 values of " Kg " have been found, the minimum heave stiffness is the highest one, as it represents the most critical case. In the majority of cases, the part of a racing car that is most likely to touch the tarmac due to low heave stiffness is the front wing and the *SC22* is no exception.

From Kg , knowing the spring stiffness and the tyre stiffness, one value of dynamic force-based installation ratio can be obtained as explained in *Equations 1.23* and *1.24*, where " Kw_{Spring} " is the spring stiffness at the wheel centre. This value will be only valid for the specified load conditions and speed.

$$Kw_{Spring} = 1/(1/Kg - 1/K_{Tyre}) \quad (1.23)$$

$$IR = \sqrt{Kw_{Spring}/K_{Spring}} \quad (1.24)$$

Maximum Roll Gradient

The Roll Gradient (RG) is an inverse measure of the suspension stiffness (suspension compliance), which correlates the lateral acceleration with the roll angle of the vehicle. Therefore, in the following paragraphs the maximum RG will be found, due to the fact that it corresponds to the softest the car can be in roll.

The RG will be determined by applying the same principle employed for the calculation of Kg . In fact, the vehicle should not be in contact with the ground also while cornering. Consequently, the same assumptions taken during the Kg 's calculation will be taken in this section. This means that, the RG will be considered constant and independent on the suspensions' travels, and the effect of damping will be neglected as the manoeuvre is considered as if steady state forces act on the vehicle.

First of all, the effect of speed and longitudinal accelerations on the height of the critical parts can be established given that Kg is known. To do so, the variation of vertical forces needs to be quantified by considering the effects of the aerodynamic forces and the result of the longitudinal acceleration as seen in the previous section in the *Equations 1.4 to 1.19*, but this time the speeds and longitudinal acceleration used will be the ones present in the Max Lateral and the Max Combined cases. Subsequently, the variation in front and rear vertical travel of the contact patches can be found by dividing the load transfers and Kg as reported in *Equation 1.25* and *1.26*, these values correspond to the front and rear ride height variation before to consider the lateral inertia.

$$Zd_f = Fd_f/kg \quad (1.25)$$

$$Zd_r = Fd_r/kg \quad (1.26)$$

Once these values have been found, the residual heights of the aerodynamic components which could touch the ground (e.i., front wing endplate and sidepods) can be determined. The residual heights' calculation should also contain the clearance. Therefore, they can be quantified as expressed in the *Equation 1.27* for the front wing and as in the *Equations 1.28* and *1.29* for the front and rear sidepods respectively.

$$Zr_{fw} = h_{fw_{end}} - ((Zd_f - Zd_r) * (wb - xf_{w_{end}})/wb + Zd_f) - clearance \quad (1.27)$$

$$Zr_{fs} = h_{sp_{front}} - ((Zd_f - Zd_r) * (wb - xsp_{front})/wb + Zd_r) - clearance \quad (1.28)$$

$$Zr_{rs} = h_{sp_{rear}} - ((Zd_f - Zd_r) * (wb - xsp_{rear})/wb + Zd_r) - clearance \quad (1.29)$$

The residual heights of the components can be leveraged to determine how much roll angle the car can develop before hitting the ground, this is done through a geometrical evaluation. In fact, considering as approximation that the car rolls along an axis on its mid-plane and the height of this axis is the initial residual height of the component considered, the maximum roll angles (*alpha*) can be quantified as follows in the *Equations 1.30, 1.31* and *1.32*.

$$\alpha_{fw} = \arctan(Zr_{fw}/y_{fw_{end}}) \quad (1.30)$$

$$\alpha_{fs} = \arctan(Zr_{fs}/y_{sp_{front}}) \quad (1.31)$$

$$\alpha_{rs} = \arctan(Zr_{rs}/y_{sp_{rear}}) \quad (1.32)$$

The process employed to find the roll angles should be done both for the Max Combined and Max Lateral conditions, as they are the most critical cases in terms of roll.

After the six values of α have been determined, the next step is to calculate the RG , which is defined as the ratio between the roll angle in *degrees* and the lateral acceleration in g .

$$RG = \alpha / a_y \quad (1.33)$$

Ultimately, the lowest RG of them should be used, as it corresponds the highest roll stiffness.

Automatising the Process

The process of quantification of maximum RG and minimum Kg has been carried out by using Matlab scripts. This enables the engineers to speed up the initial phase of the suspensions' kinematics design, by providing to them some initial values needed to determine the installation ratios of the real car and their dynamic values. Lastly, the parameters found on this chapter will enable to re-scale the suspension stiffness of the previous car to roughly match the predicted stiffness of the new car, and eventually determine the suspension travel during the vehicle's manoeuvres.

Chapter 2

Critical Corners

In racing vehicles, the design of every suspensions' kinematics is always the result of a number of trade-offs. In fact, the suspensions' kinematics can only be finely tuned for only two or three kinds of corners. Otherwise, a broader trade-off has to be considered on a series of different corners. Despite the latter approach is not considered in this thesis, the method analysed in the next chapters can be expanded to accommodate this method. For this reason, by utilising the former technique, it is of paramount importance to decide the types of corner to consider during the optimisation process.

2.1 Methodology

In this section, the most effective method to select the conditions under which the suspensions' kinematics are optimised will be explained. Moreover, the reasons why this method is not applicable in our case will be discussed and a different approach will be presented.

Drivers' Feedback and Telemetry

In order to decide the areas of the track to be analysed, drivers' feed-backs and telemetry data are often employed. As a matter of fact, drivers are really effective in identifying the parts of a circuit where the vehicle is not working properly, both in terms of grip and balance. Moreover, the telemetry data can be used to precisely identify the characteristics of this parts of the circuit and to quantify the lack of balance and grip when compared to the corners where the drivers report that the car is working properly.

On the other hand, whilst the method described is the best way to evaluate where to better the suspensions' kinematics, it requires a lot of testing, consistent track conditions and a perfect setup of the vehicle which enables the drivers to fully exploit the vehicle and thus to expose its weaknesses. In the specific case study here reported (based on the tests carried out in 2022), the comments of the drivers and the data gathered demonstrate that the vehicle's behaviour and performance was too inconsistent between the runs. This situation was mostly caused by incorrect brake bleeding between the runs and uncontrolled variation of the front tyre temperature and pressure.

GPS Data and Full-Vehicle Simulations

Due to the impossibility of clearly determining in which corners to optimise the suspensions' kinematics by using the technique above-mentioned, the vehicle is simulated in the track where the most reliable GPS data were collected. Once the vehicle has been simulated, the corners where the most time can be gained are employed as the corners where to optimise the suspensions.

2.2 Trajectory Modelling

It is fundamental to model properly the trajectory that the car will be following during the simulation process, which will be carried out through the vehicle simulation software Vi-Carrealtime. Therefore, a combination of smoothing techniques on Matlab and on Vi-Road (utility contained in Vi-Carrealtime) are employed to create a smoothed version of the vehicle trajectory that is implemented in the simulator. In this way, the trajectory obtained will also retain most of the characteristics of the real car trajectory from which it is extrapolated from.

From GPS Data to Trajectory Coordinates

First of all, the GPS data recorded are reported as latitude and longitude both in degrees. Therefore, these data need to be converted into X and Y data in metres in order to create a path to follow for the simulated vehicle. To do so, the difference between the initial GPS coordinates and the following coordinates during the lap considered has to be calculated. Consequently, it can be noticed that the angles resulting from this difference are extremely small, thus the formula reported in the *Equations 2.1* and *2.2* is a good approximation to convert latitude and longitude into metres.

$$X = R_e * \tan(\alpha_{Longitude}) \quad (2.1)$$

$$Y = R_e * \tan(\alpha_{Latitude}) \quad (2.2)$$

the parameters in the *Equations 2.1* and *2.2* stand for:

- X = track's x coordinate [m]
- Y = track's y coordinate [m]
- R_e = earth radius [m]
- $\alpha_{Longitude}$ = difference between the Longitude values during a lap and the first one [deg]
- $\alpha_{Latitude}$ = difference between the Latitude values during a lap and the first one [deg]

Trajectory Coordinate Smoothing

By directly using these data, the simulated vehicle starts turning left and right in an erratic way. This situation is caused by the fact that the x and y coordinates, obtained through this process, draw a trajectory which is too irregular to be followed by the vehicle. Therefore, the Vi-Road utility might be used on these coordinates to apply a smoothing to the trajectory. However, by just applying the smoothing

through Vi-Road, the resulting trajectory loses most of its initial characteristics, as the filtering applied by this software is too aggressive and not extensively tunable. For this reason, a smoothing in Matlab has to be applied prior to the insertion of the data into the simulation software.

In order to smooth effectively the x and y data in Matlab, firstly, they need to be parameterised as function of the distance. Once the parameterisation has been completed, the x and y data are expanded by adding new data. These additional data are computed through the modified Akima algorithm for mono-dimensional interpolation integrated in Matlab, which provides a smooth third order local polynomial fitting with a reduced quantity of oscillations of the output (to directly use a bi-dimensional interpolation did not provide an acceptable result). Then, the resulting data are smoothed again by using different moving averages to even out some residual imperfections in the trajectory which resulted from the previous steps. The positive effects of this smoothing can be observed in the example in *Figure 2.1* where the raw x and y coordinates obtained from the GPS data as reported above, are compared with the data that have been smoothed through this process.

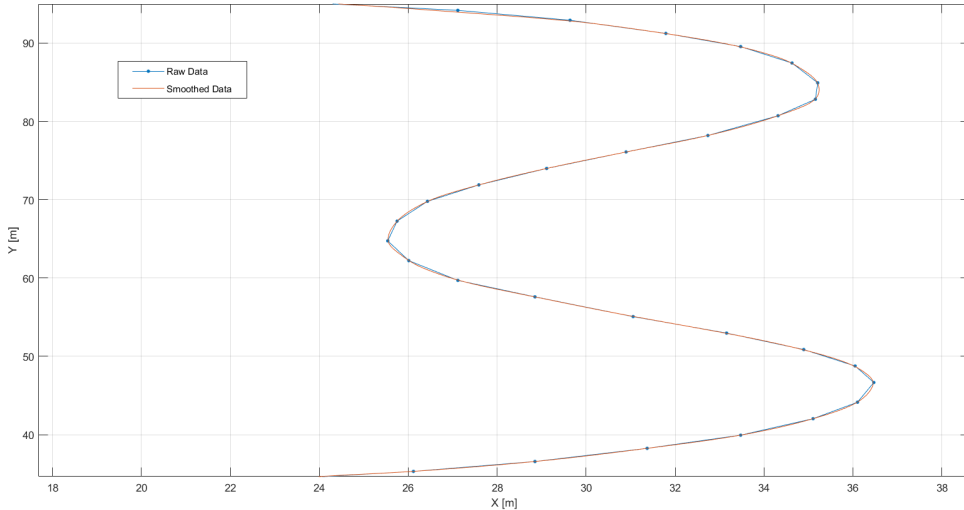


Figure 2.1: Raw Data vs Smoothed Data of some corners

After x and y coordinates data have been processed on Matlab, the resulting coordinates just need a minor smoothing on Vi-Road in order to eliminate any kind of irregular steering movement during the simulation.

2.3 Vehicle Simulations

The determination of the critical corners where to optimise the suspensions kinematics is the result of full vehicle simulations executed through Vi-Carrealtime. In particular, two simulations will be performed. Firstly, a simulation where the vehicle is not fully exploiting its full grip is executed. After that, the second simulation will have the car to be nearer to its maximum performance envelope. Then, the simulations are compared and the corners where the maximum time advantage normalised with respect to the corner length is obtained will be deemed as critical corners.

Differentiate the Simulations

In order to exploit the car in a different way during these simulations, three parameters that determine the virtual driver's behaviour in Vi-Carrealtime has to be tuned. The first one is the Longitudinal Acceleration Performance Factor. By increasing it, the virtual driver will tend to pick up the throttle earlier and to rise the aggression on the throttle. The second parameter to tune is the Longitudinal Braking Performance Factor. An increase in this performance factor results in delayed braking point and higher braking pressure during the whole braking phase, this often results in higher corner entry speeds. The last parameter to be tuned is the Lateral performance factor. Higher values of this parameter cause the driver to turn earlier and more aggressively into a corner, in general, the vehicle side-slip angle become much higher; moreover, increasing the Lateral Grip Factor also leads to less throttle lifting in fast corners.

Overall, to increase these grip factors is a convenient way to simulate enhanced vehicle grip. In fact, when a driver has more grip they can brake later into the corners, carry more speed into the corners, use more throttle during corner exit and use the steering more aggressively. Therefore, the totality of these effects may well simulated through the performance factors, that are raised from a value of 0.7 to a value of 0.9 from the first simulation to the second one.

Critical Corners

From the analysis of the data resulting from the simulation, the critical corners can be found. However, this cannot be done as long as the corners are discretised one from the others. In order to achieve this result, a visual analysis is employed. In facts, a tri-dimensional scatter of the trajectory of the vehicle during the simulation has been created. It features on the x-axis and y-axis there are respectively the x and the y coordinates of the vehicle trajectory in metres, whereas the z-axis contains the arclenght of the trajectory. Moreover, the course itself is coloured depending on the combined input on the throttle and brake, which is the throttle position in percentage minus the brake position in percentage. As it is possible to notice from *Figure 2.2*, which reports scatter described, that the starting point of each corner can be determined by looking at the points where the combined throttle and brake input goes from an high value from a low one.

As the result of the discretisation, the corners will look like in *Figure 2.3*. It can be assessed that each corner goes from its starting point to either the starting point of the next corner or the end of the lap. This is done because the effect of a corner reflects on the successive straight. However, this effect would bias the results towards the corners followed by a straight, hence it has to be compensated by normalising the time delta by the corner length.

The normalised time gain ("Normalised Delta" in *Table 2.4*) is employed as the factor that determines which corner is critical for the suspensions' kinematics optimisation. By looking at the results in *Table 2.4* it is possible to observe that the three most effective corners where to improve the vehicle's performance are the fifth, the fourth and the tenth corner. Furthermore, the linear correlation between Normalised Delta and Corner Length (in the table reported below) is small, thus the length of the corner does not influence the final result. Lastly, the three corners chosen represent a set of different characteristics. In actual fact, corner four is a

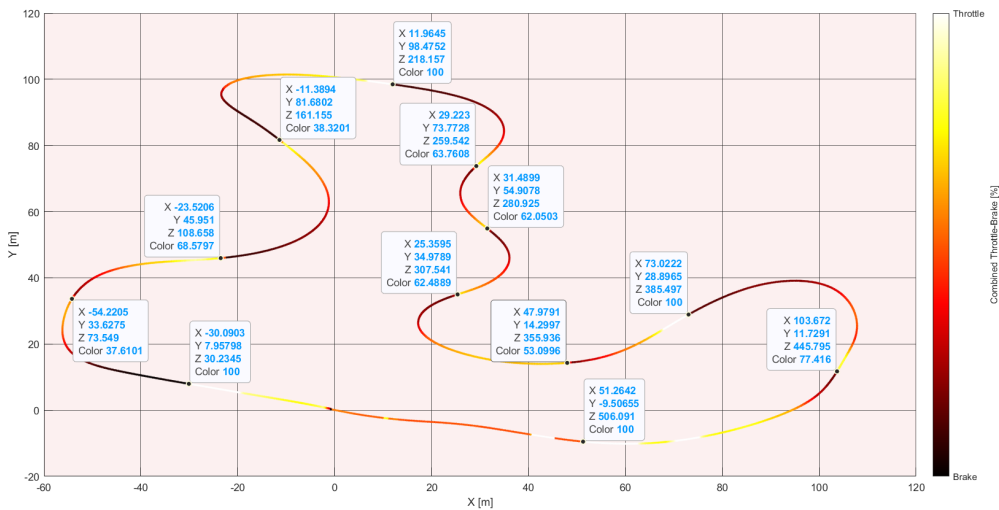


Figure 2.2: Track Map with Combined Traction and Brake Input

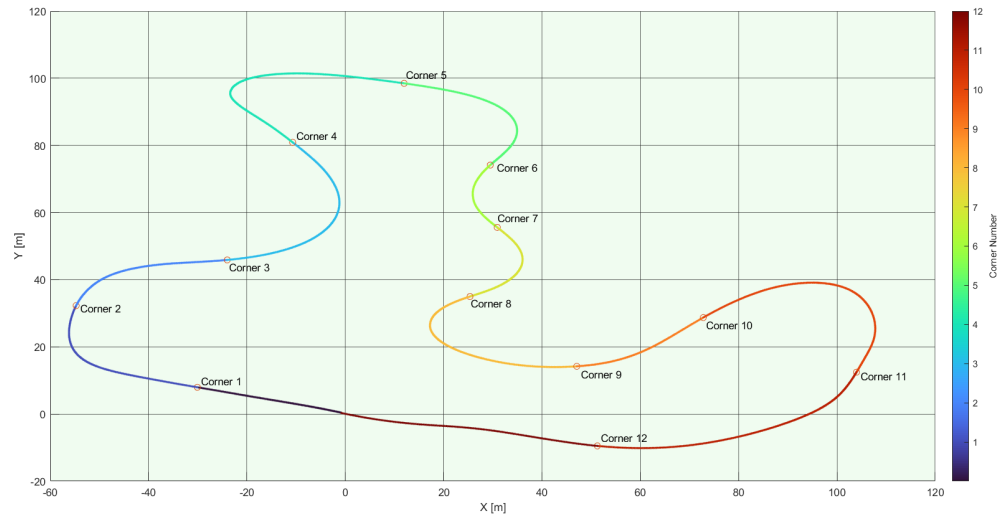


Figure 2.3: Track Map with Corner Numbers

slow corner similar to an hairpin, corner five is a medium speed corner with a change in direction in the exit, whereas corner ten is a fast turn which tightens up. All of these characteristics are common to the wide majority of the FSAE circuit where the *SC22* has competed.

Corner	Normalised Delta	Time Delta	Corner Length	Min Speed
5	0.0064	0.2600	40.8182	37.1221
4	0.0057	0.3300	57.7566	17.6981
10	0.0054	0.3200	59.5723	43.7995
6	0.0053	0.1100	20.8142	42.7567
1	0.0050	0.2100	41.7989	40.6676
2	0.0048	0.1700	35.7358	56.1169
7	0.0048	0.1300	27.3346	35.0700
9	0.0047	0.1400	29.8311	81.2780
3	0.0044	0.2300	51.8268	49.0605
8	0.0038	0.1800	47.3367	28.2560
11	0.0031	0.1900	60.7634	63.1834
12	0.0006	0.0300	53.6571	115.9722

Figure 2.4: Results of the Analysis

Chapter 3

Working Conditions of the Tyres

One of the main targets of the suspension's kinematics optimisation is to increase the grip extracted from the tyres. Therefore, it is of primary importance to define the working conditions of the tyres. In this chapter, the vehicle is simulated in order to replicate the speed and acceleration generated by the real car in the corners identified in the previous chapter. In this way, all the characteristic angles and slips, the speed and the vertical force acting on each tyre during such corners can be determined.

3.1 Methodology

In this section, the parameters needed to determine how much lateral and longitudinal force is developed by the tyres during each time instant during every time instant will be examined. Furthermore, the methods that can be adopted to determine the working conditions of the tyres will be discussed.

Tyres' Working Parameters

There are several tyre's parameters that are needed to determine the working condition of a tyre such as temperature and wear. In order to perform the analysis treated in *Chapter 4*, the values that have to be determined during each time instant needed are the vertical force (in newtons), the side-slip angle (in degrees), the camber angle (in degrees), the longitudinal slip ratio (as an adimensional number) and the longitudinal speed (in metres over seconds) of the tyre considered.

In addition to these parameters, the values of pressure, loaded radius and the turn-slip are necessary to obtain the forces generated by tyres. The pressure and the turn-slip will be both set to one due to the fact that the target hot pressures is of about 1 bar and that the tyre's deformation is best represented when the turn-slip equals 1 metre. On the other hand, the loaded radius is set to be constant at its static value.

Other parameters, such as the above-mentioned tyre temperature and tyre wear are not considered. This is mainly due to the absence of real-time data regarding

the temperature and the lack of a thorough knowledge of the effect of temperature and wear on the tyre's performance.

Despite this, it can be assumed that the variation of these parameters scales down the forces generated by the tyres, while not affecting the dependency between the forces generated by a tyres and the parameters described above. Therefore, by employing this approximation, the results obtained through the suspension's kinematics optimisation will still be significant in terms of percentage gains.

Track Tests and Sensors

In this section the sensors required to perform this kind of analysis purely based on track data will be discussed. In order to understand what sensors are adapt to calculate the tyres' conditions needed, it is firstly necessary to describe the equations that enable us to extract the values desired.

In order to better understand the equations that will be reported in this section it is opportune to refer to *Figure 3.1*.

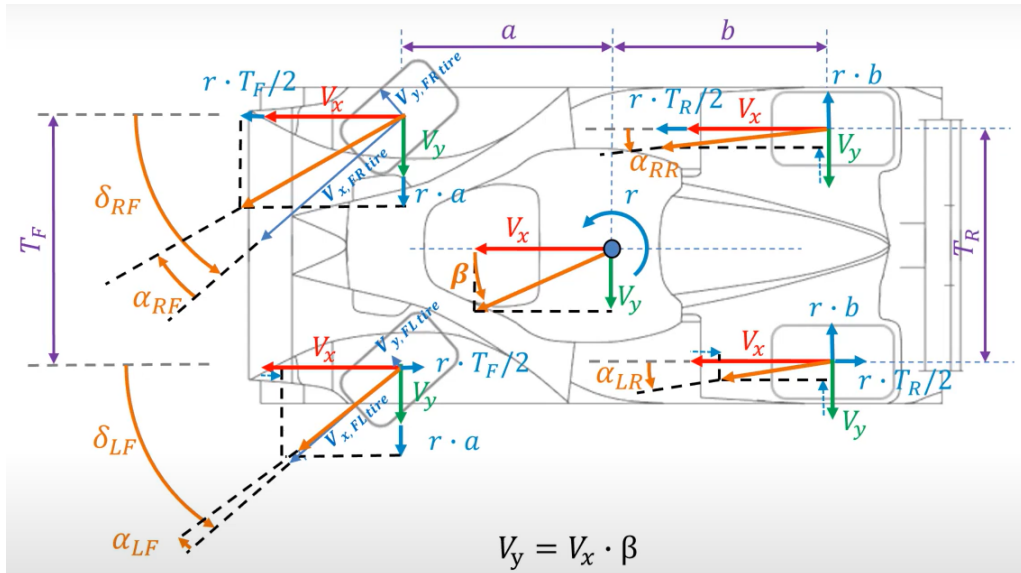


Figure 3.1: Tyres' Speed and Side-slip

The values reported in this figure are:

- **CG** = centre of gravity
- V = vehicle speed [m/s]
- β = vehicle side-slip angle [rad]
- V_x = vehicle longitudinal speed [m/s]: $V_x = V * \cos \beta$
- V_y = vehicle lateral speed [m/s]: $V_y = V * \sin \beta$
- r = yaw rate [rad/s]
- a = longitudinal distance between the CG and the front axle [m]
- b = longitudinal distance between the CG and the rear axle [m]
- T_F = front track width [m]

- T_R = rear track width [m]
- δ_{FL} = front left steering angle at the wheel [rad]
- δ_{FR} = front right steering angle at the wheel [rad]
- α_{FL} = side-slip angle front left tyre [rad]
- α_{FR} = side-slip angle front right tyre [rad]
- α_{RL} = side-slip angle rear left tyre [rad]
- α_{RR} = side-slip angle rear right tyre [rad]

All the parameters reported are obtainable from the post processing of the data coming from track testing. In fact, the longitudinal speed and the longitudinal slip ratio of each tyre can be attained by making use sensors that are widespread and commonly used in every racing environment, such as an IMU (Inertial Measurement Unit) and the rotational speed sensors of the wheels, which in our case are in the four engines (one for each wheel) of which the vehicle is provided. The data measured from these sensors are then processed as shown from *Equation 3.1* to *3.4* in order to calculate the longitudinal slips on each one of the four tyres.

$$\sigma_{FL} = \frac{(V_x - r * T_F/2) * \cos \delta_{FL} + (V_y + r * a) * \sin \delta_{FL} - \omega_{FL} * Rl_{FL}}{(V_x - r * T_F/2) * \cos \delta_{FL} + (V_y + r * a) * \sin \delta_{FL}} \quad (3.1)$$

$$\sigma_{FR} = \frac{(V_x + r * T_F/2) * \cos \delta_{FR} + (V_y + r * a) * \sin \delta_{FR} - \omega_{FR} * Rl_{FR}}{(V_x + r * T_F/2) * \cos \delta_{FR} + (V_y + r * a) * \sin \delta_{FR}} \quad (3.2)$$

$$\sigma_{RL} = \frac{(V_x - r * T_R/2) * \cos \delta_{RL} - \omega_{RL} * Rl_{RL}}{(V_x - r * T_R/2) * \cos \delta_{RL}} \quad (3.3)$$

$$\sigma_{RR} = \frac{(V_x + r * T_R/2) * \cos \delta_{RR} - \omega_{RR} * Rl_{RR}}{(V_x + r * T_R/2) * \cos \delta_{RR}} \quad (3.4)$$

The variables not specified in these equations are:

- σ_{FL} = longitudinal slip ratio of the front left tyre [-]
- σ_{FR} = longitudinal slip ratio of the front right tyre [-]
- σ_{RL} = longitudinal slip ratio of the rear left tyre [-]
- σ_{RR} = longitudinal slip ratio of the rear right tyre [-]
- ω_{FL} = rotational speed of the front left tyre [rad/s]
- ω_{FR} = rotational speed of the front right tyre [rad/s]
- ω_{RL} = rotational speed of the rear left tyre [rad/s]
- ω_{RR} = rotational speed of the rear right tyre [rad/s]
- Rl_{FL} = loaded radius of the front left tyre [m]
- Rl_{FR} = loaded radius of the front right tyre [m]
- Rl_{RL} = loaded radius of the rear left tyre [m]
- Rl_{RR} = loaded radius of the rear right tyre [m]

On the other hand, it is of fundamental importance to use four TPMSSs (Tyre and Pressure Monitoring Systems) and an optical sensor, in order precisely define the values of vertical forces and the side-slip angles acting on the tyres . In particular, whilst the tyres' side-slip angles can be calculated as in the *Equations 3.5, 3.6, 3.7*

and 3.8 , the vertical force can be found by an estimation obtained through the pressure data coming from each TPMS and a pressure distribution in the contact patch that has to properly be modelled. However, whilst this approach is really straight forward, to purchase and setup these sensors might not be possible, due to the budget for the majority FSAE teams.

$$\alpha_{FL} = \arctan \left(\frac{V_y + r * a}{V_x - r * T_F / 2} \right) - \delta_{FL} \quad (3.5)$$

$$\alpha_{FR} = \arctan \left(\frac{V_y + r * a}{V_x + r * T_F / 2} \right) - \delta_{FR} \quad (3.6)$$

$$\alpha_{RL} = \arctan \left(\frac{V_y - r * a}{V_x - r * T_F / 2} \right) \quad (3.7)$$

$$\alpha_{RR} = \arctan \left(\frac{V_y - r * a}{V_x + r * T_F / 2} \right) \quad (3.8)$$

For these reasons, the values of vertical force acting on a tyre can be calculated from the data acquired by placing strain gauge on the suspension push-rod or pull-rod, which estimates the force passing through the linkage where the strain gauge is used. Subsequently, the force obtained is converted in a force acting on the wheel centre.

Alternatively, if there is not the possibility to mount four strain gauges on the push-rods, the force acting on the wheel centre can be determined from the dampers' potentiometers. These sensors enables the us to measure the values of dampers' travel. Also the damper speed can be computed by using a numerical derivative. As a matter of fact, the damper displacement and speed can be utilised to compute the force acting on the spring and damper assembly. Once this force has been found, it can be converted to the force acting on the wheel centre by using a lookup table. Lastly, the component of the force on the wheel centre due to the torsion bar can be calculated in the a similar way of what has been done for the components of the force on the wheel centre due to damper and spring . After the total force on the centre of the wheel has been found, the only missing components is due to the inertia of the unsprung masses and the combination of jacking forces and anti-feature forces.

To follow this approach can become quite complex as it requires a thorough understanding of the suspension characteristics and, most of all, it must be possible to acquire all the lookup tables necessary to execute the process described above (installations ratios and Roll centre positions). These lookup tables are actually quite elaborate due to the fact that they depend on a multiplicity of different factors (multidimensional lookup tables). Moreover, the tyre acts as a low-pass filter for the forces that reaches the wheel centre, making the estimation of vertical force at the contact patch of the tyre imprecise.

Regarding the tyres' side-slip angle calculations, they require the value of vehicle side-slip angle (β), that can either be computed by an optical sensor or calculated from the IMU's data. In particular, the values of yaw rate and acceleration coming from the IMU can be used to compute an approximation of the vehicle side-slip angle. However, it is not always possible to avoid the side-slip angle of the vehicle to drift when it is computed from the IMU.

Overall, it is often unfeasible to accurately determine the vertical forces and side-slip angles acting on the tyres without the right sensor.

Available Data

In our specific case, the vehicle tested during the 2022 season (*SC22*) lacked some of the most critical sensors needed to determine the vertical forces acting on the tyres, such as TPMSs and strain gauges. Moreover, the estimation of β from the IMU was not accurate and the data taken from the dampers' potentiometers tended to be highly unreliable, due to high sensibility to disturbances. Therefore, the data extracted from the tests carried out on the *SC22* did not permit us to determine the tyres' working conditions.

In order to overcome the limits of the data obtained on track, the vehicle has been simulated in the critical corners found during *Chapter 2.3* in co-simulation between Vi-CarRealTime and Simulink and the accelerations recorded by the IMU are employed to match the the simulation with a real lap.

3.2 Vehicle Simulation

It is now necessary to explain more in depth the steps required to create a simulation scenario that matches a real vehicle conditions. First and foremost, the suspensions' stiffness of the model simulated has to be adapted to the values of suspension stiffness found in *Chapter 1.3* in order to better replicate the wheel travel of the final suspension. Secondly, the input of the simulated vehicle have to be scaled and tuned in order to match the trajectory and speed of the real vehicle. Lastly, the effect on the lateral and longitudinal forces created by the tyres in these corners has to be analysed by tuning the parameters of the working conditions.

Adapting the Suspensions' Stiffness

The vehicle model created on Vi-CarRealTime to simulate the *SC22* is a digital twin of the real vehicle. Particularly, the suspensions' kinematics, stiffness and damping are identical to the ones of the real car. However, at this point of our analysis, the heave stiffness of the vehicle is known as it has been determined in *Chapter 1.3*. On the other hand, component the rolling stiffness of the vehicle controlled by the torsion bar will remain unchanged in the new iteration of the suspension that is being designed in this thesis. This is mostly due to the fact that, accordingly to the drivers' feed-backs, the rolling stiffness of the vehicle tested on track was on point; moreover, the heave stiffness obtained from the calculations executed above does not change dramatically with respect to the values of the *SC22*. Therefore, the roll stiffness provided by the torsion bars do not need to change in order to guarantee a similar rolling stiffness (hence roll gradient) to the one provided from the vehicle tested.

First of all, the decision of the method employed to adapt the suspension stiffness needs to take into account that it does not make sense to modify the geometry of the upper part of the suspensions (rocker, droplink, balance bar and damper attachment point) at this point in the suspensions' design. This choice is justified by the fact that the lower part of every suspension influence the installation ratios and, most of

Variable Name	Roll Gradient Value
Wheel Centre Front	0.13307 [deg/g]
Wheel Centre Rear	0.20084 [deg/g]
Wheel Centre Overall	0.1617 [deg/g]
Tyre	0.33634 [deg/g]
Total Front	0.46941 [deg/g]
Total Rear	0.53719 [deg/g]
Total Overall	0.49804 [deg/g]

Figure 3.2: Roll Gradient Components of the *SC22*

Variable Name	Roll Gradient Value
Wheel Centre Front	0.14179 [deg/g]
Wheel Centre Rear	0.21034 [deg/g]
Wheel Centre Overall	0.17103 [deg/g]
Tyre	0.33634 [deg/g]
Total Front	0.47813 [deg/g]
Total Rear	0.54669 [deg/g]
Total Overall	0.50738 [deg/g]

Figure 3.3: Roll Gradient Components of the *SC22* with Re-scaled Heave Stiffness

all the position of the upper elements of the suspension is influenced by the location of the outer hard-point of lower control arm. As a consequence, the simplest way to re-scale the suspensions' stiffness is to change the spring stiffness in order to match the wheel centre heave stiffness that would be present in the final suspensions at the speed at which the minimum ground stiffness has been determined during *Chapter 1.3*.

The data needed in order to find the stiffness of the springs that have to be inserted in the Vi-CarRealTime model (to obtain a car featuring the new heave stiffness) are the new installation ratio and the old one for each of the four suspensions. Furthermore, the real spring stiffness is needed. The real spring stiffness is generally contained in the simulated vehicle model, whilst the old installation ratio and the new one can respectively be obtained from a suspension kinematics simulation and as a result of the calculation carried out during after the calculation of the minimum heave stiffness. In order to obtain the springs' stiffness to insert in the simulated model (spring equivalent stiffness) from these information *Equation 3.9* is applied.

$$K_{SpringEquivalent} = K_{Spring} * \left(\frac{IR_{New}}{IR_{Old}} \right)^2 \quad (3.9)$$

Although this method does not guarantee the heave stiffness to be the same that will be obtained in the final suspension during the whole wheel travel, this is a valid approximation for the preliminary analysis executed in this chapter.

Simulation Setup and Inputs Scaling

After the springs' stiffness have been tuned to match the right heave stiffness, the model is ready to be used for the simulation.

The simulation is executed starting from the a generic open loop event created in Vi-EventBuilder (a utility of Vi-CarRealTime) where the initial speed of the event and the required to carry out the simulation have to be specified. For our specific case, only the initial speed is relevant, whereas the other inputs can be set to a constant value equal to zero. This is due to the fact that all the input (but the initial speed) can be overwritten in Simulink. The initial speed (in [m/s]) of the open loop event created in Vi-EventBuilder can be modified by opening it as text file and modifying the "INITIAL SPEED" parameter of the "STARTUP" section. Once the right initial speed has been set to the initial value of the corner that has to be simulated, the openloop file is used in a FileDriven simulation executed in the test mode of Vi-CarRealTime. By running this simulation in files only mode, an svm file is generated. This file can be ran by forcing the real values of steering, throttle and brake through Simulink by taking them from the track testing data.

By just employing the raw data coming from the fast laps in the critical corners, the simulated car would not follow the same trajectory of the real one at the same speed of the real one. This is due to the fact that the simulation does not take into account the environmental external effects such as the track temperature or the tyre wear.

In order to match the speed and trajectory of the real car with the ones of the simulated vehicle, a way to evaluate the trajectory has to be defined.

When using an intrinsic coordinates system to define the vehicle's trajectory, the side-slip angle of the vehicle is needed (*Equation 3.10*), but it is not one of the values that can be found from the testing of the *SC22*. Nonetheless, an approximation can be done for small values of side-slip angle. In fact, the curvature radius of the vehicle's trajectory can be approximated as in the *Equation 3.11*. Therefore, if the lateral acceleration and the speed of the simulated vehicle is similar to the real ones, it can be assumed that the simulated trajectory matches the line made by the car during track testing.

$$R = \frac{V_t^2}{A_c} = \frac{V_x * \cos \beta - V_y * \sin \beta}{A_x * \sin \beta + A_y * \cos \beta} \quad (3.10)$$

$$R = \frac{V^2}{A_y} \quad (\text{Approx.}) \quad (3.11)$$

The elements of these equations are:

- R = **curvature radius** [m]
- A_c = **centripetal acceleration** [m/s^2]
- A_x = **longitudinal acceleration** [m/s^2]
- A_y = **lateral acceleration** [m/s^2]
- V_t = **vehicle's tangential speed** [m/s]

- V_x = vehicle's longitudinal speed [m/s]
- V_y = vehicle's lateral speed [m/s]
- V = vehicle's speed [m/s]
- β = vehicle's side-slip angle [deg]

By just scaling the input recorded from the real car a good correlation between real and simulated trajectory and speed can be obtained. In particular, in *Figure 3.4* it is reported the speed in [kph] and the lateral acceleration in [g] for the simulation and the real test. It can be noticed that the linear correlation coefficients reported in the titles are both over 80%; therefore, the simulation data are well correlated with the real ones.

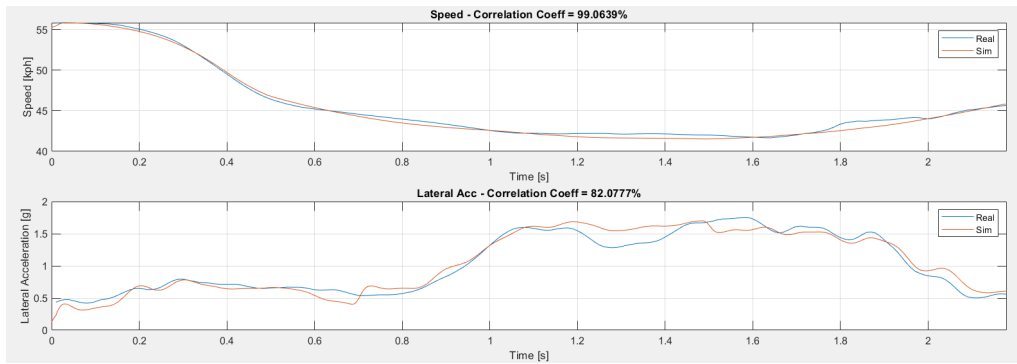


Figure 3.4: Correlation Between Simulation and Real Tests

Once the simulations have been ran for all the critical corners, the results will show up the working conditions on the four tyres.

3.3 Tyres' Working Conditions Optimisation

For the optimisation of the tyres' working conditions only the effects due to the lateral force are considered. This choice is mostly related to the fact that, in order to fully exploit the longitudinal performance of a racing vehicle, the drivers have to posses a profound knowledge of the track they are racing on, which is not usually possible to in an FSAE event where track testing is not present and the track changes from one year to the next one. Therefore, from our analyses, the drivers will always tend to not fully exploit the longitudinal forces that the tyre could develop, as they would rather optimise the execution of the corners. Ultimately, the longitudinal grip can be partially sacrificed in favour of a quantifiable increase in lateral performance of the vehicle.

The tyres' working conditions characteristics considered for this analysis are the side-slip angle and the camber angle. This is due to the fact that these two features are directly affected by the suspension kinematics. For instance, the effects related to the increase in load transfer due to higher lateral accelerations achieved through the suspension kinematics optimisation are not taken into account in this analysis.

KPI

In order to execute the optimisation procedure in a comprehensive manner, grip, balance, control and stability are evaluated on the full vehicle. These four KPIs are calculated by employing a double track model (*Figure 3.5*) and they are utilised to compare the vehicle's cornering performance before and after changing the tyres' angle above-mentioned.

The analysis of the KPIs is carried out by considering a selected number of in-

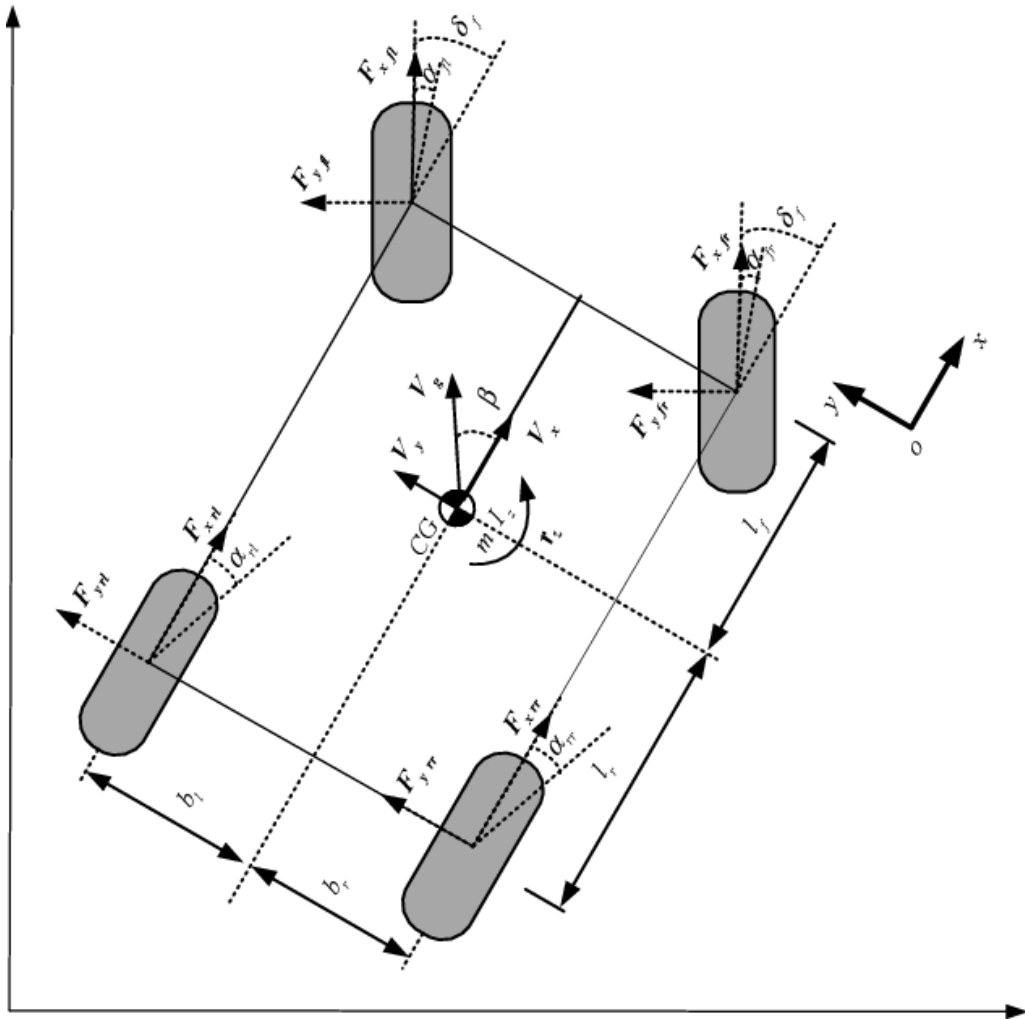


Figure 3.5: Double Track Model

stants during the critical corners. During those instances, the vehicle is assumed to be under steady state conditions.

Due to the fact that all the tyres will have certain steering angle (due to the steering and toe angle on the front tyres and just to the toe angle on the rear tyres) the lateral force in the reference frame of the tyre is decomposed into a longitudinal force ($F_{x,eq}$) and a lateral force ($F_{y,eq}$) in the reference frame of the vehicle.

For the calculation of some of these KPIs the result is computed in different ways depending on the cornering direction. This expedient enables us to simplify the simplify the sign convention at the single tyre level.

Given that quick direction changes are not present in this analysis, the difference of vertical force between one side and the other of the vehicle is used to differentiate the right corners from the left ones.

Grip

The grip of a vehicle can be defined as its ability to generate accelerations. Therefore, in order to maximise the lateral grip of the vehicle, the lateral forces produced by the tyres have to be increased.

The vehicle grip for this analysis is computed as the lateral acceleration in $[g]$:

$$Grip = \frac{F_{y,eq}^{FL} + F_{y,eq}^{FR} + F_{y,eq}^{RL} + F_{y,eq}^{RR}}{9.81 * m} \quad (3.12)$$

Where:

- $F_{y,eq}^{FL}$ = lateral force on the front left tyre on the reference frame of the vehicle
- $F_{y,eq}^{FR}$ = lateral force on the front right tyre on the reference frame of the vehicle
- $F_{y,eq}^{RL}$ = lateral force on the rear left tyre on the reference frame of the vehicle
- $F_{y,eq}^{RR}$ = lateral force on the rear right tyre on the reference frame of the vehicle
- m = total vehicle mass

Balance

The vehicle balance consists in its tendency to understeer or oversteer. In the simplest terms, a vehicle oversteers when its rear part tends to align with the vehicle trajectory. Vice-versa, it understeers when the front of the vehicle has a tendency to stay aligned with the vehicle trajectory.

In a real case scenario, a driver feels the understeer as a lack of rotation during cornering, whilst the oversteer is perceived by the driver as an excess of vehicle rotation. This rotation can be quantified by using the yaw rate that is the time derivative of the angle between the x-axis of a global reference frame (fixed to the ground) and the x-axis of the vehicle's reference frame.

A net yaw moment acting on the vehicle (moment in on the CG in top view) causes the yaw rate to change during time, hence resulting in a yaw acceleration. High and positive values of yaw acceleration translates into the tendency of the vehicle to become oversteering, whereas high and negative yaw accelerations result in a shift of the vehicle behaviour towards understeer.

As a result of the connection between yaw moment and yaw rate, the yaw moment is used as a measure of balance:

$$\begin{aligned} Balance \ (Left \ Corner) &= (F_{y,eq}^{FL} + F_{y,eq}^{FR}) * a - (F_{y,eq}^{RL} + F_{y,eq}^{RR}) * b \\ &\quad + (F_{x,eq}^{FL} - F_{x,eq}^{FR}) * t_f / 2 - (F_{x,eq}^{RL} + F_{x,eq}^{RR}) * t_r / 2 \end{aligned} \quad (3.13)$$

$$\begin{aligned} Balance \ (Left \ Corner) &= (F_{y,eq}^{FL} + F_{y,eq}^{FR}) * a - (F_{y,eq}^{RL} + F_{y,eq}^{RR}) * b \\ &\quad + (F_{x,eq}^{FR} - F_{x,eq}^{FL}) * t_f / 2 - (F_{x,eq}^{RL} + F_{x,eq}^{RR}) * t_r / 2 \end{aligned} \quad (3.14)$$

Where:

- a = longitudinal distance between the front axle contact patch and CG
- b = longitudinal distance between the rear axle contact patch and CG
- t_f = front track
- t_r = rear track

Control

The control quantifies the capacity of the vehicle to follow a steering input. Therefore, it is only influenced by the front tyres.

The control can be defined by considering the variation of yaw moment due to a small increase of steering angle. This steering angle variation is considered as an increase of side-slip angle around the chosen the working point.

As a result, the control is defined as follows:

$$\text{Control (Left Corners)} = (dF_{y,eq}^{FL} + dF_{y,eq}^{FR}) * a + (dF_{x,eq}^{FL} - dF_{x,eq}^{FR}) * t_f / 2 \quad (3.15)$$

$$\text{Control (Right Corners)} = (dF_{y,eq}^{FL} + dF_{y,eq}^{FR}) * a + (dF_{x,eq}^{FR} - dF_{x,eq}^{FL}) * t_f / 2 \quad (3.16)$$

where:

- $dF_{y,eq}^{FL}$ = variation of $F_{y,eq}^{FL}$ caused by a small change of δ
- $dF_{y,eq}^{FR}$ = variation of $F_{y,eq}^{FR}$ caused by a small change of δ
- $dF_{x,eq}^{FL}$ = variation of $F_{x,eq}^{FL}$ caused by a small change of δ
- $dF_{x,eq}^{FR}$ = variation of $F_{x,eq}^{FR}$ caused by a small change of δ

In general, high and positive values of control guarantee the vehicle to respond well to steering inputs.

Despite the fact that the value of control calculated in this way does not take into account the variation of steering angle, it is still valid if the variations just described are computed considering the same differential of side-slip angle on the front tyres independently of the working point chosen.

Stability

The stability value indicates the variation yaw moment due to an increase of side-slip angle of the vehicle.

The increase in side-slip angle translates into a variation of all the side-slip angles on the tyres in such a way that the variation of the tyres' side slip-angles equal the variation of vehicle's side-slip angle. The differential of side-slip angle causes a differential of the forces generated by the tyres. Ultimately, this force variation causes a yaw moment differential that can be used to quantify the stability of the vehicle.

$$\begin{aligned} \text{Stability (Left Corners)} &= (dF_{y,eq}^{FL} + dF_{y,eq}^{FR}) * a - (dF_{y,eq}^{RL} + dF_{y,eq}^{RR}) * b \\ &\quad + (dF_{x,eq}^{FL} - dF_{x,eq}^{FR}) * t_f / 2 - (dF_{x,eq}^{RL} + dF_{x,eq}^{RR}) * t_r / 2 \end{aligned} \quad (3.17)$$

$$\begin{aligned} \text{Stability (Right Corners)} = & (dF_{y,eq}^{FL} + dF_{y,eq}^{FR}) * a - (dF_{y,eq}^{RL} + dF_{y,eq}^{RR}) * b \\ & + (dF_{x,eq}^{FR} - dF_{x,eq}^{FL}) * t_f / 2 - (dF_{x,eq}^{RL} + dF_{x,eq}^{RR}) * t_r / 2 \end{aligned} \quad (3.18)$$

The stability is considered high when negative. A negative value of stability is beneficial due to the fact that this results into the vehicle tending to realign to its trajectory when sliding.

On the other hand, it is possible to notice that high values of control result in low values of stability. Therefore, a trade-off between the two values has to be considered.

As for the control, despite the fact that the value of stability calculated in this way does not take into account the variation of steering angle, it is still valid if the variations just described are computed considering the same differential of side-slip angle on all four tyres independently of the working point chosen.

Targets

Given that the analysis carried out in this thesis regards a racing vehicle, the main focus is to maximise the vehicle grip.

The increase of lateral acceleration causes the yaw rate to rise. An explanation of this phenomenon can be obtained by assuming that the trajectory of the vehicle does not change by increasing the grip. The vehicle trajectory can be defined (in an approximated way) as seen in *Equation 3.11*.

By considering the same approximations the heading speed of the vehicle (r_H) can be defined as follows:

$$r_H = \frac{A_y}{V} \quad (3.19)$$

The heading velocity is the angular speed of the vector " V " in the global reference frame. Considering that the vehicle side-slip angle and its variation are not massive when compared to the yaw rate, it is safe to suppose that the yaw rate changes accordingly to the heading velocity variation.

By recalling *Equation 3.11* it can be noted that also a variation in the lateral grip of the vehicle affects the vehicle speed if the trajectory remains the same.

$$\Delta A_y = A_y * m \rightarrow \Delta V = V * (\sqrt{1+m} - 1) \quad (3.20)$$

In these equations m is the percentage variation of lateral grip.

From the definition r_H (*Equation 3.19*), also the variation of r_H can be determined as function of m :

$$\Delta r_H = r_H * (\sqrt{1+m} - 1) \quad (3.21)$$

By considering small values of m , the square of the binomial can be substituted by the first term of its Taylor expansion series:

$$\Delta r_H = r_H * \frac{m}{2} \quad (3.22)$$

Over-all, the increase in grip has to be joined with a yaw rate rise. The percent of yaw rate variation is approximately half of the percent of the grip variation.

The growth of yaw rate can be associated to an equal enlargement in yaw acceleration. This is due to the fact that the variation of yaw rate is a constant multiplied to the yaw rate, thus in the time derivation of the yaw rate this constant is remains the same.

Given that the yaw acceleration is directly proportional to the yaw moment, a percentage increase of grip has to be accompanied by a rise in balance equal to half the percentage of the grip variation.

In terms of control and stability, these two KPIs do not need to be tuned unless the vehicle does not suffer from instability and lack of reactivity to the steering inputs.

By considering how the lateral force increases as function of the tyre's side-slip angle, while its derivative (cornering stiffness) falls (*Figure 3.6*). Therefore, the main constraint to be kept in mind when increasing the grip of the vehicle is to not compromise control and stability.

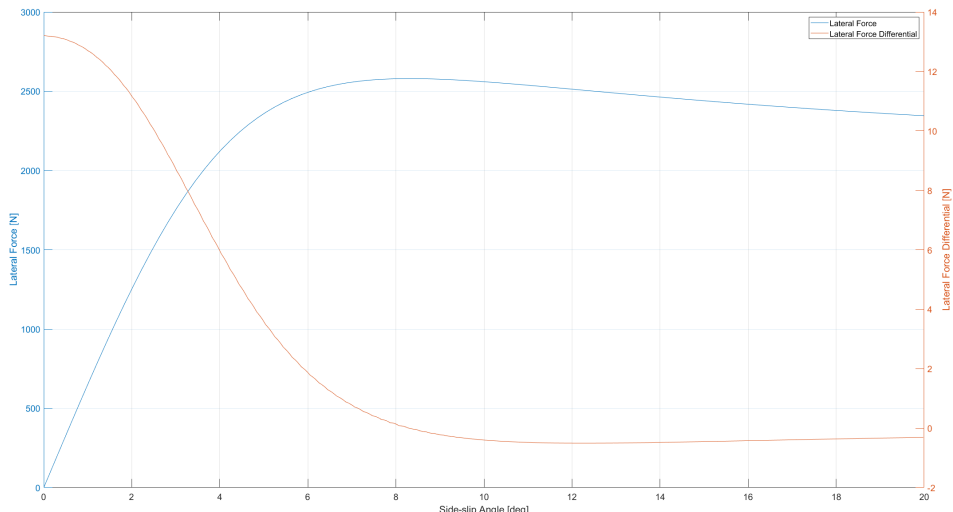


Figure 3.6: Lateral Force and Lateral Force Differential

Procedure

The optimisation of the vehicle performance through the exploitation of the tyres' lateral force is carried out by considering the effect on the KPI (grip, balance, control and stability) when changing the side-slip angle and camber angle on a single tyre.

This process is executed on a graphical interface created on Matlab (*Figure 3.7*), and enables the observation of the trends for different combinations of camber and side-slip angle, hence aiding the choice of the angles camber and side-slip angles. In

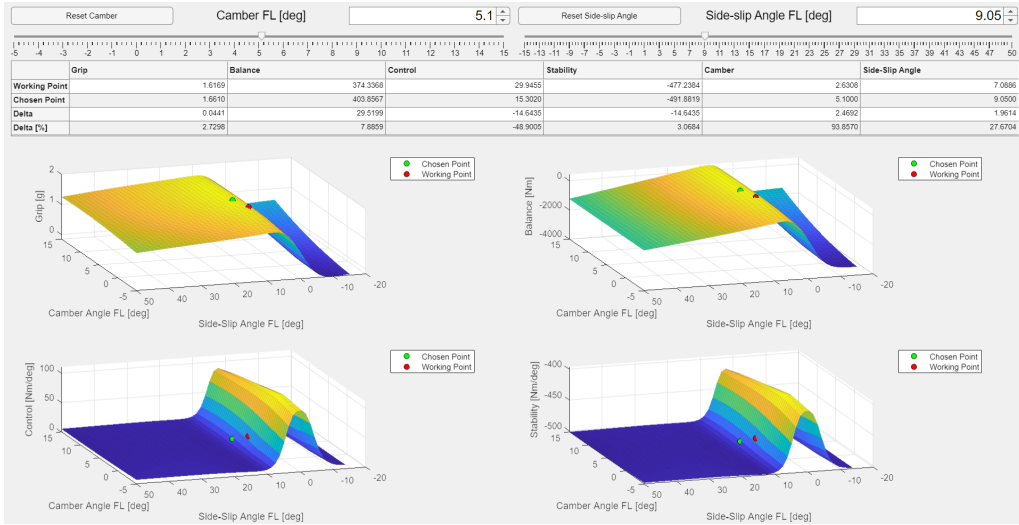


Figure 3.7: KPI Interface - Front Left Tyre

order to change the side-slip angle of a tyre, the steering angle value has to be modified. The only way to change the steering angle without changing the drive input or the steering ratio is by acting on the toe angle. The toe angle is the difference in steering angles between the two tyres of the same axle. It can either be set in static condition or a consequence of the suspension kinematics.

Due to the fact that the target side-slip is reached through the generation of a toe angle, if the side-slip is increased of certain amount on one tyre it should be reduced of the same quantity on the other tyre of the same axle. This is not necessarily true if the effect considered in the toe angle generation is mainly due to bump-steer. However, the principal effect causing the dynamic toe during cornering is the ackermann steering configuration, which provides roughly symmetrical results on the right tyre and on the left tyre.

The ackermann steering configuration is only effective in the axle of the vehicle that is endowed with steering capability, thus in the front one. Therefore, the toe angle reachable on the rear axle is mostly achieved through the static toe angle and the bump-steer characteristic of the suspension. Ultimately, this results more limited side-slip angle tuning on the front rear axle of the vehicle.

Results

The result of this process consists in the determination of the target values of toe and camber in the points chosen for the analysis.

In terms of the KPI values, their variation from values obtained in the base suspension is reported in the following table: As it is possible to notice from the table, the increase in grip does not come to a sacrifice to the stability and control of the vehicle. In particular, the control is measurably increased by following this approach.

The increase in control is a positive effect as the drivers expressed the general lack of control of the vehicle trajectory during cornering.

Grip Variation	9.23%
Balance Variation	5.17%
Control Variation	11.76%
Stability Variation	0.40%

Table 3.1: KPI Variation

Possible Improvements

It is possible to fully automate this process and to not only consider some points of each corner but the whole track.

In this specific case, the process has been carried out manually, in order to verify the feasibility of the method and to understand how to develop an effective tuning strategy.

Chapter 4

Suspensions' Lower Parts Kinematics

The lower part of the suspensions is the one that controls how much the position and the angles of the wheel change for a given quantity of vertical wheel travel variation and steering input. Therefore, given that one of the main objective of the suspensions kinematics optimisation process is to improve how the tyres interact with the ground, the optimisation of the lower suspension kinematics is quintessential for the achievement of such objective.

The *SC22* is the latest FSAE vehicle created by Squadra Corse PoliTo that completed during 2021/2022 season and it will be harnessed as a reference during the following analysis.

4.1 Components of the Lower Part of the SC22's Suspensions

The front and the rear suspensions of the vehicle under analysis both present a double wishbone scheme. That being the case, in all four suspensions there is an upper control arm (UCA) and a lower control arm (LCA).

The components that make each one of the control arms are two brackets joined in their extremities to shape a triangle. Therefore, the UCA and the LCA are called wishbones as they resemble the appearance of a wishbone that is bone present in the vast majority of birds which presents a triangular shape.

Furthermore, every suspension feature a tie-rod that is a bracket needed to control the rotational degree of freedom not locked by the two wishbones, which can be used to enable steering.

The two vertexes of each wishbone triangle attached to the chassis are defined as inner hardpoints due to the fact that they are the nearest to the centre of the vehicle; whereas the other vertex is connected to the upright and it is labelled as outer hardpoint.

The two inner hardpoints of each wishbone are then denominated as front or rear

hardpoint depending on they distance from the foremost point in the vehicle. In particular, the nearest inner hardpoint to the foremost point in the vehicle is the front one, while the other point is the rear hardpoint.

The tie-rod hardpoint can be described in a similar way of what has been done for the the UCA and the LCA. As a matter of fact, the extremity of the tie-rod which is connected to the upright is an outer hardpoint, whilst the other one is an inner hardpoint.

The inner hardpoint of the tie-rod can either be connected to the chassis or a steering rack. Whilst in the former case the wheel cannot steer, in the latter it can. Given that the *SC22* is a two wheel steering vehicle, the front tyres' tie-rods are the only one to be connected to a steering rack.

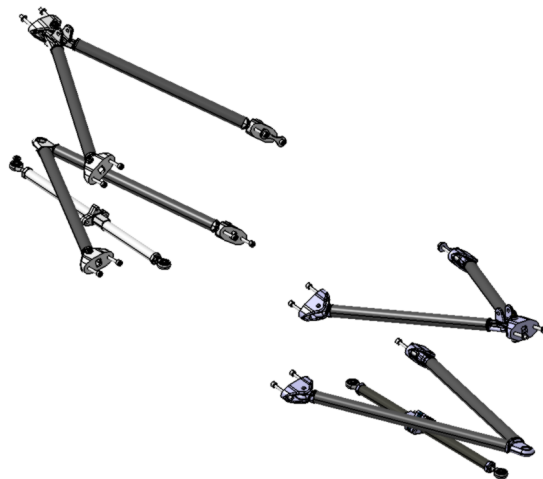


Figure 4.1: Front Suspension SC22 lower part

4.2 Hardpoints' Position Calculation Methods

There are different methods to define the location of the hardpoints in a suspension. The first way to find the right points is to manually insert the value of these points into a software that enables the designer to simulate and visualise the evolution of some specific characteristics of the suspension kinematics, such as the camber angle and the installation ratio of the damper, when changing the values of the hardpoints. This kind of software also allow to visualise the evolution of the parameters chosen by the designer as function of the vertical wheel travel or the steering angle of a suspension, hence to analyse their dynamic values.

Despite the apparent simplicity of the method, it can be extremely time demanding to adjust the kinematics of a suspension by manually tuning one point at the time. This is mostly due to the fact that by changing one hardpoint at the time a multiplicity of suspension characteristic are modified both in terms of static values and dynamic values.

On the other hand, the static position of the hardpoints of a suspension can be used to determine some specific parameters of a suspension. The combination of a subgroup of these parameters can uniquely identify a combination of hardpoints that define a suspension. This process is called suspension parameterisation and the result of it is a parametric model of the suspension.

The parametric model of a suspension takes as input some specific parameters of the suspension to be modelled and gives back the resulting hardpoints as its output. Therefore, this model enables the designer to obtain a combination of hardpoints that is the one that guarantees the characteristics requested by the designer in static conditions, hence when both the vertical wheel travel of the suspension and the steering angle of the suspension are equal to zero.

The version of the suspension that is created through the parametric model will be compliant to the designer' specifications only in static conditions (as a consequence of fact that the parametric model generates the suspension based on its static conditions). Therefore, in order to tune the dynamic characteristics of the suspension kinematics, the suspension's hardpoints gets finely tuned manually by the user. This means that the parametric model is only the starting point of the hardpoint definition process.

As it is possible to notice neither the manual nor the parametric model ought to generate the suspension hardpoints that fit all the static and dynamic characteristics required by the designer in one step, due to the fact that these methods require multiple manual iterations. That being the case, the most efficient way to generate a suspension is by employing an optimisation model. This model takes the dynamic characteristics of the suspension kinematics and through a series of iterative simulations tries to make the suspension's kinematics to the target dynamic characteristics by rearranging the hardpoints of the suspension.

There are different algorithms that can be used to implement an optimisation model. In fact, the hardpoints can be randomly changed, or some approximating functions can be used, or in other cases machine learning techniques can be actuated in order to fit some characteristics that cannot be modelled through a formula or that would be too time consuming to be randomly iterated.

4.3 Suspension Kinematics Parameters

A parametric model will be used in this chapter to generate the hardpoints' locations of the suspensions that are going to be optimised.

In order to create a suspension through a parametric model we first need to define the parameters that are taken as input from the model and explain their effects. These parameters can be divided in front view parameters, side-view parameters and top-view parameters.

Front view parameters:

- **fvs_a** = *front view swing arm*
- **RC** = *roll center*
- **KP Angle** = *kingpin inclination*
- **scrub radius**

Side view parameters:

- **svsa** = *side view swing arm*
- **anti-features**
- **caster angle**
- **caster trail**
- **PC** = *pitch centre*

Top view parameters:

- **wishbone aperture**

Furthermore, also the parameters imposed by the tie rod location have to be considered:

- **ackermann percentage**
- **bump steer**

In the following sections these parameters will be described in terms of how they are defined and what are their effects on the suspension kinematics and on the vehicle dynamics.

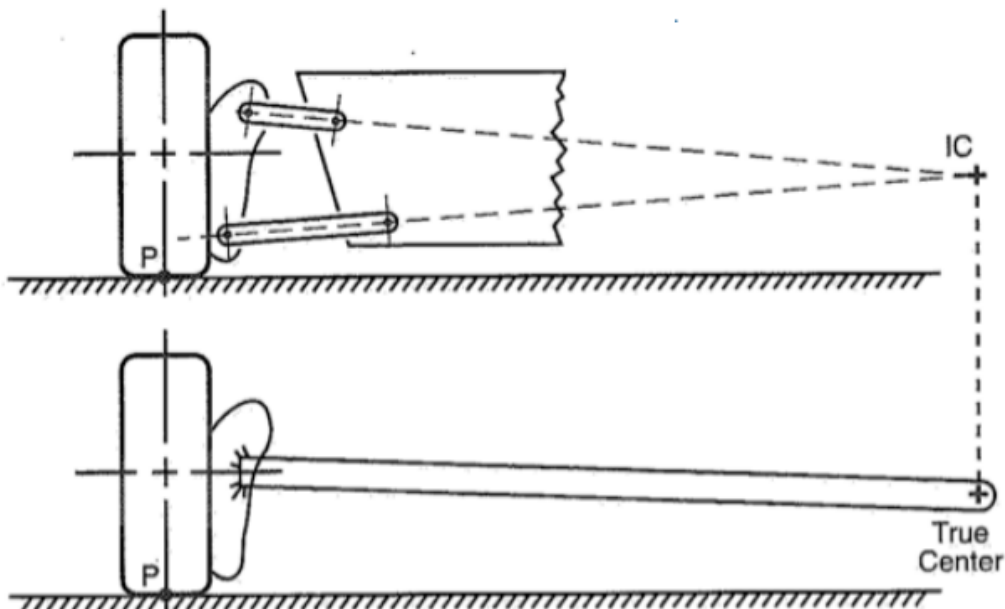


Figure 4.2: Front View Instant Centre

4.3.1 Front View Swing Arm

Front View Instant Centre Location

In a double wishbone suspension the motion of wheel hub around the chassis is dictated by the hardpoint locations of the two control arms (*reference to 4.1*). When looking at the front view of the suspension, the triangles that represent the wishbone geometry can be simplified into one rod for each wishbone. This process is executed by merging the two inner hardpoints of a wishbone, therefore creating a virtual inner hardpoint.

There are three methods for creating this hardpoint. The first method is to use the midpoint between the real inner hardpoints of the suspension. The second method is to consider the line that connects the two inner hardpoints and to take the point that has the same y-coordinate of the outer hardpoint of the wishbone that is taken in consideration during the process. Lastly, the final method to determine the line passing through the two inner hardpoints, the interception point between this line and a line perpendicular to the one just defined passing through the outer hardpoint can be used as inner hardpoint approximation.

Despite the fact that the first way of determining the virtual inner hardpoint appears more intuitive, following a validation on Adams' Car that is a software that simulate the suspension kinematics without making any kinematic approximation, the second method results to be the most accurate in determining the front view kinematics of the suspension.

On the other hand, it can be argued that Adams car consider the contact patch movement to determine the front view instant centre location. Therefore, its position can also vary by tuning the tie-rod location. This is caused by the fact that the contact parch does not coincide with the kingpin axis (axis where the two outer hardpoints lay), thus the movement of the contact patch is partially affected by the tie-rod location. Ultimately, Adams' Car is not always adapt to evaluate whether one of these methods is more adapt.

Furthermore, in all the methods above-mentioned, it should be considered that there is not really a front view instant centre of the suspension but there is an instant axis. Consequently, the front view instant centre location should be the interception of the instant axis and the z-y plane passing through the wheel centre of the axle considered. In this case, the instant axis is defined as the line passing through the side view instant centre (interception in side view of the lines that connects the inner hardpoints of the wishbones) and the interception between lines that connects the approximated control arms in front view.

For sake of simplicity, the virtual inner hardpoint is taken by using the same y-coordinate of the outer hardpoint of the wishbone considered. Lastly, the rod that approximates a wishbone corresponds with the segment that connects the outer hardpoint of a wishbone with its virtual inner hardpoint.

Once the wishbones have been approximated with two rods, it is possible to identify the front view instant centre (IC Front) of the wheel hub with respect to the chassis

as the intersection of the lines that contain the approximated rods.

The instant centre of a generic body 1 with respect to a body 2 (to which the first body is connected) is the point around which every point of body 1 only rotate (without any translation) in the reference frame of body 2 in a certain time instant. Consequently, by determining the IC Front of the wheel hub in reference to the chassis, also the wheel rotation around the chassis can be defined in a precise instant of time.

Camber Gain and Camber Recovery

The location of the the IC Front can be used to calculate the camber recovery characteristic of a suspension that is a measure of how much the camber of the tyre attached to the suspension considered changes during the roll of the vehicle, this result is in the reference frame of the chassis.

When a vehicle goes through a corner, the two suspension on the same axle are subjected to two opposite vertical forces on the wheels to compensate the moment generated by the equal and opposite lateral force on the centre of gravity and on the tyres.

As a consequence of this phenomenon (called lateral load transfer), the vehicle suspensions will be subjected to a vertical wheel travel (wrt their undisturbed position) that causes the vehicle to roll.

These wheel travels are proportional to the roll angle of the vehicle. In order to describe the camber recovery with a mathematical model, a some simplifications have to be made.

First of all, the absolute value of the suspension vertical travel is consider to be the same on the right and on the left suspension. Secondly, we will consider that all the roll is only caused by the suspension movement; therefore, the tyre deflection is neglected. This approach ultimately results in *Figure 4.3*.

The symbols reported in *Figure 4.3* are:

- $\Delta\gamma$ = camber recovered
- Δz = vertical wheel travel of the suspension
- t = track of the axle taken into consideration
- fvs = front view swing arm
- ϕ = roll angle of the chassis

By taking this approach it can be observed that:

$$\Delta z = \frac{t}{2} * \tan \phi \quad (4.1)$$

If the arc created by the tyre's contact patch during this motion is approximated with Δz , the $\Delta\gamma$ can be explained through the following relation:

$$\Delta\gamma = \frac{\Delta z}{fvs} \quad (4.2)$$

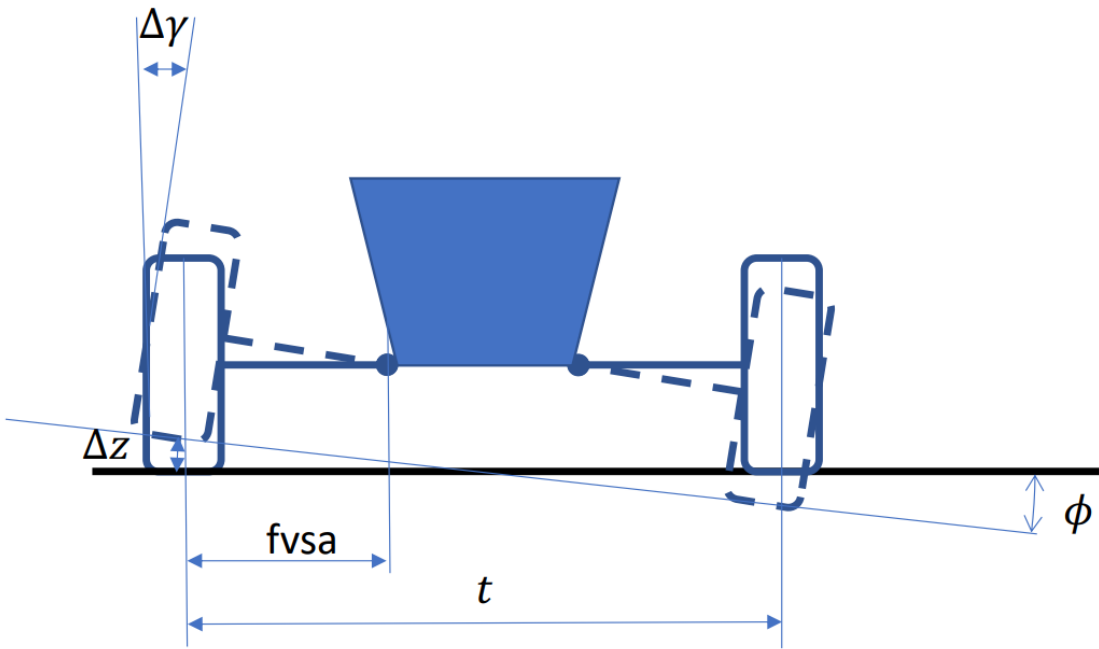


Figure 4.3: Roll and Vertical Wheel Travel Relation

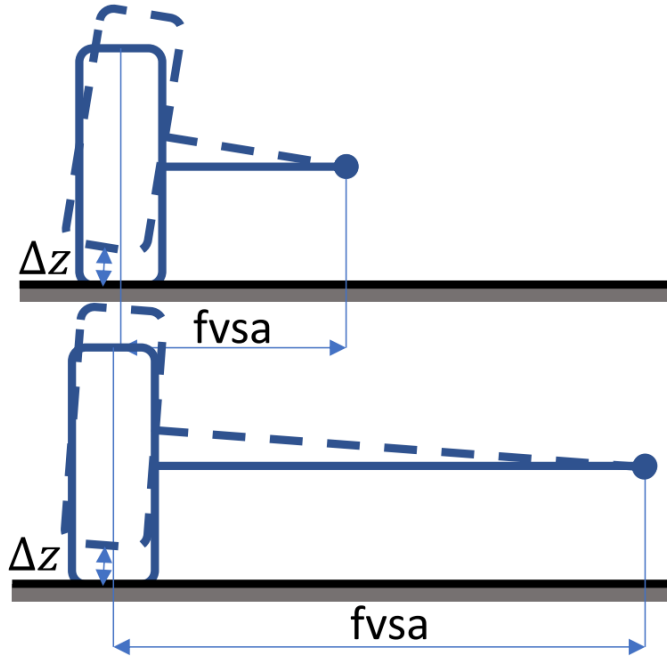


Figure 4.4: Camber Gain Sensitivity to fvsa

From the [Equation 4.2](#) it is possible to observe that, given a certain Δz , the smaller the $fvsa$ the higher the camber recovered is. Furthermore, the [Equation 4.1](#) can be applied to the [Equation 4.2](#) in order to obtain the following formula:

$$\Delta\gamma = \frac{\frac{t}{2} * \tan\phi}{fvsa} \quad (4.3)$$

To generalise the concept of camber recovered independently of the roll angle, the camber recovery has to be defined as the gain of camber due to a roll angle, hence

the ratio between the camber recovered and the roll angle that causes such camber gradient.

In order to obtain the camber recovery, another approximation has to be considered. In fact, the tangent of roll angle can always be substituted with the roll angle (in radians) itself. This is due to the fact that the roll angle is extremely unlikely to go over 7 degrees. This is especially true in racing cars like the one taken in consideration during the analysis carried out along this thesis, on which the roll angle will never go over 2 degrees under normal racing conditions.

By applying this approximation to the *Equation 4.3* the camber recovery can be described as:

$$\frac{\Delta\gamma}{\phi} = \frac{\frac{t}{2}}{fvsa} \quad (4.4)$$

The *Equation 4.4* enables us to identify two limit cases. The first one is the case where the fvsa length equals half the track width, whereas the second one is the case where the fvsa length is infinite.

In the former case, the suspension has a unitary camber recovery. Therefore, when a car goes through a corner the variation camber angle with respect to the chassis will be the same as the roll angle of the chassis. In the latter case, the camber recovery of the suspension is null. This results in the camber with respect to the chassis being constant when the vehicle is rolling.

Due to the fact that when a vehicle roll of certain angle ϕ the whole vehicle will lean more toward the outside of the corner of an angle equal to ϕ , a unitary camber recovery does not make the tyre change its camber angle with respect to the ground. On the other hand, if the camber recovery is equal to zero, the tyre will lean following the chassis during roll and this effect is not compensated.

When a tyre leans to the outside of a corner it generates a camber force that works against the lateral force generated by tyre through its side-slip angle hence reducing the cornering capabilities of the vehicle. Therefore, a unitary camber recovery compensate the negative effect of rolling on both internal and external tyres of a vehicle during cornering, in contrast to a null camber recovery that does not make up for the camber lost caused by the vehicle rolling during a corner.

In turn, a short front view swing arm is more desirable than longer one during cornering. In fact, it can be also argued that a front view swing arm that is shorter than half the track width of vehicle can be beneficial to the turning capabilities of the vehicle. Due to the fact that in such case the tyres will lean towards the inside of the corner creating camber forces enhance the cornering grip of the vehicle.

Although it might appear like a shorter front view swing arm is the obvious choice when designing the kinematics of a suspension, this choice comes with some trade-offs.

Firstly, the high values of camber angle induced by a short front view swing arm

may lead to uneven and quick tyre wear as the most loaded tyre during cornering will always be more stressed in the part of the tread that is nearer to the inside of the corner is more stressed than the other parts due to the excessive camber angle.

Secondly, the increase in camber actually decreases the amount of lateral force generated by a tyre through its side-slip angle. In fact, the net variation of lateral force developed by a tyre is given by the sum of the force gained through camber and the force lost for the same working conditions. This phenomenon leads to a reduction of lateral performance of a tyre subjected to excessive values of camber, which can be caused by the camber recovery.

Moreover, the variation of camber due to the front view swing arm is not only directly caused by the roll of the vehicle, but is a consequence of the vertical motion of the wheel. As a matter of fact, the camber gradient normalised by the vertical wheel travel is defined as camber gain, it can be calculated by manipulating the *Equation 4.2* as follows:

$$\frac{\Delta\gamma}{\Delta z} = \frac{1}{fvsa} \quad (4.5)$$

The camber gain is a paramount factor when deciding the front view swing arm length as it defines the quantity of camber generated during pitch and heave of a vehicle. In actual fact, cars with a short front view swing arm also causes non-negligible values of camber during braking, traction or as the result of the aerodynamic load acting on the vehicle as the speed increases.

Despite the camber angle has a positive effect on the lateral force generated by tyres, it negatively impacts the longitudinal grip. As a consequence, whilst a small fvsa is desirable in order to develop grip while cornering, it is not during straight line braking and traction.

Ultimately, The choice of the fvsa length is the result of a compromise between reaching the ideal camber angle needed to traverse each corner, the longitudinal capabilities of the vehicle and the tyre wear. The result of this trade-off is highly dependent on a series of factors.

First of all, whether the lap-time on the circuits where the vehicle has to compete is more sensible to the longitudinal grip or the lateral grip of the vehicle. Secondly, how the tyre reacts to the camber angle under different working conditions. For instance, some tyres are only sensible to camber when subjected to small values of side-slip angle (or vice-versa). As a consequence, higher values of camber can be detrimental for the overall vehicle performance in certain types of corners depending on the quantity of side-slip developed. Finally, the appropriate camber recovery setting for a racing car's suspension is contingent upon the specific format of the competition, which, in turn, determines the significance of tire wear within that competition.

Front View N-Line and Front IC Height

The line that connects the IC front of a suspension to the contact patch of the tyre attached to that suspension is named front view n-line.

What has been studied in the previous paragraph is the length of its projection on the ground, which has been defined as the *fvs_a*. However, also its inclination plays an important role on the kinematics of a suspension. The n-line inclination can be analysed in terms of front view instant centre height. In fact, once the loaded radius of a tyre is determined and the fvs_a length is known, the inclination of the fvs_a is only given by the front view instant centre height.

Induced Side-Slip

The height of the front view instant centre of a suspension influences the car behaviour over bumps.

As it can be observed from *Figure 4.5*, if the front view instant centre is at the level of the ground, the front view n-line is parallel to the ground. Given that the contact patch rotates around the instant centre as any other point of the wheel, the contact patch moves orthogonally to the n-line. In turn, this leads to the track width not changing by a considerable amount when the suspension movement is some order of magnitude smaller than the length of the n-line. On the other hand, in case the front view instant centre is either above or below the ground, the track width varies because of the suspension movement.

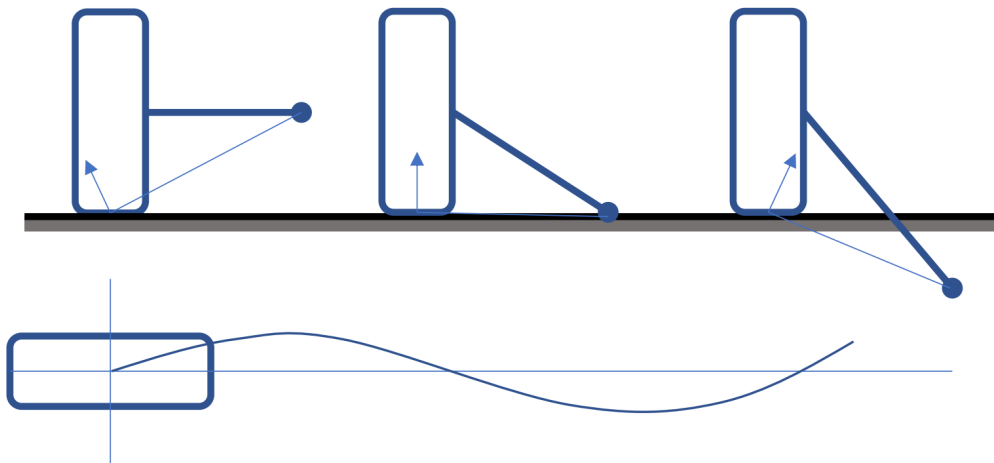


Figure 4.5: front view Instant Centre Effect

This dynamic track variation can be interpreted as a lateral speed of the tyre added to its original speed. Therefore, the instant centre height can cause side-slip angle when the suspension is subjected to quick vertical movements. Such phenomenon, can unsettle the car over bumps as the a lateral force is developed on the tyre when the steering wheel is straight.

From a mathematical point of view, the side-slip angle induced by the front view

instant centre can be quantified as follows:

$$\Delta y = \Delta z * \frac{h_{IC}}{fvsa_{Prog}} \quad (4.6)$$

$$v_y = v_z * \frac{h_{IC}}{fvsa} \quad (4.7)$$

$$\alpha = \arctan \frac{v_y}{v_x} = \arctan \frac{v_z}{v_x} * \frac{h_{IC}}{fvsa} \quad (4.8)$$

The elements of the *Equations* from 4.6 to 4.8 are:

- Δy = lateral displacement of the contact patch
- Δz = vertical displacement of the contact patch
- v_y = lateral speed of the contact patch
- v_z = vertical speed of the contact patch
- h_{IC} = front view instant centre height
- $fvsa$ = length of the front view swing arm projection to the ground, which coincides with the length of the front view n-line projection on the ground

The effect described, despite present, is not so influential to the vehicle stability because of two main reasons. First of all, it only affects a vehicle over the bumps and curbs. Sometimes, this side-slip angle can also be harnessed to aid the vehicle rotation over when hitting a curb.

Furthermore, given that the side-slip induced by the bumps is only present as long as the vertical speed of the suspension travel is not zero, it does not last for a long enough time to generate a considerable lateral force on the vehicle. In fact, a tyre, in order to generate a force, needs a certain amount of time after being put under a certain load condition.

This behaviour of tyres is quantified in terms of distance traveled before the force produced by a tyre reaches the 63% of its steady-state value. In terms of the lateral force generated by a side-slip angle, the relaxation length is non negligible when considering the distance traveled over a bump. However, the camber force presents a relaxation length that is almost zero. Therefore, the vertical force variation caused by a bump might generate a lateral camber force that may unsettle the vehicle, but this effect is more dependent on the initial suspension setup (in particular the static camber value) rather than the suspension's kinematics.

One sizeable effect of the side-slip angle caused by the front view instant centre height is linked to the tyres' temperatures. In point of fact, a tyre that slides over the tarmac, even on the straights, will get warm quickly. The negative effect of this practice is that it also induces increased tyre wear, making it favorable only when the track conditions do not permit a correct temperature of the tyres' tread.

Ultimately, the parameters of front view instant centre height and, as a consequence, the n-line inclination are not chosen in order to minimise the side-slip angle induced by uneven tarmac surface, but to obtain the roll centre position chosen by the designer. The roll centre location is one of the most important characteristics of

the kinematics of a suspension as it controls heave and the load transfer distribution between rolling and non-rolling during the roll of the vehicle. The topic in question will be thoroughly described and explained in the next section regarding the [Roll Centre](#).

Dynamic Effects on the FVSA

Being the result of the projection of two approximated wishbone, the front view instant centre changes position as the suspension moves. In terms of $fvsa$, the result of these changes can be predicted depending on the length and inclination of the approximated wishbones.

To reduce the front view swing arm as the suspension is subjected to a compression may have positive result on the overall grip generated by the vehicle. This characteristic translates in the suspension generating more camber than a case where the fvsa length is constant for the same value of vertical force applied on the wheel in addition to the static vertical force due to the vehicle weight.

The higher the vertical force the larger will be the camber differential between a configuration with a fvsa that gets shorter as the suspension compresses and another suspension where the fvsa length is constant. This is favourable in terms of performance because for most tyres higher values of camber are more effective when combined with high vertical forces.

In some extreme cases, the front view instant centre can change its location drastically by shifting to the opposite side of the wheel while the suspension is undergoing a compression. In fact, by looking to a right suspension in front view, the front view instant centre is normally located on the left side of the wheel. If when the suspension is compressed, the wishbones of the right suspension go from converging in the left side of the vehicle to becoming parallel and ultimately, converging on the right side of the wheel. Therefore, the fvsa length goes at first from positive to infinite and then it changes sign as the front view instant centre moves on the right side of the wheel.

This kind of movement would cause the camber recovery to become negative. As a consequence of the negative camber recovery, the camber recovered would be added to the one caused by the roll of the vehicle instead of being subtracted. Essentially, the camber force created by the camber recovered would work against the side-slip force of the tyre, thus reducing the cornering capabilities of the vehicle. Furthermore, the vertical and lateral of the roll centre would drastically change during heave and roll of the vehicle, leading to the car becoming drastically softer as the suspensions compresses (for reference to "roll centre" go to the section [Roll Centre](#)). This may cause the car to bottoming when going at high speeds.

One method used to reduce the fvsa length as the suspension is compressed is to create a Short Long Arm configuration (SLA). The SLA is characterised by the approximation of the upper wishbone in front view being shorter than the lower one. As a matter of fact, if we consider as an approximation that the vertical travel of the two outer hardpoints is the same, the upper wishbone has to do a larger angle

in order to cover a the vertical distance required when compared to the longer lower wishbone. As a result, the two the axis of the two wishbones will tend to converge in a nearer front view instant centre, resulting in a fvsa that gets shorter as the suspension is compressed.

In order to verify whether the inclination of the upper control arm in front view (the wishbones are also called control arms) can affect the dynamic fvsa length a simple model has been created. This model simulates the suspension movement in front view by using the approximated wishbone also employed to calculate the front view instant centre (section [Front View Instant Centre](#) for reference). The simulation is performed by imposing a vertical wheel travel of 30mm and by locking the distances in front view (the x coordinate is not considered) among the elements that do not change their locations when compared to each other.

The creation of the data set has been made in such a way that the upper control arm has a series of lengths that go from 350mm to 450mm with steps of 25mm, combined with inclinations between 5deg and 20deg in 4 steps. These combinations of lengths and inclinations of the upper wishbone are obtained by moving the outer hardpoint of the upper control arm.

The results of this analysis are displayed in [Figure 4.6](#) as the percentage variation of the front view swing arm length between the static condition of the suspension and the suspension subjected to a 30mm travel.

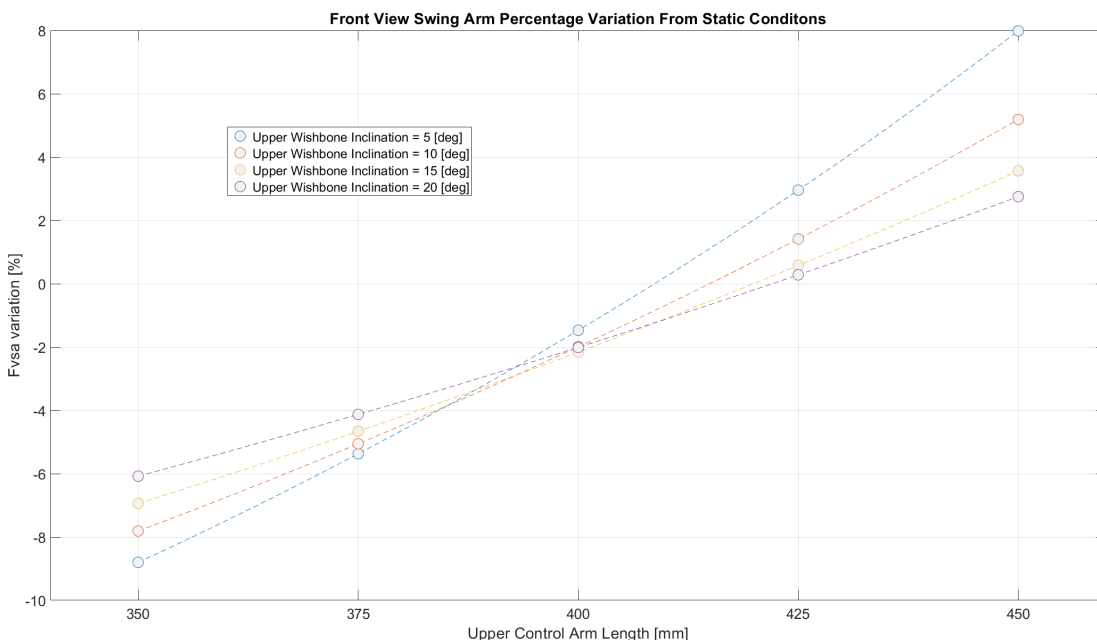


Figure 4.6: Fvsa sensitivity to upper wishbone length and inclination

From the figure above, it can be noticed that, whilst the effect of the upper control arm length corresponds to the one just described, the entity of this effect varies depending on the upper control arm inclination. In fact, its inclination reduces the effect of the upper control arm length on the *fvsa* variation. This relation can be harnessed when the packaging does not allow for an upper wishbone enough shorter

than the lower one.

4.3.2 Roll Centre

Definition and Location

The roll centres (RC) of a vehicle are points that define the axis around which a vehicle rolls. In a car there are at least two roll centres, one at the front axle and another at the rear axle (the number of RC equals the number of axles).

In order to identify the RC position in an axle, the front view of the two suspensions of the axle have to be drawn in front view. First of all, the two front view instant centre must be identified as already seen previously (in the subsection regarding *Front View Instant Centre*). Once the instant centres locations are known, it has to be considered that a vehicle rolls with respect to the ground and the only points of contact between the ground and the vehicle are the tyres' contact patches. Therefore, given that the roll of the vehicle is a result of the suspension movement generated by the chassis movement with respect to the ground, the roll centre will be located on the line that connects the front view instant centre to the contact patch of the suspension analysed (front view n-line).

Considering that there are two suspensions for each axle, the RC will be located in the interception of the two axle that connect the front view instant centre to the respective contact patch. If the vehicle is in static conditions, the suspension will be symmetric (at least this is the case in a formula SAE vehicle), thus the static location of the RC is on the mid-plane of the vehicle. As a consequence, the RC position is on the interception between the front view n-line and the mid-plane of the vehicle.

From this brief description it is possible to understand that an high roll centre is indicative of high levels of n-line inclinations and of a vertical position of the front view instant centre that is located at an higher point than what a low RC permits for the same f_{vsa} .

Lateral Load Transfer

The RC location influences how a vehicle reacts to a lateral load transfer. Therefore, in order to understand how the RC works, the phenomenon of lateral load transfer will be briefly explained in this section. For the sake of convenience, in the forthcoming pages, the lateral load transfer phenomenon will be analysed under steady state cornering conditions.

When a vehicle traverses a corner it generates a lateral acceleration. This acceleration leads to an inertial lateral force which is proportional to the lateral acceleration and to the mass of the vehicle. This force is applied to the centre of gravity of the vehicle and it is compensated by a real force generated by the tyres.

Given that all the elements of the vehicle are located above the ground, the centre of gravity will never be at the height of the contact patches, where the tyres' forces are applied. Therefore, whilst the lateral force generated by the tyres is applied at

the ground, the inertial force is not. In turn, this leads to a rolling moment.

The rolling moment has to be counterbalanced by opposing vertical forces acting on the tyres of the vehicle. These forces are called lateral load transfer. They are characterised by the fact that their resultant is null and their value on the right side of the vehicle is equal and opposite to their value on the left side of the vehicle .

In the *Figure 4.7* it is possible to recognise the inertial lateral force (F_y), the lateral force generated by the tyres (F_{yt}) and the load transfer (as the sum of $\Delta F_{z,r}$ and $\Delta F_{z,nr}$ that will be referred as ΔF_z from now on).

Given that ΔF_z is obtained from a equilibrium of moments (in particular it can be obtained from the equilibrium of moments around the left contact patch in *Equation 4.9*), the resultant of the forces acting on a tyre ($F_y/2$ and ΔF_z) is directed in the CG.

$$F_y * h = \Delta F_z * t \quad (4.9)$$

In *Equation 4.9* the term "h" is the height of CG from the ground.

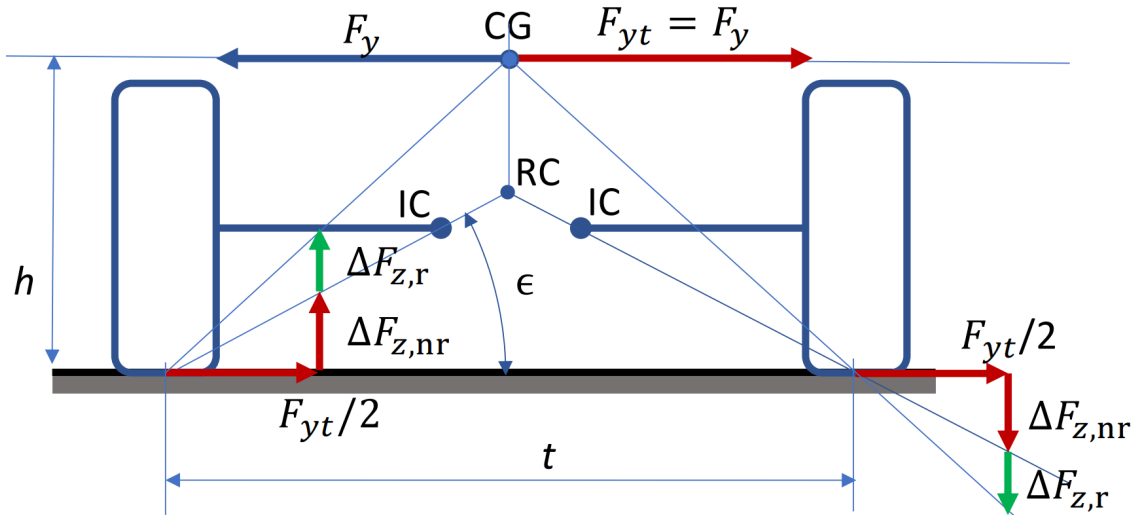


Figure 4.7: Roll Centre Height

Rolling and Non-Rolling Load Transfer Distribution

In order to understand how the vehicle reacts differently during cornering depending on the RC location, we need to take in consideration a simplified suspension in front view, which is depicted in the *Figure 4.8*. This suspension is only made by a rigid tyre attached to the chassis with a beam, thus the front view instant centre coincide with the linkage between the beam and the chassis.

If a lateral force $F_{y,t}$ (F_y in the picture) is applied to the tyre's contact patch, the wheel and beam assembly would rotate around the front view instant centre (IC). In case the tyre is kept in place by a lateral load transfer (which is plausible given the direction of the lateral force in the picture above) it means that a part of ΔF_z compensates the moment generated around the IC by $F_{y,t}$.

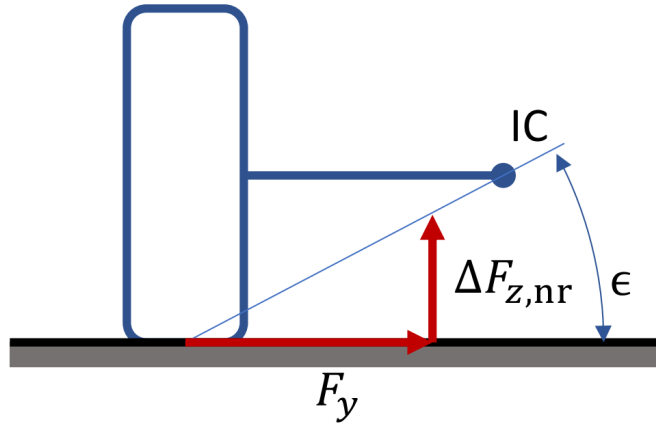


Figure 4.8: Simplified Model of the Front View of a Suspension

This part of ΔF_z is defined as non rolling load transfer ($\Delta F_{z,nr}$), because when it acts on the vehicle there will be no suspension movement. In fact, if on a suspension the only forces applied are a lateral force $F_{y,t}$ and a vertical force equal to $\Delta F_{z,nr}$ the suspension would not deflect from a kinematic point of view (its displacement would only be caused by the compliance of the system).

Given that the system analysed to study the $\Delta F_{z,nr}$ does not present any coil over damper assembly, the forces acting on the tyre are transmitted to the chassis by the wheel, the upright and the beam that connects the upright to the IC.

This phenomenon also happens in a real suspension. In fact, the load transfer is partially transmitted to chassis by the compliant elements of the suspension (shock absorber and spring) and partially by the rigid elements of the suspension.

The non rolling load transfer (also called geometric load transfer) can ultimately be determined by considering the equilibrium of moments around the front view instant centre of the vehicle as reported in *Equation 4.10*.

$$F_{y,t} * \text{nlinefwlength} * \sin \epsilon = \Delta F_{z,nr} * \text{nlinefwlength} * \cos \epsilon \quad (4.10)$$

The variables of this equation are taken from *Figure 4.8* and they can be described as follows:

- $F_{y,t}$ = lateral force applied to the tyre's contact patch
- nlinefwlength = length of the front view n-line (that connects the front view instant centre to the contact patch)
- ϵ = front view n-line inclination

By manipulating *Equation 4.10* we can obtain an analytical definition of the geometric load transfer:

$$\Delta F_{z,nr} = F_{y,t} * \tan \epsilon \quad (4.11)$$

Given that the front view n-line passes through the RC, $\Delta F_{z,nr}$ can also be seen as function of the height from the ground of RC (h_{RC}) and the track (t). Given

that the tangent of ϵ would be equal to the ratio between h_{RC} and t , $\Delta F_{z,nr}$ can be defined as:

$$\Delta F_{z,nr} = \frac{F_{y,t} * h_{RC}}{\frac{t}{2}} \quad (4.12)$$

Because of the fact that in this simplified representation the lateral force on the single tyre ($F_{y,t}$) is considered as half of the total lateral force acting on CG (F_y), the previous equation can be rewritten as follows:

$$\Delta F_{z,nr} = \frac{F_y * h_{RC}}{t} \quad (4.13)$$

From this definition of the non-rolling load transfer (*Equation 4.11*) and from *Figure 4.8* it is possible to notice that the resultant of the lateral force and the non rolling load transfer will always be aligned with the front view n-line.

This is due to the fact that the equilibrium of moments is considered in order to determine $\Delta F_{z,nr}$ and that the two forces in the system in *Figure 4.8* (that are F_y and $\Delta F_{z,nr}$) are applied to the contact patch, thus the resultant of these forces is directed on the line that connects the contact patch to the front view instant centre, that is the front view n-line . As a consequence, such resultant passes through the front view instant centre and from the roll centre not generating a moment around them.

In a real case scenario, when a vehicle traverses a corner the inertial lateral forces acts on the CG.

Unless the RC and the CG are not coincident, the inertial lateral force generates also a component of the load transfer that contributes to the vehicle roll, that is called rolling load transfer ($\Delta F_{z,r}$).

The component $\Delta F_{z,r}$ of ΔF_z can be obtained from the difference between ΔF_z and $\Delta F_{z,nr}$. This relation is reported in *Equation 4.14* :

$$\Delta F_{z,r} = \Delta F_z - \Delta F_{z,nr} = \frac{F_y * (h - h_{RC})}{t} \quad (4.14)$$

It is possible to observe from *Equation 4.14* that the rolling component is dependent on the difference between the height of the RC and the CG from the ground. This is due to the fact that the total load transfer is obtained through the equilibrium of moments around the CG, whereas the non rolling load transfer is calculated either considering the equilibrium of moments around the front view instant centre or the roll centre.

The resultant of F_y and ΔF_z does not pass through RC, but points towards CG. As a consequence, we can define an equivalent system of forces where F_y is applied on RC and a transport moment M_r is added to the system:

$$M_r = F_y * (h - h_{RC}) \quad (4.15)$$

M_r is the rolling moment (acting on the axle considered). Due to the fact that this moment makes the chassis to rotate around the RC it is not unloaded on the elements that define the geometry of the suspension. Therefore, M_r acts on the shock

absorber of the suspension. Given that the shock absorbers are compliant elements, their deformation will cause a movement of the vehicle around the RC, causing the roll of the body of the vehicle.

By considering the definitions of M_r (*Equation 4.15*) and $\Delta F_{z,r}$ (*Equation 4.14*), it is possible to notice that the two quantities are linked (*Equation 4.16*). Therefore, $\Delta F_{z,r}$ is the component of ΔF_z sustained by the shock absorber.

$$\Delta F_{z,r} = \frac{M_r}{t} \quad (4.16)$$

Based on the vertical distance from the ground of the RC and the CG, three cases that can be distinguished:

- CG higher than RC
- CG lower than RC
- CG and RC on the same height

Starting from the first case, when CG is higher than RC, ΔF_z exceeds $\Delta F_{z,nr}$. Therefore, this leads to $\Delta F_{z,r}$ to be in the same direction of $\Delta F_{z,nr}$, thus M_r rolls the vehicle in such a way that it leans on the outside of the corner. This situation is pictured in *Figure 4.7*.

If CG is lower than RC, ΔF_z is inferior than $\Delta F_{z,nr}$. Subsequently, $\Delta F_{z,r}$ acts in the opposite direction of $\Delta F_{z,nr}$. Ultimately, this leads to M_r rolling the vehicle in such a way that it leans toward the inside of the corner.

Lastly, if CG and RC are on the same height, ΔF_z and $\Delta F_{z,nr}$ will coincide. Therefore, both $\Delta F_{z,r}$ and M_r are null and the only roll of the vehicle will be due to the deflection of the tyres.

The height of the RC in the front axle and in the rear axle of a vehicle influences the load transfer distribution between front and rear, ultimately affecting the vehicle behaviour during cornering.

As a matter of fact, the load transfer has a negative net effect on the grip. This is due to the fact that the friction coefficient of the tyres decreases as the vertical force increases. Therefore, despite higher vertical forces on a tyre enable larger lateral forces, the lateral force capability that is lost in the less loaded tyre of an axle is not recovered in the more loaded tyre of the same axle (*Figure 4.9*). As a consequence, to redistribute the load transfer between the front and the rear axle can make one axle loose more grip than the other. This phenomenon can be used as a way to tune the balance of the vehicle (from understeer to oversteer and vice-versa).

In order to quantify the front and rear lateral load transfer, we need to consider the side view of a vehicle, where:

- RC_f = front roll centre
- RC_r = rear roll centre
- h_{RC_f} = front roll centre height [m]
- h_{RC_r} = rear roll centre height [m]

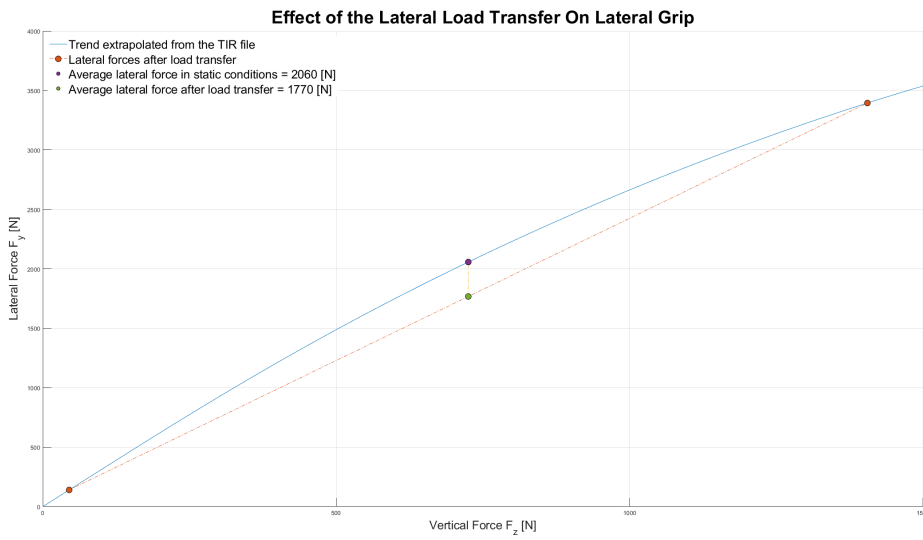


Figure 4.9: Lateral force potential of a tyre during cornering with 2g of lateral acceleration

- d = distance between CG and roll axis (can be substituted to $h - h_{RC}$ in [Equation 4.14](#)) [m]
- F_y = lateral force [N]
- $F_{y,f}$ = front lateral force [N]
- $F_{y,r}$ = rear lateral force [N]
- M_r = rolling moment [Nm]
- $M_{r,f}$ = front rolling moment [Nm]
- $M_{r,r}$ = rear rolling moment [Nm]
- a = longitudinal distance between CG and the front axle's contact patch [m]
- b = longitudinal distance between CG and the rear axle's contact patch [m]
- ϕ = roll angle (not considering the deflection of the tyres) [deg]
- ϕ_f = front roll angle (not considering the deflection of the tyres) [deg]
- ϕ_r = rear roll angle (not considering the deflection of the tyres) [deg]
- $K_{r,f}$ = front suspension roll stiffness [Nm/deg]
- $K_{r,r}$ = rear suspension roll stiffness [Nm/deg]
- t_f = front track [m]
- t_r = rear track [m]
- l = wheelbase [m]
- roll axis = has to be defined as the line that connects RC_f and RC_r .

First of all, F_y can be transported to the roll axis and the transport moment M_r can be defined as:

$$M_r = F_y * d \quad (4.17)$$

Given that M_r is the moment that makes the vehicle body to roll, its distribution between front and rear axle can be calculated considering the two roll stiffness

mentioned above. As a matter of fact, if the chassis is considered completely rigid (infinite roll stiffness of the chassis), $M_{r,f/r}$ are proportional to $K_{r,f/r}$ because in that case the roll angle will be identical on the front axle and on the rear one (*Equations 4.18 and 4.19*).

$$M_{r,f} = K_{r,f} * \phi_f = K_{r,f} * \phi \quad (4.18)$$

$$M_{r,r} = K_{r,r} * \phi_r = K_{r,r} * \phi \quad (4.19)$$

$$M_r = M_{r,f} + M_{r,r} \quad (4.20)$$

Accordingly to *Equation 4.18* to *4.20* the M_r distribution can be described as follows:

$$M_{r,f} = M_r * \frac{K_{r,f}}{K_{r,f} + K_{r,r}} \quad (4.21)$$

$$M_{r,r} = M_r * \frac{K_{r,r}}{K_{r,f} + K_{r,r}} \quad (4.22)$$

Starting from $M_{r,f}$ and $M_{r,r}$, the rolling component of load transfer on the front and on the rear axle of the vehicle can be calculated:

$$\Delta F_{z,r,f} = \frac{M_{r,f}}{t_f} = \frac{M_r}{t_f} * \frac{K_{r,f}}{K_{r,f} + K_{r,r}} = \frac{F_y * d}{t_f} * \frac{K_{r,f}}{K_{r,f} + K_{r,r}} \quad (4.23)$$

$$\Delta F_{z,r,r} = \frac{M_{r,r}}{t_r} = \frac{M_r}{t_r} * \frac{K_{r,r}}{K_{r,f} + K_{r,r}} = \frac{F_y * d}{t_r} * \frac{K_{r,r}}{K_{r,f} + K_{r,r}} \quad (4.24)$$

For the purpose to calculate the front and rear values of the non rolling lateral load transfer, the vehicle will be considered as a supported isostatic beam with a force acting on it that corresponds to the F_y . This approximation is only valid if the angular velocity of the vehicle is not changing (steady-state condition), otherwise also the effect of the inertial forces has to be considered. In the context of this approximation we can obtain:

$$F_{y,f} = F_y * \frac{b}{l} \quad (4.25)$$

$$F_{y,r} = F_y * \frac{a}{l} \quad (4.26)$$

Taking under consideration that F_y is applied to roll axis, we can consider $F_{y,f}$ applied to RC_f and $F_{y,r}$ acting on RC_r . Consequently, the non rolling load transfer can be defined as follows:

$$\Delta F_{z,nr,f} = F_{y,f} * \frac{h_{RC_f}}{t_f} \quad (4.27)$$

$$\Delta F_{z,nr,r} = F_{y,r} * \frac{h_{RC_r}}{t_r} \quad (4.28)$$

To sum up, the total lateral load transfer at the font and at the rear axle is dependent on the height of the roll centres of the vehicle along with the roll stiffness distribution:

$$\Delta F_{z,f} = \Delta F_{z,r,f} + \Delta F_{z,nr,f} \quad (4.29)$$

$$\Delta F_{z,r} = \Delta F_{z,r,r} + \Delta F_{z,nr,r} \quad (4.30)$$

Until now, F_y has not been explicitly defined. It has been implied that F_y is the product of the mass of the vehicle and the lateral acceleration endured during the

steady state cornering manoeuvre considered.

In order to understand how to more accurately define the rolling and non-rolling components of the load transfer, a more comprehensive analysis of the causes of the phenomenon is needed.

For this purpose, the difference between unsprung mass and sprung (or suspended) mass has to be explained.

The unsprung mass is made by the elements that are moving that follow the tarmac profile if the tyre is considered completely rigid and it never loses contact with the ground. As a consequence, The components that are part of the unsprung mass are those that move vertically all together with the upright while the vehicle (they are part of) is moving. For instance, parts such as the wheel and the upright of a vehicle will always be part of the unsprung mass. In turn, if there are four wheels on the vehicle there will also be four unsprung masses in its sides.

The suspended mass is the sum of all the components that are not contained in the unsprung mass. Due to the fact that the suspended mass components are connected to the sprung mass by means of the suspension, their vertical motion is filtered by the spring, the damper and the torsion bar (if present) that are the compliant elements of the suspension.

There are some elements that cannot be classified neither as unsprung mass nor as sprung mass. A prime example of these components are the control arms of the suspension. In fact, they are connected to the unsprung mass in their outer hard-points, whilst being connected to the chassis, which is part of the suspended mass.

Each one of the components that do not clearly belong to one of the two masses above-mentioned are modelled as two distinct elements, one of them belonging to the unsprung mass and the other one to the sprung mass. These elements can be modelled in such a way that the total mass, the centre of gravity location and the moment of inertia of the couple of masses is equal to the ones of the considered component (an additional moment of inertia is needed for the equation). However, for sake of simplicity, generally two thirds of the mass of these elements is considered part of the unsprung mass and the remaining third is part of the suspended mass. As a matter of fact, the total load transfer is the result of three distinct elements obtained by decoupling the unsprung mass and the suspended mass contributions:

- Unsprung mass load transfer
- Suspended mass geometric load transfer
- Suspended mass elastic load transfer

The unsprung mass load transfer can be defined by considering the equilibrium of moments between the lateral force on the two unsprung masses on one axle and the

load transfer needed to balance them (*Equations 4.31* and *4.32*).

$$\Delta F_{z,u,f} = \frac{m_{u,f} * a_y * h_{u,f}}{t_f} \quad (4.31)$$

$$\Delta F_{z,u,r} = \frac{m_{u,r} * a_y * h_{u,r}}{t_r} \quad (4.32)$$

Where:

- $\Delta F_{z,u,f}$ = unsprung mass load transfer on the front axle [N]
- $\Delta F_{z,u,r}$ = unsprung mass load transfer on the rear axle [N]
- $m_{u,f}$ = front unsprung mass [kg]
- $m_{u,r}$ = rear unsprung mass [kg]
- $h_{u,f}$ = front unsprung mass centre of gravity [m]
- $h_{u,r}$ = rear unsprung mass centre of gravity [m]
- a_y = lateral acceleration [m/s²]

The unsprung mass load transfer is not divided in rolling and non rolling components because the unsprung mass is not sustained by the suspension system.

The suspended mass geometric load transfer corresponds to the non rolling component of the load transfer defined above. It is described as "geometric" due to the fact that the roll centre location, which defines the amount of the geometric load transfer, is dependent on the suspension geometry.

From an analytical point of view, the suspended mass geometric load transfer can be defined by considering " F_y " in the *Equations 4.23* and *4.24* as only caused by the suspended mass (m_s).

$$\Delta F_{z,r,f} = \frac{m_s * a_y * d}{t_f} * \frac{K_{r,f}}{K_{r,f} + K_{r,r}} \quad (4.33)$$

$$\Delta F_{z,r,r} = \frac{m_s * a_y * d}{t_r} * \frac{K_{r,r}}{K_{r,f} + K_{r,r}} \quad (4.34)$$

In a similar fashion, the suspended mass elastic load transfer corresponds to the rolling component of the load transfer defined above. It is delineated as "elastic" due to the fact that the force is unloaded through the compliant components of the suspension.

From an analytical point of view, the suspended mass geometric load transfer can be defined by considering " F_y " in the *Equations 4.27* and *4.28* as only caused by the suspended mass.

$$\Delta F_{z,nr,f} = m_s * a_y * \frac{b}{l} * \frac{h_{RC_f}}{t_f} \quad (4.35)$$

$$\Delta F_{z,nr,r} = m_s * a_y * \frac{a}{l} * \frac{h_{RC_r}}{t_r} \quad (4.36)$$

The total load transfer on each axle can be obtained by summing the rolling, non rolling and unsprung mass load transfer.

The crucial point of this analysis regards the fact that the roll centre height affects how the load transfer is unloaded through the suspension components. As a matter of facts, higher RC locations will result in higher components of non rolling load transfer, as $\Delta F_{z,r,f}$ and $\Delta F_{z,r,r}$ are proportional to h_{RC_f} and h_{RC_r} (*Equations 4.35* and *4.36*), and lower values of rolling load transfer, because 'd' in $\Delta F_{z,nr,f}$ and $\Delta F_{z,nr,r}$ is dependent on the height of the front and of the rear RC (*Equations 4.27* and *4.28*).

Transient Load Transfer Components

Even though a shift in load transfer between the rolling and non rolling components of the suspended mass load transfer has no significant effects in terms of vehicle behaviour in a steady state cornering manoeuvre, it definitely affects the transient behaviour of the vehicle. In order to demonstrate qualitatively this effect, a simple suspended mass model with a spring and a damper has been tuned in order to take into account the components of load transfer during a more realistic corner manoeuvre (*Figure 4.10*).

The left end side of *Figure 4.10* illustrates the the main three components of load

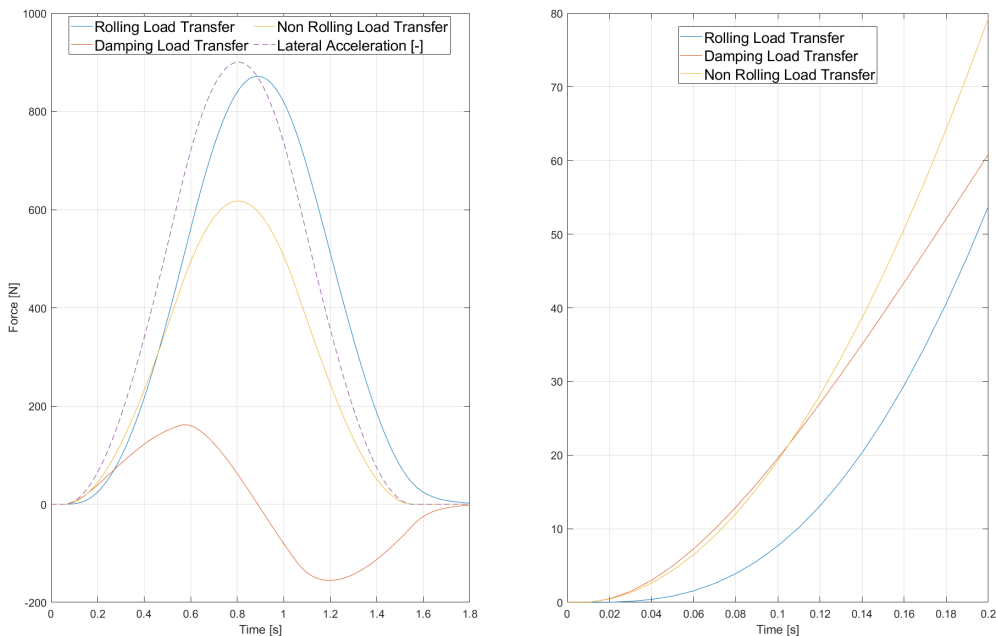


Figure 4.10: Lateral Load Transfer Components in Non Steady State Cornering

transfer during the whole manoeuvre, while on the left hand side the first two tenths of a second of the cornering are reported.

It can be noticed that, whilst on the complete corner the rolling components of the load transfer has the highest effect on the total load transfer, during corner entry the non rolling component and the damping component of the load transfer have the greatest effect.

This result is related to the fact that the forces in the non rolling load transfer are transmitted through the non compliant elements of the suspension. In fact,

being the control arms much more rigid than the spring, the force grows without needing a large movement of the suspended mass. In turn, this leads to a lower delay in the non rolling load transfer (when compared to the rolling one) due to the smaller effect of the inertia on the rigid elements.

In practical terms, the roll centre height has the largest effect on distributing the load transfer between front and rear axle during corner entry.

Dynamic RC Height

Overall, the load transfer distribution between the front and rear axle is influenced by the difference in height of the front and rear roll centres (thus by the roll axis inclination in side view) and this effect is more evident in corner entry.

Given that one of the target of the suspensions kinematic design is to provide vehicle reactivity in slow corners and limit instability in fast corners and considering, for instance, that the rear roll centre is always in an higher location than the front one, the vertical distance between the two should be larger in slow corner than what it is in fast corners.

A variation in relative RC height guarantees more lateral load transfer at the rear axle during low speed cornering and less at the front, whilst enabling less load transfer at the rear and more at the front during high speed turning. As a consequence, the car will be more oversteering in the slow speed sections, and so more reactive, but it will understeer more in the high speed parts, thus being more stable in these sections.

As a result of the dynamic variation of vertical wheel travel in high speed and low speed corners due to the aerodynamic load on the formula car analysed, the suspension kinematics can be tuned in order to achieve the vertical movement of RC described above.

Roll Centre Height Limit Cases

It can be demonstrated that, if the roll centre is under the ground, the sign of the non rolling load transfer will be the inverted. Therefore, during the corner entry, the total load transfer can either be lowered by this phenomenon or it can be reversed (depending on the entity of the negative non rolling load transfer). Ultimately, the total load transfer will not be dependent on the roll centre height during mind corner, but just on the track, the weight distribution, the height of the centre of gravity and the lateral acceleration.

It can be argued that a reversed load transfer in the first phase of the cornering operation can provide an higher yaw rate than what would be obtainable an higher location of the roll centre. In fact, by analysing the double track model in *Figure 4.11*, it is possible to notice that the yaw moment generated by the internal tyre is larger than the one generated by the external one if the lateral force on both tyres is the same. Therefore, in order to maximise the yaw rate during corner entry, the lateral force on the internal tyre has to be increased as much as possible. This can be achieved by increasing the vertical load on the internal tyre, which can be done by

inverting the lateral load transfer. Although to model the suspension kinematics in

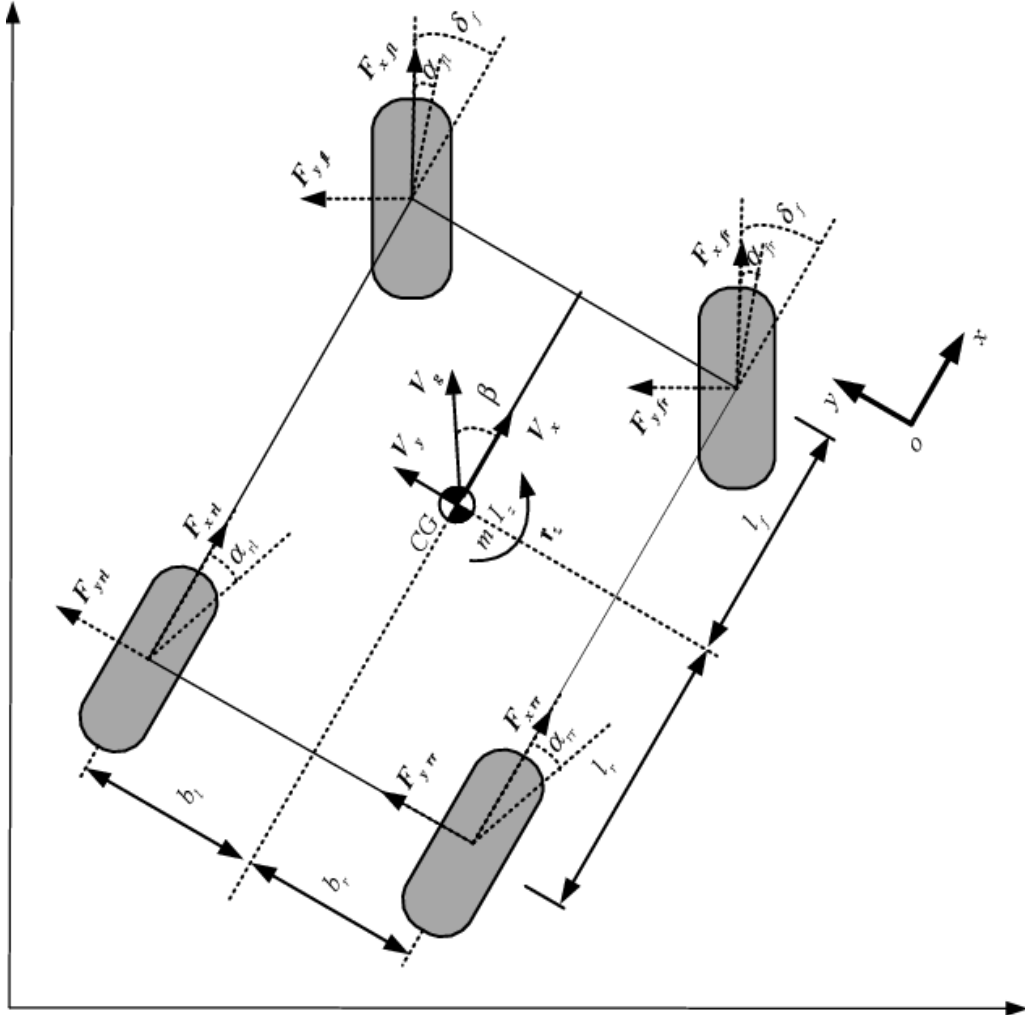


Figure 4.11: Double Track Model of a Vehicle

such a way to obtain a RC location that is under the ground might seem beneficial, this solution has two major drawbacks which make it practically never applied in modern vehicles.

First and foremost, the more the roll centres get distant from the ground the higher the inertia of the vehicle around the roll axis will increase. As a consequence of this increase in inertia, the car becomes less reactive to the drivers input during cornering.

Secondly, a decrease of the non rolling load transfer results in the increase of the rolling load transfer, given that the total load transfer during mid corner is not dependent height of the roll centre. Therefore, the compliant elements of the suspension will need to endure higher forces, being either more stressed, thus thicker, hence heavier.

On the other hand, higher magnitude of non rolling load transfer result into higher forces unloaded through the rigid elements of the suspension, making them more stressed (the magnitude of the forces on the control arms are not dependent on whether RC is locate under the ground or above it, but only on the vertical

distance between the ground and RC). However, in most cases these components are dimensioned under braking conditions, which is much more critical in terms of loads acting on those elements.

Another method that might be taken when choosing the RC location is to make the roll axis to pass through the centre of gravity. This approach would lead to the lateral load transfer to be completely unloaded on the rigid elements of the suspensions, without loading the compliant ones during pure cornering manoeuvres. Therefore, the load transfer distribution cannot be tuned by acting on the springs, torsion bars and dampers. For this reason, the roll axis will always be under the roll centre.

Generally, to use extremely high or extremely low values of RC height is detrimental either for the vehicle performance or for its setup range.

Jacking Forces and Dynamic RC Lateral Position

Another crucial point in the suspensions kinematics design is the lateral movement of the roll centre due to rolling during a cornering manoeuvre.

In order to analyse this kinematic characteristic, the front view of a vehicle is considered as shown in *Figure 4.12*.

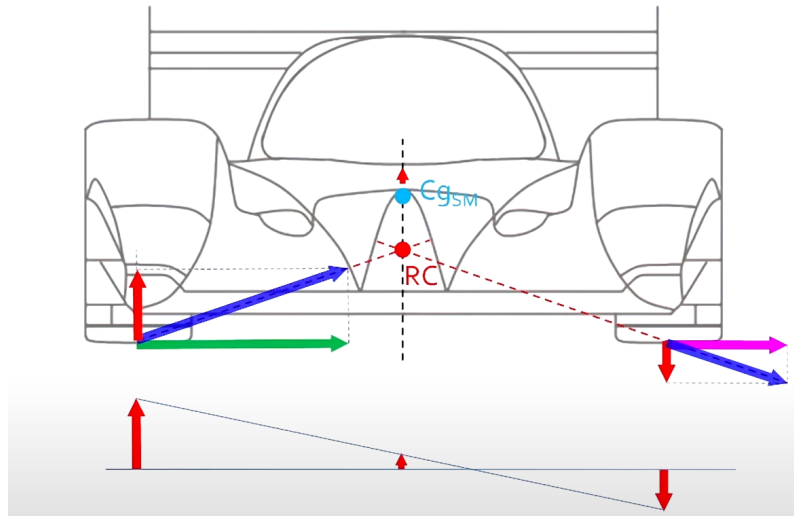


Figure 4.12: Front View of a Vehicle Featuring a Centred Roll Centre

During cornering, the lateral load transfer will result in the external tyre being more loaded than the internal one. Therefore, also the lateral force on the external tyre will be greater than the ones developed on the internal tyre, leading to larger values of the non rolling load transfer on the external tyre. As a consequence, the net effect of the non rolling load transfer does not just consist in a torque, but also in a force. The vertical component of this resultant force will act on the RC jacking up the car, hence, it is named "jacking force".

If instead of considering the RC position on the mid-plane of the vehicle it is moved towards the inside of the corner (*Figure 4.13*), the jacking force can be reduced or even inverted. This condition results in the vehicle getting closer to the ground while rolling. In turn, the vehicle can generate larger aerodynamic forces and will be subjected to less load transfer overall (because also the centre of gravity gets closer to the ground). Ultimately, the movement of the RC toward the inside of the corner is a positive effect.

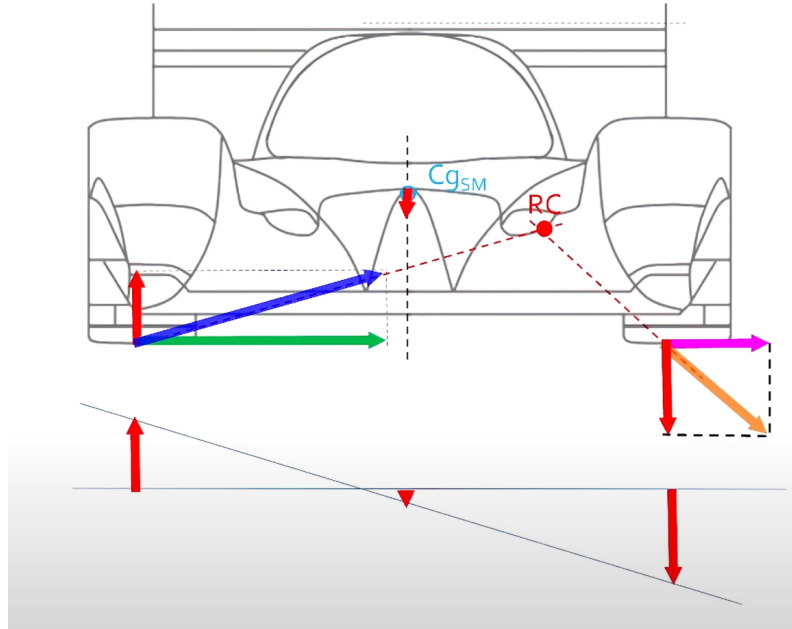


Figure 4.13: Front View of a Vehicle Featuring a Roll Centre Moved Towards the Internal Side of the Corner

On the other hand, if the RC is moved toward the outside of the corner (*Figure 4.14*), the jacking force will increase. Subsequently, the centre of gravity will become higher, causing larger values of load transfer, and the aerodynamic load developed by the vehicle is likely to decrease.

Effect of RC Height on the Tyres

Lastly, the vertical position of the RC also affects the vertical location of the front view instant centre. It can be regarded as certain that the higher h_{CR_f} the larger h_{IC} .

From the *Equation 4.6*, it is possible to observe that when the front view instant centre is above the ground, the tyre will undergo different side-slip angles as the vehicle travels over bumps. Sometimes, this phenomenon is called "bump steer".

In addition to the side-slip angle effect, higher RC locations result into the suspension being stiffer. This is a consequence of part of the work getting shifted from the compliant components of the suspension to the rigid ones. In turn, this leads to the damper moving less and absorbing a lower portion of the energy passing through the tyre.

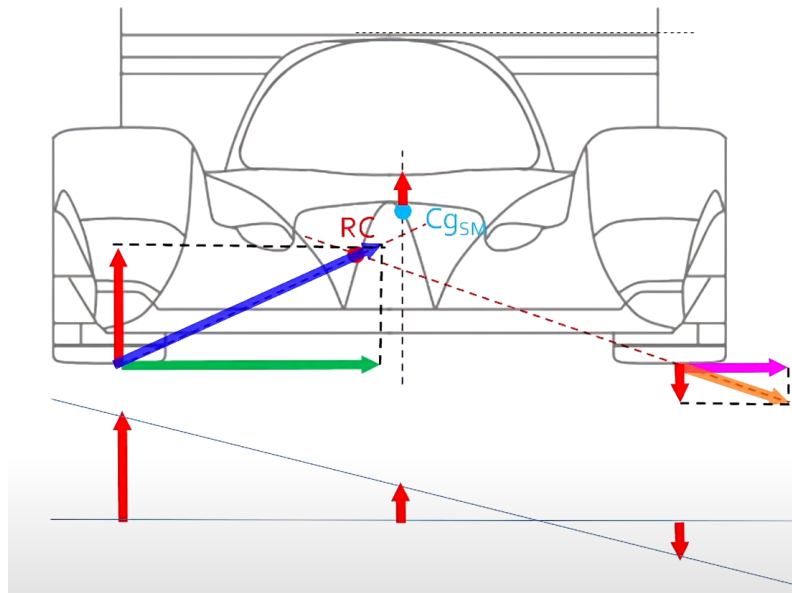


Figure 4.14: Front View of a Vehicle Featuring a Roll Centre Moved Towards the External Side of the Corner

The combined effect of the bump steer and the higher quantity of energy dissipated by the tyre leads to the tyre warming up faster and reaching higher temperatures when the suspension presents high values of RC height.

For these reasons, to locate the RC above CG is less desirable than to position it under CG.

4.3.3 Front View Analysis of the Kingpin Axis

Definition of the Front View Kingpin Axis

The axis around which the wheel rotates when steered is called kingpin axis (*Figure 4.15*). Given that the wheel is attached to the control arms by means of the outer hardpoints of the suspension (called Upper Ball Joint and Lower Ball Joint in the figure below), the kingpin axis is the line that passes through them.

When the kingpin axis is analysed in front view, it is a line on the z-y plane. Therefore, it can be described using the equation of a line:

$$y = mz + q \quad (4.37)$$

The reference frame of this line is centered in the projection on the ground of the wheel centre.

Starting from this equation, the kingpin inclination (KP_{Angle}) can be defined as the inclination of $y(z)$ and it is positive when considered as in the *Figure 4.15*:

$$KP_{Angle} = \arctan(m) \quad (4.38)$$

On the other hand, the coefficient q in combination with m determines the to the scrub radius, which is the front view distance between the projection on the ground

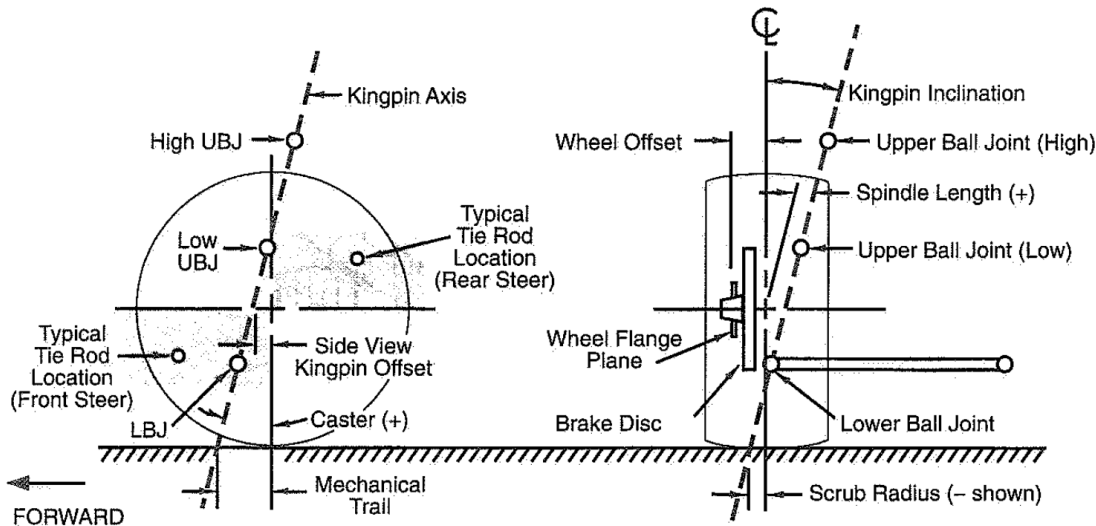


Figure 4.15: Kingpin Geometry

of the wheel centre and the interception between the kingpin axis and the ground:

$$sr = m * (-R_L) + q \quad (4.39)$$

Where:

- sr = scrub radius [mm]
- R_L = tyre's loaded radius (the reference frame of the tyre is centered in the wheel centre) [mm]

Another important parameter of the kingpin axis is the spindle length that is the distance between the wheel centre and the kingpin axis in front view. It is not present as a constrain in a parametric model due to the fact that it is completely identifiable starting from the KP_{Angle} and the scrub radius.

The presence of non null values of KP_{Angle} and scrub radius is unavoidable. This is related to packaging and clearance reasons.

Depending on the front view location of the kingpin axis, a series of characteristics of the suspension kinematics during steering can be delineated.

Steer to Camber Characteristic

The KP_{Angle} affects the camber during steering manoeuvres. In fact, the higher the KP_{Angle} the higher the camber variation. In particular, during a corner, the KP_{Angle} increases the camber (or it reduces the negative camber) on the external tyre and it raises the negative camber on the internal tyre, providing a decrease of the lateral generated by the front axle of the vehicle.

The variation of the camber angle while steering can be obtained by considering the three dimensional rotation of two random points (P_1 and P_2) around an axis inclined on the KP_{Angle} with respect to the vertical line. This way of modeling the phenomenon is described in the [Figure 4.16](#).

The calculations related to this method are carried out considering the two planes (p_1 and p_2) passing respectively through P_1 and P_2 and perpendicular to the kingpin axis, that is considered to not be inclined in side view. In this way, the trajectories of the two points analysed are two circumferences. The variation of the x and y-coordinates in the planes p_1 and p_2 of can be converted in the reference frame of the tyre (Δx_i^p and Δy_i^p). Ultimately, this enables the calculation of the camber angle.

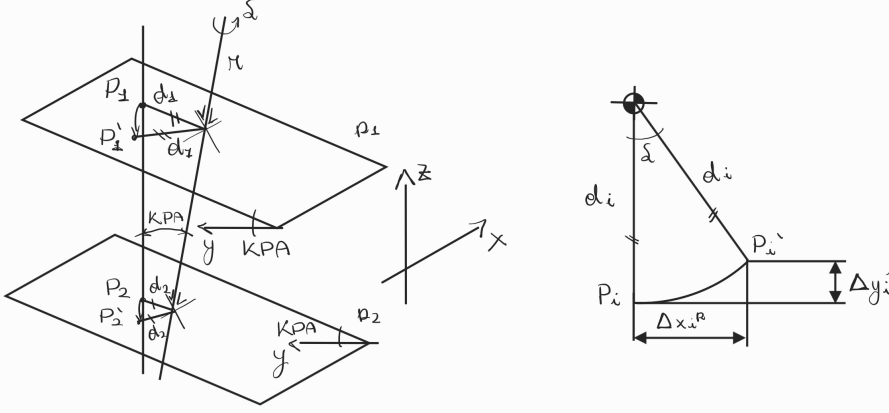


Figure 4.16: Model Used to Determine the Camber Variation Due to the Kingpin Inclination

As a first approximation, the effect of Δx_i^p is neglected. As a result, the *Equation 4.40* is obtained. By taking into account this equation and considering the small angles and that the two points are taken in such a way that their distance in z-direction equals one and their distance in y-direction is null, the *Equation 4.41* can be attained.

$$\Delta\gamma_{KP} = \arcsin \left(\frac{y_{P_2} - y_{P_1} + \tan(KP_{Angle}) * (z_{P_1} - z_{P_2})}{(z_{P_1} - z_{P_2}) * \sqrt{1 + \tan(KP_{Angle})^2}} * (1 - \cos \delta) * \cos(KP_{Angle}) \right) \quad (4.40)$$

$$\Delta\gamma_{KP} = KP_{Angle}[rad] * (1 - \cos \delta) \quad (4.41)$$

The two equations above have been validated by comparing the results with a suspension featuring the same KP_{Angle} (and no caster angle or caster trail) simulated in Adams' Car. The results are reported in *Figure 4.17*.

Is it possible to notice on *Figure 4.17* that both the models are precise enough to describe accurately the effect of the KP_{Angle} on the camber angle when steering. Therefore, the simplest model (*Equation 4.41*) will be utilised in the subsequent analyses.

The small discrepancies between all these models and the Adams' Car results are mostly related to the fact that the steering angle has been considered on a plane perpendicular to the kingpin axis instead of an horizontal plane. As a result of simulations carried out considering a range of kingpin inclinations and caster angles between zero and 15 degrees, the discrepancy between the real steering angle and the one considered on the plane perpendicular to the kingpin axis is under 5%.

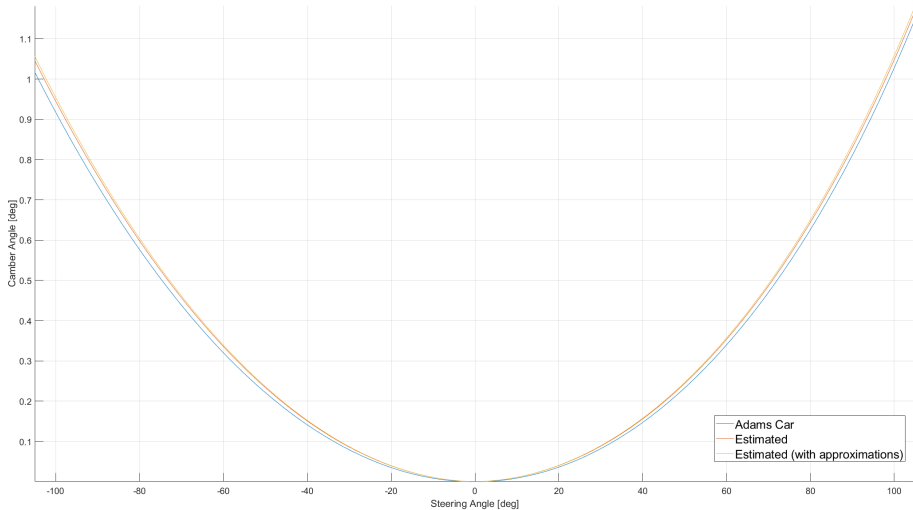


Figure 4.17: Steering Wheel Angle to Camber Angle Curve Due to a Kingpin Inclination of 5.9 degrees

Therefore, this approximation will also be used in the following analysis regarding the steering kinematics.

If the caster trail is not considered as null, the kingpin axis in *Figure 4.16* needs to be shifted along the longitudinal axis. Therefore, *Equation 4.42* is obtained.

$$\Delta\gamma_{KP} = KP_{Angle} * (\cos \delta_1 - \cos \delta_2) \quad (4.42)$$

In this equation, the steering angle is not δ anymore, but is the difference of δ_1 and δ_2 . The variable δ_1 is the inclination of the line that connects P_1 to the kingpin axis with respect to the projection of the y-axis on the plane p_1 , whilst δ_2 is the inclination of the line that connects P'_1 to the kingpin axis with respect to the projection of the y-axis on the plane p_1 . For small values of KP_{Angle} , δ_1 and δ_2 can be considered equal for the point P_2 and P'_2 respectively.

Furthermore, also the effect of the caster angle can be in combination with what has been described above. However, the effects of caster angle and the KP_{Angle} on camber will be considered as completely decoupled.

Steering Effort

The combination of non null values of KP_{Angle} and spindle length determine the motion of the wheel centre while steering. In fact, in a similar way to what has been done for the camber generated by the steering wheel due to the KP_{Angle} , the trajectory of the wheel centre can be considered as a circumference on the plane perpendicular to the kingpin axis and passing through the wheel centre.

Due to the fact that the wheel centre is moving on this trajectory, while steering (if the caster angle is null) the wheel centre will be shifted downwards independently on the steering direction. The net effect of this movement is to jack up the front of the car.

In order to raise the car, a work has to be provided to the system to enable the variation of the potential energy of the mass, for the energy conservation principle. This work is developed by the steering torque on the wheel, which ultimately translates in a torque on the steering wheel. In particular, by considering the *Figure 4.18*, the average steering torque can be defined as in the *Equation 4.44*.

Energy Conservation: $W = \Delta E_p \rightarrow$

$$M_{KP} * \Delta\delta = F_w * \Delta h = \frac{1}{2} * m_s * \frac{b}{l} * \Delta h \rightarrow \quad (4.43)$$

$$M_{KP} * \Delta\delta = \frac{1}{2} * m_s * \frac{b}{l} * \Delta h$$

$$M_{KP} = \frac{1}{2} * m_s * \frac{b}{l} * SL * \frac{(\cos \delta_1 - \cos \delta_2) * \sin (KP_{Angle})}{\delta_2 - \delta_1} \quad (4.44)$$

Where:

- M_{KP} = average moment around the kingpin axis (average steering torque on the wheel) [Nm]
- F_w = weight force (vertical force acting on one of the front tyres under static conditions) [N]
- m_s = suspended mass [kg]
- b = longitudinal distance between the CG and the rear axle [m]
- l = wheelbase of the vehicle [m]
- Δh = vertical movement of the wheel centre [m]
- δ_1 = initial value of the steering angle on the wheel [deg]
- δ_2 = final value of the steering angle on the wheel [deg]
- $\Delta\delta$ = variation of the steering angle on the wheel [deg]
- SL = spindle length [m]

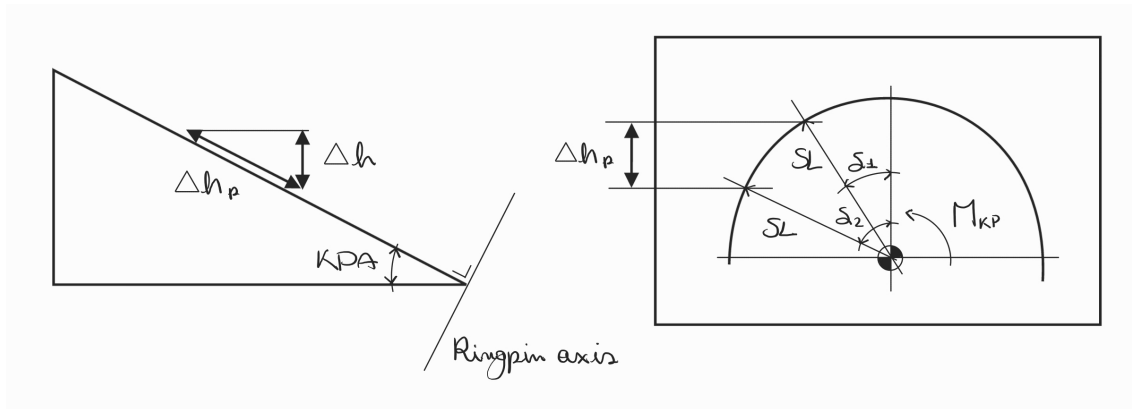


Figure 4.18: Wheel Centre Trajectory Around the Kingpin Axis

As it is possible to observe from the *Equation 4.44*, the moment on the steering rises when the spindle length or the KP_{Angle} become higher. Therefore, in order to minimise the torque on the steering wheel due to the wheel centre vertical movement during steering the front view of kingpin axis should be as close as possible at the wheel centre. By reducing SL , also the vertical movement of the front axle due

steering is decreased.

During this analysis an approximation has been utilised. In fact, the wheel centre has been considered as the application point of the weight. In reality, the line where the vertical force vector lays is dependent on the location of the contact patch. This location dynamically changes due to the load condition on the tyre and its angles. Therefore, the distance between the axis where the weight force is applied and the kingpin axis should be contained (rather than SL). The spindle length is just a first approximation of this distance.

An important effect related to the value of the scrub radius is the steering torque due to the longitudinal force acting on the tyre (F_x). As a matter of fact, F_x has an offset with respect to the kingpin axis, which causes a steering torque. This offset is mostly dependent on the scrub radius (SR) and slightly influenced by the KP_{Angle} . Moreover, considering that the application point of F_x moves in y-direction due to the load conditions on the on the tyre and its angles, its offset with respect to the projection on the ground of the wheel centre (y_{F_x}) has to be considered.

$$d_{F_x} = \frac{SR - y_{F_x}}{\cos(KP_{Angle})} \sim SR - y_{F_x} \quad (4.45)$$

The steering torque can be defined as follows.

$$M_{F_x} = F_x * d_{F_x} \sim F_x * (SR - y_{F_x}) \quad (4.46)$$

Considering a braking manoeuvre under the conditions where the braking moments applied on the two front tyres is the same and they are not locking, the two M_{F_x} acting on the wheels of the front axle will compensate themselves. Although this leads to the net torque on the steering due to F_x to be null, the tie-rod, the upright and the steering rack will be subjected to stress during braking and traction.

From the description of M_{F_x} , it might appear like to reduce the scrub radius can only provide positive effects. Nevertheless, M_{F_x} can enable the driver to feel the locking of one of the front tyres on the steering wheel. In fact, when one of the tyre is locking during a braking manoeuvre, the F_x produced by that tyre will drop. In turn, this leads to different values of M_{F_x} on the two wheels. Ultimately, the unbalance of M_{F_x} results in a net torque on the steering wheel.

Despite the unbalance in M_{F_x} between the two sides of the front axle may be a positive effect in terms driving feeling while braking, this is not necessarily the case in the traction phases.

For instance, lets consider that the vehicle is provided of torque vectoring and the controls are balancing some understeer by providing more torque on the external tyre of the front axle the one provided on the intern one. In this case, considering that the kingpin in most of the cases touches the ground in a more internal location than the application point of F_x , the net torque on the steering wheel due to M_{F_x} is in the same direction of the turning. Dependently on the actuation speed of the torque vectoring, the driver could feel this as an increase in understeer or as snap oversteer. Whilst the former case can lead the driver to decrease the amount of throttle actuation to compensate the understeer, thus reducing the effect of the

torque vectoring, the latter case is more critical. Due to the fact that the driver will tend to correct the trajectory (because of the steering wheel becoming quickly lighter) the effect of the torque vectoring can be nullified.

The scrub radius can also result in an impulsive steering torque when the vehicle travels over a bump. This is due to the fact that when a tyre hits a bump, a F_x will be generated on the tyre.

Effect of the Camber Gain

The camber gain (*Equation 4.5*) changes the inclination of the upright in front view when the wheel is subjected to a vertical travel. Therefore, also the KP_{Angle} is not constant when the suspension moves. In fact, it changes accordingly to the camber gain (*Equation 4.2*).

General Considerations

To sum up, the scrub radius can be tuned in different ways depending on the target of the design. However, in most of the cases, the scrub radius is the result of the suspension packaging.

Taking this into consideration, the kingpin axis can be optimised on the rear suspension with the only target of reducing the moments acting on the wheel, in order to decrease the stresses on the upright and on the tie-rod during traction. This is related to the fact that the rear wheels of the vehicle considered cannot steer.

In order to reduce the stresses on the elements above-mentioned during traction, the scrub radius has to be tuned in such a way that the kingpin axis is in the nearest position possible during most of the traction phases.

4.3.4 Side View Analysis of the Kingpin Axis

Definition of the Front View Kingpin Axis

The side view examination of the kingpin will follow what has just seen for the [front view](#).

The side view geometry of the kingpin axis (*Figure 4.15*) can be represented as a line on the x-z plane:

$$x = mz + q \quad (4.47)$$

The origin of the reference frame used to create this equation coincide with the projection of the wheel centre on the ground. Therefore, the coefficients m and q can be used to define the caster angle (c_{Angle}) and the caster trail (ct):

- $m = \tan(c_{Angle}) \rightarrow c_{Angle} = \arctan(m)$
- $ct = m * (-R_L) + q$

Steer to Camber Characteristic

As for the KP_{Angle} , a non null value of caster angle affects the steering to camber curve. However, whilst the KP_{Angle} is detrimental for the lateral grip on the front tyres due to the loss of negative camber angle, the same is not true for the c_{Angle} .

As a matter of fact, during cornering, the positive caster trail (*Figure 4.15*) results in an increase of negative camber on the front outside tyre and a rise of positive camber on the front inside tyre. In turn, this lead to both the tyres leaning towards the inside of the corner, this results in camber forces that work in the same direction of the lateral force generated through the side-slip of the tyre. Ultimately, the grip generated from the front axle will be enhanced, unless the tyres are in a work condition where the camber effect on F_y make it saturate or drop.

In order to model the camber variation due caster angle while steering, the modelling procedure employed to determine the steering to camber relation due to the KP_{Angle} can be applied again. This procedure, if applied without any approximation, results into *Equation 4.48*.

$$\Delta\gamma_{ca} = \arcsin \left(\frac{(x_{P_2} - x_{P_1} + \tan(c_{Angle})) / (\sqrt{1 + \tan(c_{Angle})^2}) * \sin \delta}{z_{P_1} - z_{P_2} + \frac{x_{P_1} - x_{P_2} + \tan(c_{Angle})}{\sqrt{1 + \tan(c_{Angle})^2}} * (1 - \cos \delta) * \sin(c_{Angle})} \right) \quad (4.48)$$

By neglecting the effect of Δx_{P_1} and Δx_{P_2} a more convenient formula can be obtained:

$$\Delta\gamma_{ca} = \arcsin \left(\frac{(x_{P_2} - x_{P_1} + \tan(c_{Angle})) * \sin \delta / (\sqrt{1 + \tan(c_{Angle})^2})}{z_{P_1} - z_{P_2}} \right) \quad (4.49)$$

By adding further approximations to the formula the result will be:

$$\Delta\gamma_{ca} = c_{Angle} [rad] * \sin(\delta) \quad (4.50)$$

As it is possible to notice from *Figure 4.19* that all the three formulations are precise enough to describe the phenomenon, the simplest one (*Equation 4.48*) will be utilised. In particular, the estimated effect on the external tyre (negative steering wheel angles) follow really accurately the real curve found through Adams' Car. Therefore, the values of camber angle provided by the estimation are more precise in the most loaded tyre.

Induced Roll

When steering the suspension moves on trajectory that is perpendicular to the kingpin axis. Therefore, the wheel centre moves on a circumference on a plane perpendicular to the kingpin axis an passing through the wheel centre.

As a result of non null values of caster angle and spindle length, the wheel centre moves vertically when steering. Considering the case where the longitudinal distance between the wheel centre and the kingpin axis is null, the quantity of vertical movement will just change its sign when changing steering direction. Therefore,

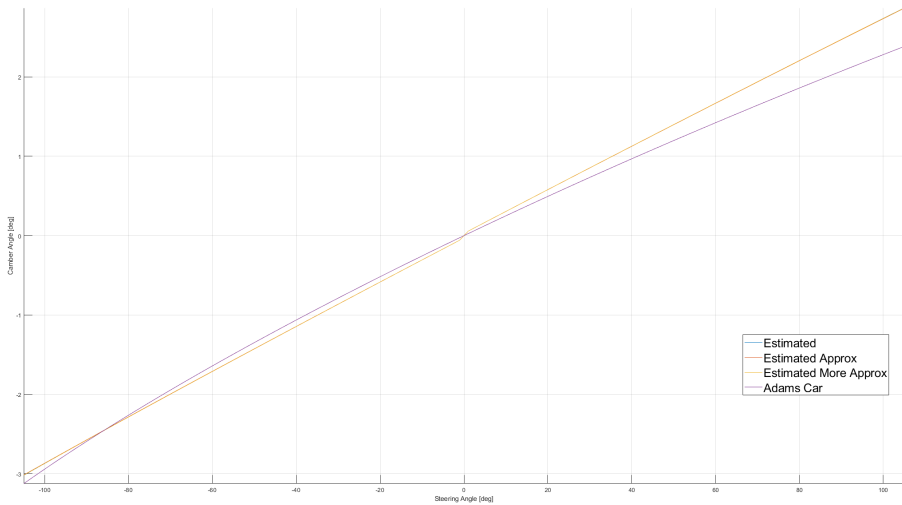


Figure 4.19: Steering Wheel Angle to Camber Angle Curve Due to a Caster Angle of 6.3 degrees

if the steering is rotated in one direction, the net effect will just be a roll of the body of the vehicle without any vertical movement. Lastly, the fact that the left and the right wheel centres move vertically in two opposite directions and of the same amount results in the net torque on the steering to be influenced by the caster angle.

Given that the vehicle has a certain roll stiffness, the roll angle caused by the opposite vertical movements of the wheel centres while steering will translate in a rolling torque acting on the front axle. Therefore, steering the front tyres will cause a load transfer due to the combination of the caster angle and spindle length.

In order to quantify such load transfer, the roll angle has to be calculated. This process is carried out by modelling the vertical motion of the wheel centre as a function of the steering angle. To create this relation the model in *Figure 4.20* has been utilised.

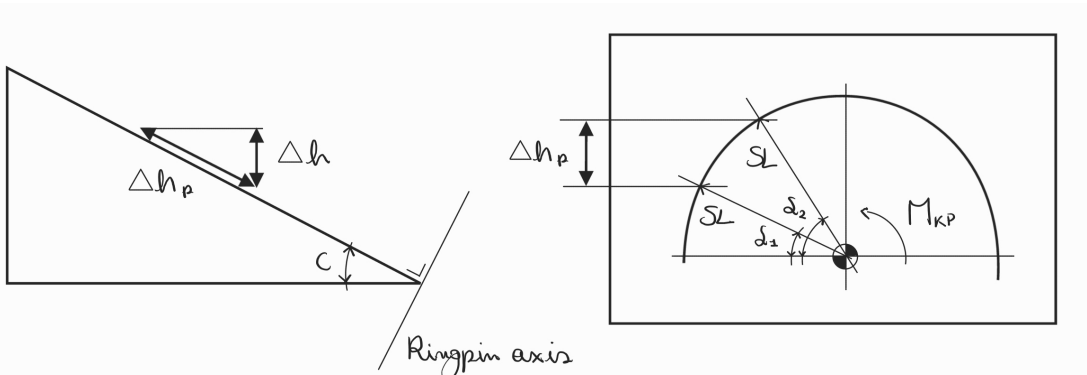


Figure 4.20: Wheel Centre Trajectory Around the Kingpin Axis - Camber Effect

$$\Delta h = SL * (\sin \delta_1 - \sin \delta_2) * \sin(c_{Angle}) \quad (4.51)$$

$$\Delta\phi = \arctan\left(\frac{2\Delta h}{t}\right) = \arctan\left(\frac{2SL(\sin \delta_1 - \sin \delta_2) \sin(c_{Angle})}{t}\right) \quad (4.52)$$

$$\Delta M = K_{r,f} * \Delta\phi = K_{r,f} * \arctan\left(\frac{2SL(\sin \delta_1 - \sin \delta_2) \sin(c_{Angle})}{t}\right) \quad (4.53)$$

$$\Delta F_z = \frac{M}{t} = \frac{K_{r,f}}{t} \arctan\left(\frac{2SL(\sin \delta_1 - \sin \delta_2) \sin(c_{Angle})}{t}\right) \quad (4.54)$$

Given that the load transfer is null when the steering angle is equal to zero, the total load transfer for a given angle can be computed by considering the initial steering angle δ_1 null.

$$\Delta F_z = \frac{M}{t} = \frac{K_{r,f}}{t} \arctan\left(\frac{2 * SL * \sin \delta_2 * \sin(c_{Angle})}{t}\right) \quad (4.55)$$

Overall, this effect causes a load transfer on the front axle. In particular, the load is transferred on the outside tyre. Therefore, the combination of caster angle and spindle length results in a increase in the front load transfer, hence a reduction of the rear load transfer (diagonal load transfer). Ultimately, this load transfer result in a slight increase of the vehicle understeer.

Furthermore, the phenomenon above-mentioned leads to an increase in stress on the rack components, on the tie-rod and on the upright.

Steering Effort

The side view of the kingpin plays a crucial role in the self-stabilizing effect of the tire, in particular, when a lateral force is generated due to a side-slip angle. In particular, the caster trail has the largest contribution to this phenomenon.

In order to understand the self alignment characteristics of a wheel, an analysis of the moment around the z-axis (M_z) generated by a lateral force (F_y) is needed. In fact, F_y is not centred in the centre of the reference frame created to define the characteristics of the kingpin axis, instead it changes position accordingly to the loads acting on the tyre. As a result of these movement, F_y creates a moment M_z (along with M_x); therefore, also this moment is dependent on the load condition on the tyre.

When a tyre is developing a lateral force, the longitudinal offset that causes M_z is labelled with the letter " d_{F_y} ". Therefore, M_z can be defined as follows:

$$M_z = F_y * d_{F_y} \quad (4.56)$$

If all the characteristics of a tyre, but the sides-slip angle and d_{F_y} , are considered constant, the value of d_{F_y} changes as function of the side-slip angle.

As a matter of fact, for small values of side-slip angle acting on the tyre, the tangential pressure distribution on the contact patch " τ_y " (that results in F_y) is linearly increasing along the length of the contact patch. This is due to the fact that small side-slip angles do not cause the tread to slide significantly on the tarmac, thus the

lateral force is developed by exploiting the linear elastic characteristics of the tyre along the majority of the contact patch.

On the other hand, when the side-slip increases, part of the lateral force is generated from sliding friction mechanisms. Therefore, τ_y does not increase linearly along the contact patch and its peak value will move forwards. As a consequence, d_{F_y} becomes shorter and shorter and eventually it changes sign. Eventually, M_z can change sign due to the variation in d_{F_y} . From the analysis of the trends of F_y and

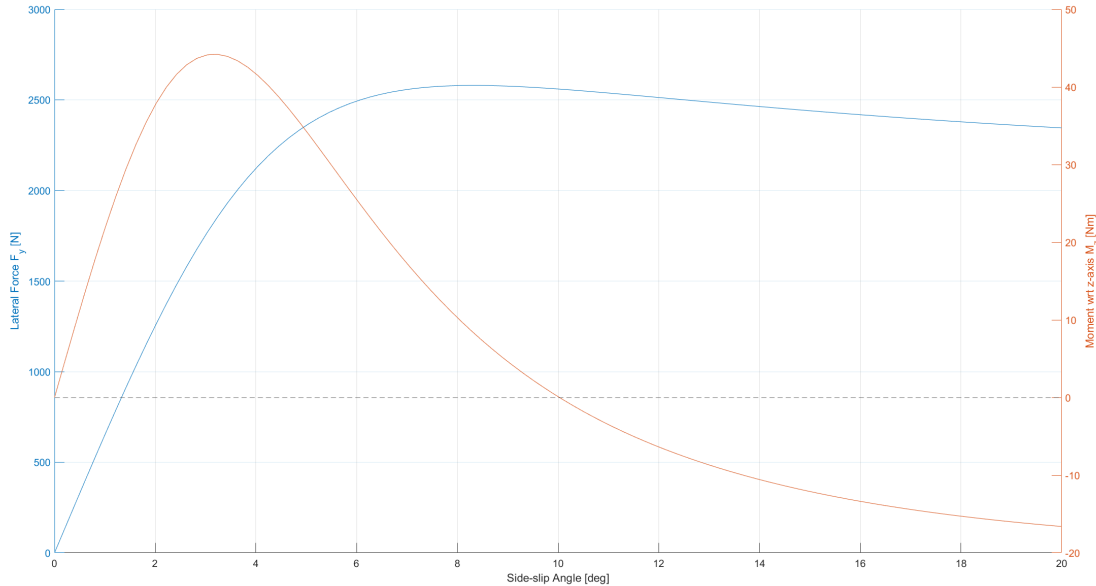


Figure 4.21: Lateral Force and Moment on the Z-Axis Versus Side-slip Angle

M_z as functions of the side-slip angles (Figure 4.21), there are some differences that can be noticed. In fact, whilst for side-slip angles lower than two degrees both F_y and M_z increase linearly, the shortening of d_{F_y} causes M_z to decrease before the peak of F_y . When the value of side-slip reaches ten degrees, M_z goes to 0, while the F_y is yet to decrease by a substantial amount from its peak value.

As a first approximation, M_z can be considered as the self-aligning moment of the tyre. When this moment is positive and F_y is produced by a side-slip angle due to a steering angle, it causes the x-axis of the reference frame of the wheel to re-align with the x-axis on the reference frame of the vehicle. This is due to the fact that, for positive values of M_z , F_y is applied behind the z-axis of the tyre's reference frame and F_y on the tyre has always a opposite direction with respect to the side-slip angle (when not considering conicity and ply-steer characteristics of the tyre). Ultimately, M_z works against the side-slip when positive, whereas it tends to increase the side-slip when negative.

The self-aligning moment is proportional to the torque on the steering wheel. Therefore, this moment provides to the driver feed-backs on the level of grip on the front axle. If the self-aligning moment coincides with M_z , than the driver feels a drop in steering torque much before the peak of F_y .

The phenomenon described above may result in two limit situations. As a matter of fact, the driver could either use the tyre only in the range of side-slip angles where the M_z is high or guess where the peak lateral force really is.

In former case, F_y can be significantly lower than its peak value. Therefore, the drivers are not fully exploiting the grip that the tyres can provide, as they are too conservative with their steering inputs (under-driving).

In the latter case, the driver would be able to better exploit the grip of the tyre, but they can only rely on their feeling of the yaw-acceleration and of the lateral acceleration acting on their body.

Another problem that may occur when the self-aligning moment coincides with M_z regards the point where the moment changes sign. In point of fact, if the steering torque quickly drops to zero and becomes negative, the driver is likely to interpret that as a snap of oversteer. Consequently, this characteristic of M_z leads to the driver either to apply steering corrections when it is not needed or to tremendously under-drive the vehicle. This can happen especially during fast corners, where the aerodynamic load acting on the tyres enables large values of side-slip angles.

In a real case, M_z coincides with the self aligning moment only if both the caster angle and the caster trail are equal to zero. In fact, the calculation of the self-aligning moment (M_{F_y}) should be performed in relation to the kingpin axis, as it serves as the steering axis for the wheel.

$$M_{F_y} = F_y * (d_{F_y} + ct) * \cos(c_{Angle}) \quad (4.57)$$

$$\text{For small values of } c_{Angle} \rightarrow M_{F_y} = F_y * (d_{F_y} + ct) = M_z + M_t \quad (4.58)$$

In the *Equation 4.48*, M_{F_y} is the sum M_z and a transport moment " M_t ". Given that M_t is directly proportional to ct , which can be considered roughly constant, its trend is dictated by F_y . In *Figure 4.22*, the combination of effects that causes M_{F_y} is portrayed as function of the side-slip angle. It is possible to notice that, due to M_t caused by ct , the peak of self-aligning moment is shifted nearer to the peak of F_y . This leads to a better feeling on the steering wheel of the actual lateral grip provided by the tyres.

Furthermore, the value of side-slip angle for which M_{F_y} changes sign is shifted forward by increasing ct . In turn, this results in a better coupling of what the driver feels through the accelerations and the steering torque, thus enabling them to better exploit the vehicle performance.

Although it may appear like to increase ct only causes positive effects, this is not necessarily true, especially if the car is not provided with power steering. In fact, a longer ct causes the overall steering torque to significantly rise. Therefore, this is a negative effect both in terms of vehicle drivability and loads acting on the upright and on the steering system.

In addition to this, positioning the peak of the self-aligning moment too close to the maximum value of lateral force could lead to a delayed sensation of front grip loss in the steering.

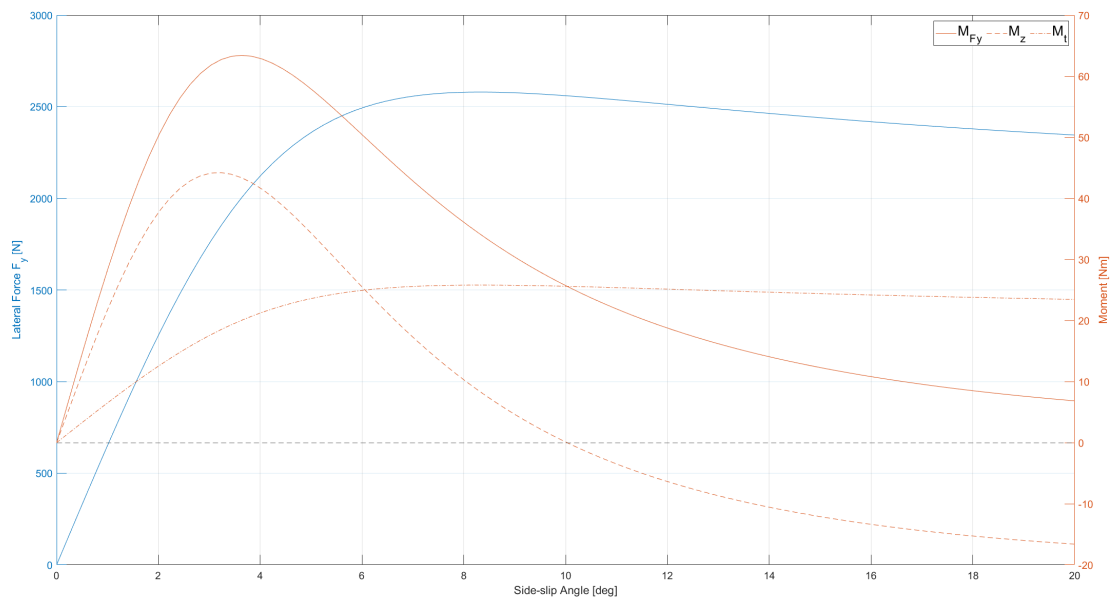


Figure 4.22: Lateral Force and Self-aligning Moment Components Versus Side-slip Angle - Caster Trail = 10 [mm]

General Considerations

In most of the cases, in a formula student vehicle, one of the targets of the design of the front suspensions has to be to increase the c_{Angle} as much as needed to reach a value of camber variation, that in combination with the static camber and the camber recovery, provides a satisfactory value of camber in most of the conditions, but particularly during cornering. On the other hand, ct has to be reduced as much as possible to minimise the steering torque without causing M_{Fy} to become negative under normal racing conditions.

In order to achieve high c_{Angle} and small ct , the point on the kingpin axis that has the same z-coordinate of the wheel centre has to be positioned behind the wheel centre.

When the rear suspension is considered instead, the design has to account for the fact that, in the vehicle considered during this analysis, the rear wheels cannot steer. Therefore, the only effects related to steering are caused by the tie-rod and the upright compliance, which are negligible.

As a consequence of the impossibility to steer the rear tyres, the kingpin axis in side view will be a consequence of the packaging on rear suspension components. The only thing that may be optimised is the caster trail. In fact, it should be chosen in such a way to minimise the moment generated when the rear tyre under consideration is highly loaded with lateral forces. This is done to reduce the stresses on the upright and on the tie-rod.

4.3.5 Side View Swing Arm

Side View Instant Centre Definition

In a double wishbone suspension, the side view motion of the wheel hub with respect to the chassis is dependent on the x-z location of the inner hardpoints.

The outer hardpoint of LCA can move in side view on a line perpendicular to the axis that connects the two inner hardpoint of the LCA. The same is true for the UCA.

Given that the upright can be considered as a rigid element, the instant centre of rotation in side view can be found from the interception of at least two lines perpendicular to the side view motion of two points of the upright. For the sake of convenience, the points considered in order to find the side view instant centre are the outer hardpoints of the UCA and of the LCA. Therefore, the position of the side view instant centre is the interception of the line that connect the inner hardpoints on the LCA and the line that connects the inner hardpoints of the UCA.

Side View Swing Arm Definition

The side view location of the instant centre can be used to determine the upright side view motion when the wheel centre is subjected to a vertical displacement. In particular, the side view swing arm and the side view instant centre height have to be considered to analyse the upright movement.

The side view swing arm (*svsa*) is the longitudinal distance between the side view instant centre and the wheel centre, whilst the side side view instant centre height (h_{IC_s}) is the vertical distance between the side view instant centre and the ground.

Another important parameter is the inclination of the side view n-line (ϵ) with respect to the ground. The side view n-line is the line that connects the contact patch to the side view instant centre. Therefore, its inclination can be determined as function of the *svsa* and and of the h_{IC_s} as it is reported in *Equation 4.59*.

$$\epsilon = \arctan \left(\frac{h_{IC_s}}{svsa} \right) \quad (4.59)$$

The characteristics of the side view n-line can also be visualised in terms of n-line length (l_{nl}) as described in *Equation 4.60*.

$$l_{nl} = \sqrt{svsa^2 + h_{IC_s}^2} \quad (4.60)$$

Caster Gain and Wheelbase Variation

Given that upright will tend to rotate around the side view instant centre, also the caster angle changes accordingly. This phenomenon can be modeled how it has been done for the camber gain (*Equation 4.61*).

$$\frac{\Delta c_{Angle}}{\Delta z} = 1/svsa \quad (4.61)$$

From this relation, it can be stated that, when the suspension is compressed, the caster angle on the wheel increases. The shorter the *svsa*, the larger Δc_{Angle} .

The caster gain can be exploited to obtain larger values of camber in fast corners. This is caused by the aerodynamic forces that push the car down increasing the value of caster. However, it causes the caster to decrease during corner exit, which may lead to understeer.

Moreover, with the caster gain also the caster trail increases. However, this effect is compensated by the tyre compression that reduces the caster trail itself (the net result of the combination of these effects has to be analysed case by case).

On the other hand, as the wheel centre rotates, the wheelbase of the vehicle (wb) changes. For instance, by considering the side view instant centre over the wheel centre, the vertical movement of the wheel results in an increase in the wheelbase. This phenomenon is identical on the rear wheels and on the front wheels.

From a mathematical point of view the wheelbase variation is related to the $svsa$ and to the angle between the x-axis and the line that connects the side view instant centre and the wheel centre (ϕ). Although the $svsa$ changes during the suspension compression, it is considered constant in order to obtain [Equation 4.62](#).

$$\Delta wb = l'_{nl} * (\cos(\arcsin(\sin(\phi) - \Delta z/l'_{nl})) - \cos(\phi)) \quad (4.62)$$

Considering [Equation 4.60](#) and [4.62](#):

$$\Delta wb = \sqrt{svsa^2 + z_{IC_s}^2} * (\cos(\arcsin(\sin(\phi) - \Delta z/\sqrt{svsa^2 + z_{IC_s}^2})) - \cos(\phi)) \quad (4.63)$$

Where:

- l'_{nl} = length of the line connecting the side view instant centre to the wheel centre
- z_{IC_s} = z-coordinate of the side view instant centre

It is possible to notice from this equation that the Δwb due to Δz increases with longer l'_{nl} (or higher $svsa$) and with higher values of ϕ .

The increase in wheelbase has a stabilising effect on the vehicle. Given that it is a result of the vertical movement of the suspension, this effect will be present when the vehicle is subjected to high vertical loads. For instance, during high speed cornering, it is positive for a vehicle to be provided of a long wheelbase, as the yaw-rates are comparatively lower than the one obtained during low speed cornering.

During breaking and traction the increase of the wheel base due to one axle and the reduction related to the other one can compensate each other. Therefore, the net effect is a variation of the position of the centre of gravity with respect to the front and rear wheel centre. In the vast majority of cases, this effect is minor can be ignored.

Overall, it can be noticed that tuning the $svsa$ is a choice between maximising the wheelbase variation or to gain caster during fast corners.

If the side view instant centre of the front suspension is lower than the wheel centre,

it is better to prioritise the caster gain over the wheelbase variation and vice-versa. On the other hand, on the rear suspensions it may be better to prioritise the wheelbase variation due to the fact that the caster angle has no meaningful effect on the rear axle kinematics.

4.3.6 Anti-Features

Longitudinal Load Transfer

When a vehicle is subjected to a longitudinal acceleration, an inertial longitudinal force is developed on its centre of gravity. This force is dependent on the longitudinal acceleration and on the vehicle mass and it is caused by the real longitudinal forces acting on the tyres.

Due to the fact that the centre of gravity is always located to an higher position with respect to the contact patches of the tyres, the longitudinal force acting on the system generates a moment. This moment is compensated by a longitudinal load transfer.

The longitudinal load transfer consists in four vertical forces. Two of them act on the front axle and they are identical both in terms of value and direction. The other two forces are identical between them and they have the same value of front ones but opposite direction.

The load transfer acting on an entire axle can be calculated as follows:

$$\Delta F_z = m * a_x * h_{CG}/wb = F_x * h_{CG}/wb \quad (4.64)$$

Where:

- ΔF_z = load transfer on one axle [N]
- m = vehicle mass [kg]
- a_x = longitudinal acceleration [m/s^2]
- h_{CG} = height of the centre of gravity [m]
- wb = wheelbase [m]

The longitudinal load transfer creates a moment around the y-axis of the vehicle (pitching moment). The effect of the pitching moment is to make the vehicle lean towards the front during braking (dive) or tilt towards the rear in traction (squat).

Pitching and Non Pitching Load Transfer

The suspensions kinematics affects the pitch motion of the vehicle in a similar way in which it influenced the roll motion.

In order to demonstrate the interaction between the suspension kinematics and the vehicle pitch, a simplified model of the side view of the suspension has to be taken into account. In particular, the wheel is considered to be connected to its side view instant centre through a rigid beam, which is attached to the side view instant centre through a hinge.

When a longitudinal force ($F_{x,f}$) is applied to the contact patch of the front wheel and the side view instant centre is not aligned with that contact patch, a moment is generated on the system.

In the case where a breaking load condition is considered, $F_{x,f}$ is directed rearwards. Given that in the majority of cases the side view instant centre is above the ground ($h_{IC_s} > 0$), the moment generated by $F_{x,f}$ tends to rotate the wheel in anti-clockwise direction. Therefore, the front of the vehicle is jacked up by this effect. If instead the side view instant centre is under the ground ($h_{IC_s} < 0$), the moment caused by the $F_{x,f}$ and h_{IC_s} tends to drop the front of the vehicle.

The moment above-mentioned can be compensated by a vertical force acting on the contact patch, which can be defined as reported in the *Equation 4.65*.

$$svsa * \Delta F_{z,np,f} = h_{IC_s} * F_{x,f} \rightarrow \Delta F_{z,np,f} = F_{x,f} * \frac{h_{IC_s}}{svsa} = F_{x,f} * \tan \epsilon_f \quad (4.65)$$

Where ϵ_f is the front n-line inclination.

If the vehicle considered is braking, the longitudinal load transfer on the front axle is a vertical force directed upwards. Considering the case where also that the side view instant centre is above the ground, also $\Delta F_{z,np,f}$ is directed upwards. Therefore, a part of the load transfer equal to $\Delta F_{z,np,f}$ is used to compensate the moment applied by $F_{x,f}$, thus it does not make the vehicle pitch. As a consequence, $\Delta F_{z,np,f}$ is the non pitching front load transfer.

In a similar manner to what has been explained for the lateral load transfer, the non pitching component of the load transfer is unloaded through the rigid elements of the suspension, whilst the remaining part is the pitching component of the load transfer which is unloaded through the compliant element of the suspension, thus causing pitch.

In the limit case where the vehicle is only braking on the front axle and the side view instant centre of the front suspension lies on the line connecting the contact patch to the centre of gravity (the side view n-line of the front suspension passes through the CG), the ratio of h_{IC_s} and $svsa$ equals the ratio of h_{CG} and a . Therefore, all the load transfer will be non pitching, and the only pitch on the vehicle will be caused by the tyres deforming.

Anti-Features Definition

In order to quantify the proportion between non pitching and total component of longitudinal load transfer, the anti-features coefficients are defined.

There are four anti-features coefficients that can be used depending on whether the vehicle considered is braking or accelerating and depending on the axle considered:

- *anti-dive "A_d"* = tendency of the **front** suspensions to **not compress** during **braking** [-]
- *anti-lift rear "A_{l,r}"* = tendency of the **rear** suspensions to **not extend** during **braking** [-]

- *anti-squat* " A_s " = tendency of the **rear** suspensions to **not compress** during **traction** [-]
- *anti-lift front* " $A_{l,f}$ " = tendency of the **front** suspensions to **not extend** during **traction** [-]

Often, when considering the traction related anti-features, the engine torque has to be considered as an external moment acting on the wheel. As a consequence, this torque has to be introduced in the balance of moments when determining the non pitching component of the load transfer. Nevertheless, due to the formula vehicle employed for this case study featuring outboard engines, the engine torque is internal to the wheel system and has no effect on the calculation executed above. Ultimately, all the anti-features can be defined in a similar way (*Equations* for 4.66 to 4.69).

$$A_d = \frac{\Delta F_{z,np,f}}{\Delta F_z} = \frac{bb_f * \tan \epsilon_f}{h_{CG}/wb} = bb_f * \tan \epsilon_f * \frac{wb}{h_{CG}} \quad (4.66)$$

$$A_{l,r} = (1 - bb_f) * \tan \epsilon_r * \frac{wb}{h_{CG}} \quad (4.67)$$

$$A_s = tb_r * \tan \epsilon_f * \frac{wb}{h_{CG}} \quad (4.68)$$

$$A_{l,f} = (1 - tb_r) * \tan \epsilon_r * \frac{wb}{h_{CG}} \quad (4.69)$$

Where:

- bb_f = front braking force over the total one [-]
- tb_r = rear traction force over the total one [-]

Generally, the anti-features are employed to control the front and rear ride heights when the vehicle undergoes a longitudinal acceleration. Therefore, they are particularly useful in vehicles featuring aerodynamic components, where the distance from the ground of elements such as the front wing and the rear diffuser have to be kept low without them hitting the ground.

General Consideration

The anti-features enable for lower heave and pitch stiffness and damping without compromising the ride heights of the vehicle in corner entry and exit. This results to achieve the best mechanical grip possible by tuning the damping and the stiffness of the suspension and keeping the ride height under control at the same time.

4.3.7 Pitch Centre

Definition

The pitch centre (PC) of a vehicle is the side view of the axis around which the vehicle pitches (pitch axis).

The pitch centre location can be found in a similar way to what has been done for the roll centre. In fact, it will be positioned in the interception of the side view n-lines of the front and of the rear axles.

Chassis Movement Due to Longitudinal Load Transfer

The PC location on the x-z plane influences how the vehicle moves when subjected to longitudinal or vertical forces acting on CG.

First of all, let's consider the effect of the vertical location of PC when the vehicle is subjected to a longitudinal force. In this situation there are two cases that can be identified. The former is the condition where PC is under CG. In this case a braking force creates a moment that tends to dive the vehicle, whereas a traction force generates a moment that makes the vehicle squat. If instead PC is over CG the effects of the braking forces and the traction forces are inverted. In the latter case, the forces unloaded through the control arms are higher than the one generated when the PC is under CG.

In both cases, it is of primary importance to keep in mind that the steady state longitudinal load transfer is not impacted by the location of PC, whilst the transient longitudinal load transfer is affected by PC in a similar way in which the transient lateral load transfer is affected by RC. Therefore, the higher PC the faster load transfer builds up.

On the other hand, the longitudinal location of PC influences the vehicle's body motion when it is subjected to time variant vertical forces. For instance, if the vehicle considered passes over a bump there will be a spike of vertical force that results in an oscillating heave motion of the chassis (the pitch motion due to the fact that the rear wheels encounter the bump after the front one is neglected). If the x-location of PC does not coincide with the x-coordinate of CG the vertical force generates a pitching moment, which results in a pitching oscillation that is combined with the heave of the chassis.

Chassis Movement Due to Aerodynamic Effects

In a vehicle featuring significant values of aerodynamic load, also the relative location of PC and the pressure point (PP) of the vehicle has to be taken into account. As a matter of fact, if PC is over PP, the aerodynamic drag generates a moment that squats the vehicle and vice-versa if the PC is under PP. Instead if PC is behind PP, the aerodynamic downforce causes the vehicle to squat, whilst the vehicle dives if PC is in front of PP. These effects are all dependent on the square of the speed of the vehicle and can be harnessed to better control the vehicle platform at high speeds.

4.3.8 Wishbones Aperture Angle

Definition

The distance between the inner hardpoints of a double wishbone suspension can be tuned in order to balance the forces acting on the chassis and on the wishbone when the tyre is subjected to lateral and longitudinal forces.

For starters, the effect of the lateral force of is evaluated on a simplified model. For this analysis a single wishbone is considered, and it is modelled as a truss made by two rods (*Figure 4.23*).

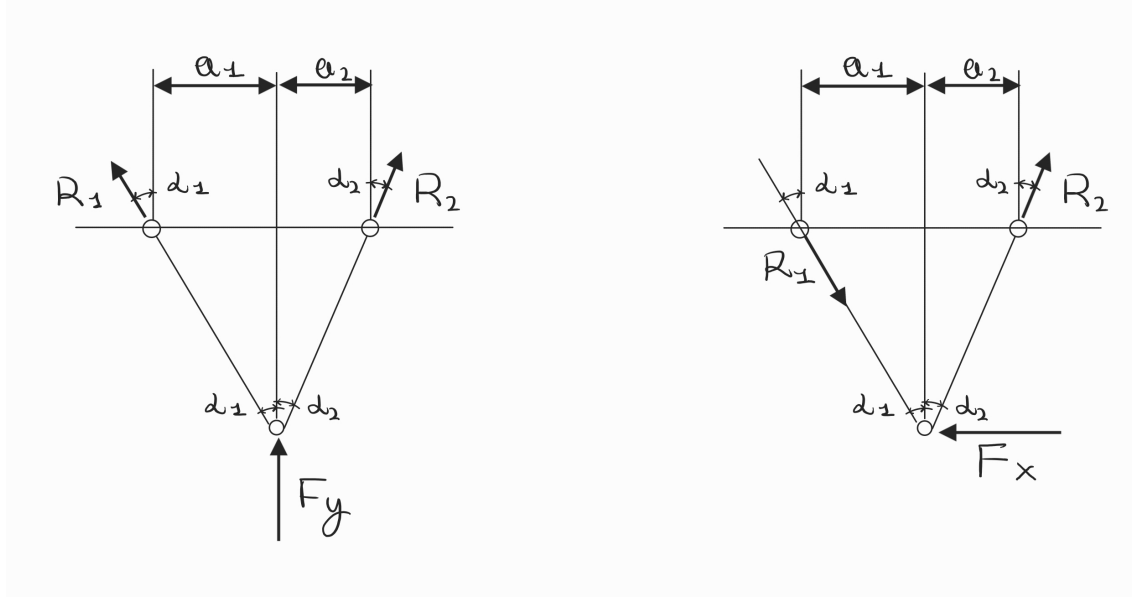


Figure 4.23: Upper View of a Simplified Wishbone

Forces Evaluation

By considering the equilibrium of forces on the lateral direction, it is possible to notice that the larger the aperture angles of the wishbones (α_1 and α_2) are, the larger the resultant forces on the chassis (R_1 and R_2) are.

$$R_1 * \cos \alpha_1 + R_2 * \cos \alpha_2 = F_y \quad (4.70)$$

A similar analysis can be done when studying the effects of a longitudinal force acting on the outer hardpoint of the wishbone. In this case, larger values of α_1 and α_2 result in lower R_1 and R_2 acting on the chassis.

$$R_1 * \sin \alpha_1 + R_2 * \sin \alpha_2 = F_x \quad (4.71)$$

If F_y and F_x are considered to have the same peak value, the optimal value of α_1 and α_2 would be 45 degrees in order to reduce the peaks of R_1 and R_2 . However, it is not always possible to obtain a total aperture of the wishbone equal to 90 degrees for packaging reasons. In particular, such a high aperture could result into the wishbone interfering with the rim when steering.

In general term, the target is always to maximise the distance between the two inner hardpoints as long as the rim and the wishbone's brackets do not interfere under any circumstance and the inner hardpoints end up in the plane of the monocoque designed to sustain the load applied by the wishbones.

4.3.9 Ackermann Percentage

Modelling of the Steering System

When the front wheels of a steady vehicle are steered, it is most likely that the steering angles of the front tyres are different. This phenomenon is related to the geometry of the steering system and in particular on the relative location of the

outer hardpoint of tie-rod with respect to the kingpin axis.

In order to understand the reasons behind the difference between the steering angles of the front tyres, the steering rack, the tie-rod and the upright are modelled by considering the ackermann steering geometry (*Figure 4.24*).

The ackermann geometry considers the steering rack and the tie as unique primary beam, which is connected to the front left and front right uprights by means of two hinges. The upright themselves are modelled as two beams connecting the kingpin axis to the primary beam's hinges. The system is created on a plane perpendicular to the kingpin axis. By using this geometry, the rotation that was normally present on

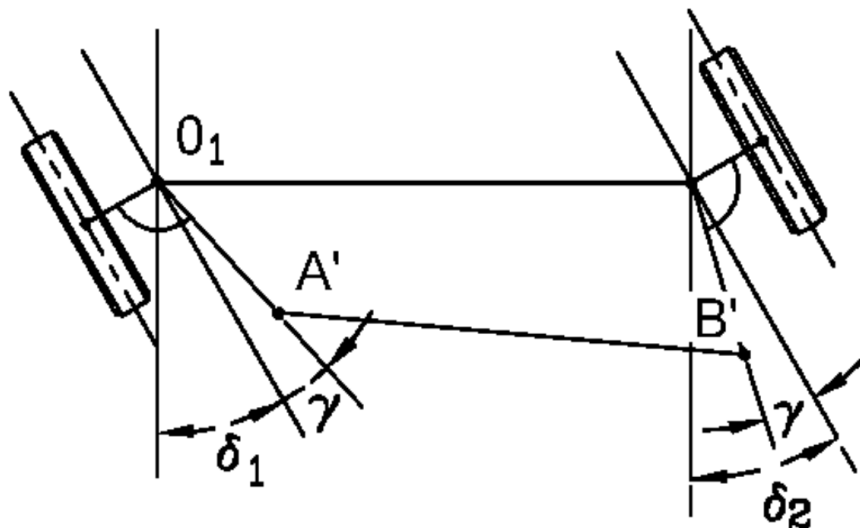


Figure 4.24: Ackermann Geometry

the tie-rod due to steering is now distributed on the primary beam. Given that the primary beam is much longer than a tie-rod, its rotation can be neglected. Therefore, the lateral movement of the outer hardpoint of the tie-rod can be considered identical on the inside and on the outside tyre.

The difference between the steering angle of the internal tyre and on the external one will be referred in this section as dynamic toe angle. This toe angle is positive when the wheels point towards the chassis (toe-in) and negative if they point outwards (toe-out). In other words, if the internal tyre steers more than the external one, the front wheels are in a toe-out configuration, vice-versa, if the external tyre steers more than the internal the front wheels are in a toe-in configuration.

Figure 4.25 is relative to the left wheel and it represents the trajectory of the outer hardpoint of the tie-rod (tie-rod out) around the kingpin axis in a plane perpendicular to the kingpin axis.

The values of steering angle on the left and right directions (δ_L and δ_R) can be considered for a given steering input as the steering angle of the internal tyre and of the external tyre respectively.

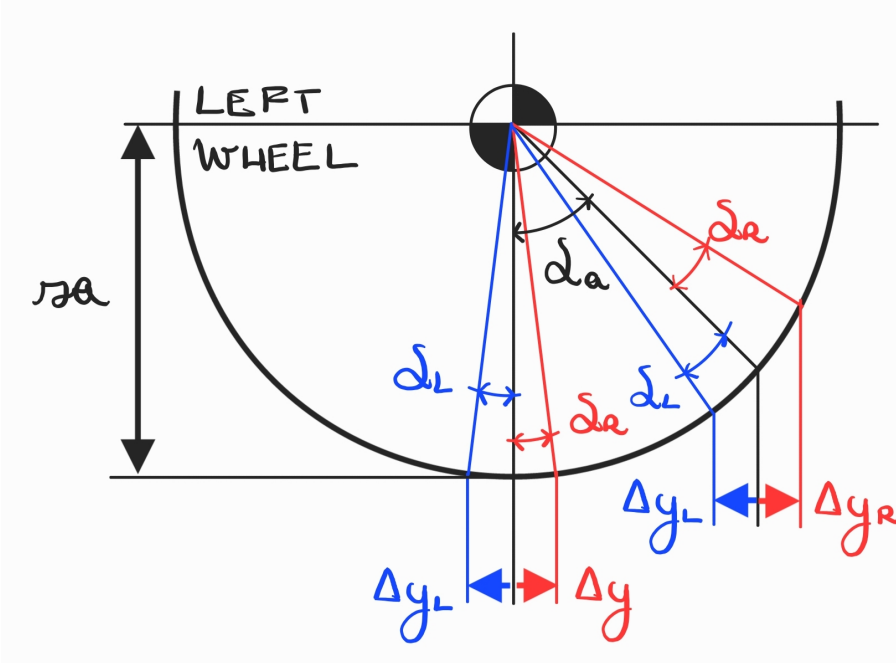


Figure 4.25: Ackermann Geometry

Steering Geometries

It is possible to notice that, for the same rack input ($\Delta y_L = \Delta y_R = \Delta y$), the resulting steering angle on the internal wheel and on the external wheel are the same only if the kingpin axis and the tie-rod out are longitudinally aligned on the plane considered in *Figure 4.25*.

The fact that δ_L and δ_R can differ may be exploited to create a dynamic toe angle during cornering. In order to accomplish this, three main steering geometries can be adopted:

- ackermann (or pro-ackermann) = the lines that connect the kingpin axis and the tie-rod out meet behind the front axle
- parallel = the lines that connect the kingpin axis and the tie-rod out are parallel
- reverse ackermann (or anti-ackermann) = the lines that connect the kingpin axis and the tie-rod out meet in front of the front axle

These three geometries have specific effects on the dynamic toe of the front wheels. As a matter of facts, ackermann steering causes toe-out when steering, parallel steering has no effect on the dynamic toe and reverse ackermann results in dynamic toe-in.

Steering Angles Estimation

Starting from *Figure 4.25* and using some trigonometrical relations, it is possible to obtain an estimation of the angle variation between the internal wheel and the external wheel of a vehicle.

$$\Delta\delta = 2 * \delta_a - \arcsin \left(\sin \delta_a - \frac{\Delta y_L}{sa} \right) - \arcsin \left(\sin \delta_a + \frac{\Delta y_R}{sa} \right) \quad (4.72)$$

In this equation the variables are:

- $\Delta\delta$ = difference in steering angle between the external wheel and the internal one ($\delta_L - \delta_R$) [deg]
- δ_a = angle steering angle offset of the static suspension when not steering [deg]
- Δy_L = external wheel's tie-rod out lateral movement [mm]
- Δy_R = internal wheel's tie-rod out lateral movement [mm]
- sa = steering arm (distance between the tie-rod out and the kingpin axis) [mm]

Given that Δy_L equals Δy_R , *Equation 4.72* can be reworked as follows:

$$\Delta\delta = 2 * \delta_a - \arcsin\left(\sin \delta_a - \frac{\Delta y}{sa}\right) - \arcsin\left(\sin \delta_a + \frac{\Delta y}{sa}\right) \quad (4.73)$$

Ackermann Percentage Definition

In order to render non-dimensional and more generic $\Delta\delta$, the ackermann percentage parameter has to be defined.

For this purpose, a reference value of difference in steering angle between the external wheel and the internal one ($\Delta\delta_{ref}$) has to be used. The value of $\Delta\delta_{ref}$ is defined as the one that respects the Jantaud condition. This means that lines that connect the kingpin axis and the tie-rod out intercepts in the mid point of the rear axle. Therefore, $\Delta\delta_{ref}$ can be obtained from *Equation 4.73* by imposing δ_a equal to the arc-tangent of the ratio between half of the front track width and the wheelbase.

$$\begin{aligned} \Delta\delta_{ref} = & 2 * \arctan\left(\frac{t}{2 * wb}\right) - \arcsin\left(\sin\left(\arctan\left(\frac{t}{2 * wb}\right)\right) - \frac{\Delta y}{sa}\right) \\ & - \arcsin\left(\sin\left(\arctan\left(\frac{t}{2 * wb}\right)\right) + \frac{\Delta y}{sa}\right) \end{aligned} \quad (4.74)$$

The ackermann percentage can ultimately be defined as the ratio of $\Delta\delta$ and $\Delta\delta_{ref}$.

$$\begin{aligned} A_k = & 100 * \left(2 * \delta_a - \arcsin\left(\sin \delta_a - \frac{\Delta y}{sa}\right) - \arcsin\left(\sin \delta_a + \frac{\Delta y}{sa}\right) \right) * \\ & \left(2 * \arctan\left(\frac{t}{2 * wb}\right) - \arcsin\left(\sin\left(\arctan\left(\frac{t}{2 * wb}\right)\right) - \frac{\Delta y}{sa}\right) \right. \\ & \left. - \arcsin\left(\sin\left(\arctan\left(\frac{t}{2 * wb}\right)\right) + \frac{\Delta y}{sa}\right) \right)^{-1} \end{aligned} \quad (4.75)$$

Model Validation

The model presented above has been validated through a comparison with the results obtained on Adams' Car. In order to perform this comparison, both the model have been tested by considering a modified version of the SC22 suspension. In particular, this configuration features a tie-rod out that has been moved by 6mm towards the chassis. This adjustment has been performed with the aim of increasing the effect of the ackermann geometry, which would be practically a parallel steer in the base configuration. The result of this process has been reported on *Figure 4.26*. As it

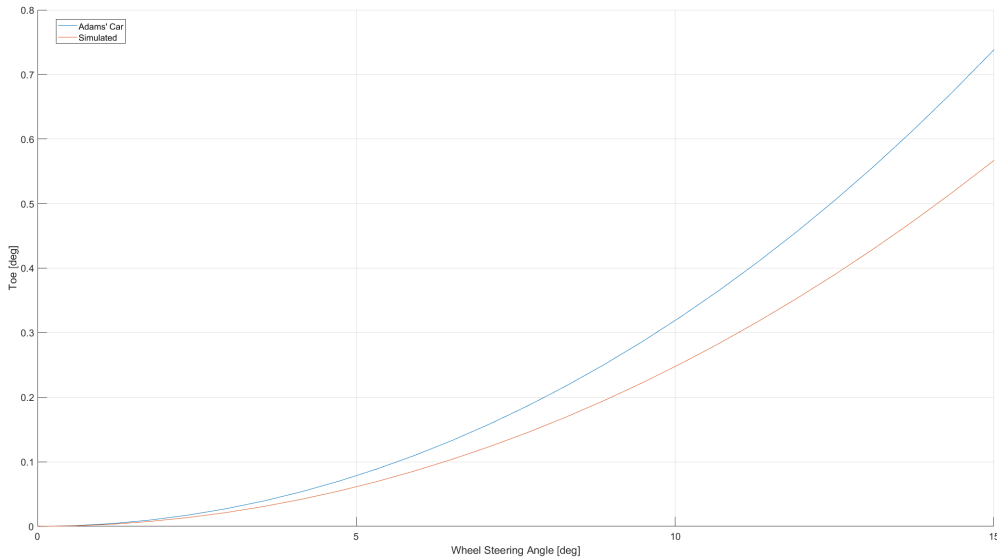


Figure 4.26: Ackermann Geometry Validation

is possible to notice from this graph, although there is a resemblance between the result obtained through Adams' Car and the simulated model, there is a noticeable difference between the results for high values of steering angle. In particular, this difference has been quantified in a series of different simulations at about 30%. Therefore, a corrective coefficient has been introduced in order to correct this error.

The corrected model is compared to Adams' Car in *Figure 4.27*.

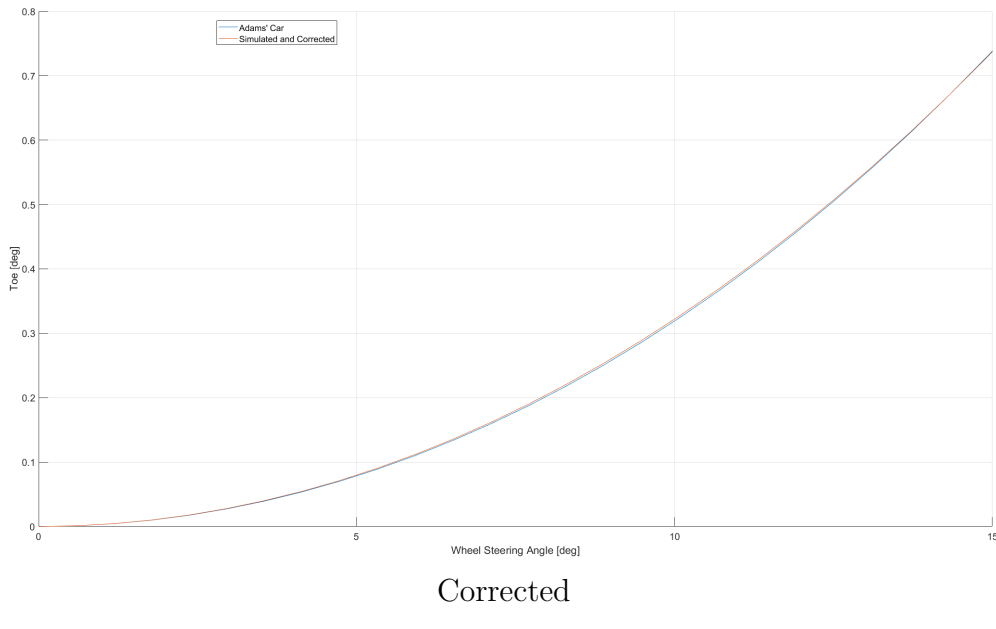


Figure 4.27: Ackermann Geometry Validation

Effect of Toe Setup Changes

The static value of toe angle in the front suspension is usually modified by tuning the length of the tie-rod. Therefore, a change of toe angle causes a variation of the

ackermann characteristic of the suspension.

In general, if the absolute static toe angle is lower than one degree, the effect on the steering geometry can be ignored. However, this result is strongly dependent on the steering geometry itself and the effect of toe regulation on ackermann has to be checked on the vehicle considered before deciding to either ignore it or take it into account in the ackermann definition.

4.3.10 Bump Steer

Definition

Considering the front view of a suspension, a vertical wheel travel results in all the points of the upright rotate around the front view instant centre. However, the tie-rod out is constrained to move on a trajectory centered in the inner hardpoint of the tie-rod (tie-rod in).

In most cases the tie-rod in and the front view instant centre do not coincide during the whole vertical travel of the wheel. Therefore, the vertical wheel travel can cause a variation of the y-coordinate of the tie-rod out which differs from the variation of the y-coordinate of the points tightly linked to the control arms (outer hardpoints of the UCA and LCA).

Given that the outer hardpoints of the UCA and LCA have a different longitudinal location relative to the tie-rod out, a vertical movement can result in a dynamic variation of the toe angle due to vertical movement. This variation changes the steering angle when the vehicle travels over a bump, hence it is named bump steer.

In case a racing vehicle is considered, the effect above-mentioned can influence the vehicle behaviour when it is subjected to a load transfer. For instance, when the vehicle is braking while entering a corner, the longitudinal load transfer results in a compression of the front suspensions and an extension of the rear suspensions, if the bump steer is not precisely tuned, the vehicle can be suffering from understeer or oversteer during the early phase of corner entry. Considering the front axle, while cornering, the effect of bump steer during cornering is generally much smaller than the one provided from ackermann.

Bump Steer Qualitative Estimation

A qualitative assessment of the bump steer can be done by considering two limit conditions. The first condition correspond to the case where the line that connects the tie-rod out and the front view instant centre passes through the tie-rod in, but the distance from the front view instant centre and the tie-rod out differs from the distance between the tie-rod out and the tie-rod in. In the second condition, these two distances have the same value, but the tie-rod in does not lay on the line connecting the tie-rod out and the front view instant centre.

The cases above-mentioned are depicted in *Figure 4.28*. In particular, the red parts are referred to the tie-rod, whilst the black lines correspond to the front view instant

centre and the upright. The left hand side of *Figure 4.28* represent the former case, while the latter case is pictured on the right side of the figure.

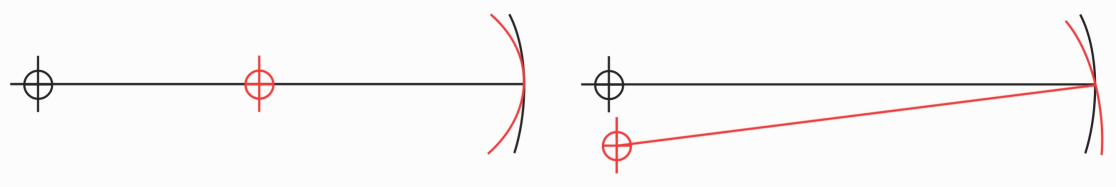


Figure 4.28: Two Limit Cases for the Bump Steer

In the first case, the lateral movement of the upright due to the vertical wheel travel is smaller than the lateral movement of the tie-rod out. In the second case, these two lateral displacements differ depending on whether the suspension undergoes a compression or an extension. The result of this tie-rod in not coinciding with the front view instant centre depends on which one between the tie-rod in and the front view instant centre is above or below the tie-rod in. Therefore, from the two cases just described three condition can be identified:

- front view instant centre and tie-rod in are aligned but not coincident
- front view instant centre is under the tie-rod in
- front view instant centre is over the tie-rod in

This difference in the two lateral displacements described above respectively coincides with the movement of the upright and the movement of the tie-rod out. For a given distance between the kingpin axis and the tie-rod out, the bump steer can be determined as a consequence of the difference in the two lateral displacements.

From the three cases above-mentioned, six conditions of can be determined depending on whether the tie-rod out is behind or in front of the kingpin axis:

- front view instant centre and tie-rod in are aligned but not coincident and the tie-rod out is behind the kingpin axis: toe-out both in compression and extension
- front view instant centre is under the tie-rod in and the tie-rod out is behind the kingpin axis: toe-out in compression and toe-in in extension
- front view instant centre is over the tie-rod in and the tie-rod out is behind the kingpin axis: toe-in in compression and toe-out in extension
- front view instant centre and tie-rod in are aligned but not coincident and the tie-rod out is in front of the kingpin axis: toe-in both in compression and extension
- front view instant centre is under the tie-rod in and the tie-rod out is in front of the kingpin axis: toe-in in compression and toe-out in extension
- front view instant centre is over the tie-rod in and the tie-rod out is in front of the kingpin axis: toe-out in compression and toe-in in extension

Bump Steer Quantitative Estimation

In order to precisely calculate the toe value due to bump steer, the dynamic locations of the front view instant centre, the tie-rod in and their variation with respect to

the tie-rod in have to be considered. Furthermore, the point on the kingpin axis that identify the distance between the tie-rod and the kingpin axis and the line that connects it to the front view instant center have to be used when considering the upright movement. However, for this simplified analysis, these effects are not considered. Moreover, the y-coordinate of the tie-rod out coincides with the one of the point of the kingpin that is used to determine the distance between the kingpin axis and the tie-rod out. In addition to that the distance between the tie-rod and the kingpin axis is considered constant. Starting from *Figure 4.29* and from

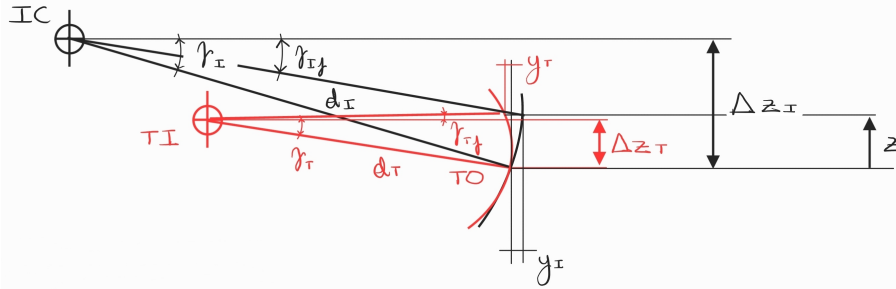


Figure 4.29: Bump Steer Model

the assumptions described above, the bump steer characteristic can be defined as follows:

$$\frac{\Delta\delta}{z} = \arctan((d_T * (\cos(\arcsin((z - \Delta z_T)/d_T)) - \cos(\arcsin((\Delta z_T/d_T)))) - d_I * (\cos(\arcsin((z - \Delta z_I)/d_I)) - \cos(\arcsin(\Delta z_I/d_I))))/ar)/z \quad (4.76)$$

Where:

- $\Delta\delta$ = toe angle [deg]
- z = wheel vertical travel [mm]
- d_I = distance between the front view instant centre and the tie-rod out [mm]
- d_T = distance between the inner hardpoint of the tie-rod and the tie-rod out [mm]
- Δz_I = vertical between the front view instant centre and the tie-rod out [mm]
- Δz_T = vertical distance between the inner hardpoint of the tie-rod and the tie-rod out [mm]
- ar = longitudinal distance between the tie-rod out and the point of the kingpin axis at the same z-coordinate of the tie-rod out [mm]

Validation

The model validation has been carried out though a comparison with the result obtained in Adams' Car. For this analysis, the SC22 front suspension has been modified in order to exacerbate the bump steer, that otherwise would be practically null in the base configuration.

By comparing the result of the model presented above with Adams' Car (*Figure 4.30*), it can be noted that this model is only valid for small values of wheel travel.

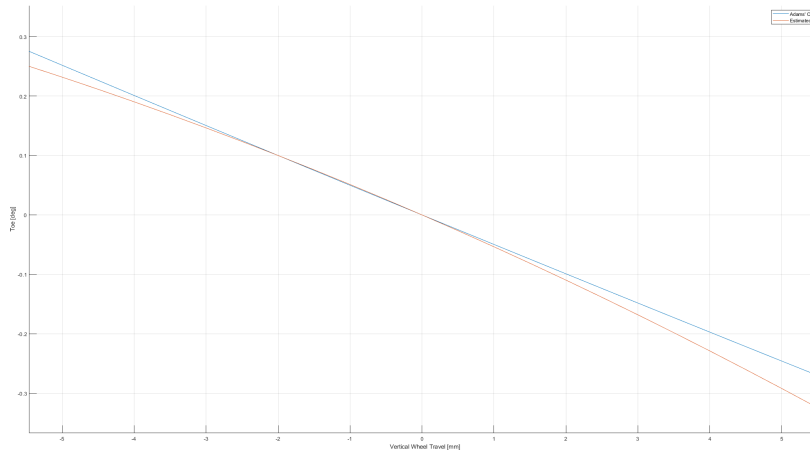


Figure 4.30: Bump Steer Model

Even by introducing the effects of the movement of the front view instant centre and considering the fact that the tie-rod out and the point on the kingpin axis consider have not the same y-coordinate, the model does not converge to the result obtained in Adams' Car.

The imprecision of the model is a consequence of a characteristic of the bump steer. As a matter of fact, the dynamic toe due to the vertical wheel travel is extremely sensitive to small changes of the hardpoints' locations. Therefore, even a small imprecision in the model results in measurable variations of the bump steer curve.

Alternative Bump Steer Quantitative Estimation

In order to address the inaccuracy of the previous model, the movement of the two control arms of the suspension considered is simulated in 2D.

In this process, the lengths of the (approximated) 2D control arms is fixed, their z-coordinate is increased of a value " z " and the resulting variation of their y-coordinate is simulated through Matlab scripting. The vertical movement " z " corresponds to an input of vertical wheel travel which is also applied to all the outer hardpoints of the suspension in order to simplify the system.

Once the new locations of the outer hardpoints have been determined, the new side view of the kingpin axis can be calculated. Therefore, the lateral movement of the kingpin axis at the height of the outer tie-rod hardpoint can be found before and after the vertical movement of the wheel centre.

Due to the fact that also the outer hardpoint of the tie-rod moves vertically, the same procedure can be carried out to determine the lateral movement of the tie-rod out.

Considering the difference of the kingpin axis lateral movement and the tie-rod out lateral movement and the relative location and distance between the tie-rod and

the kingpin axis, the toe angle generated by the vertical movement of the wheel centre can be determined as follows:

$$dy = dy_T - dy_P \quad (4.77)$$

$$toe = \arctan(\tan(Da) + dy/sa) - Da \quad (4.78)$$

Where:

- dy_T = tie-rod outer hardpoint lateral movement
- dy_P = lateral movement of the point on the kingpin axis at the same height of the tie-rod outer (P)
- Da = angle between the longitudinal axis of the tyre and the line that connects P to the tie-rod outer (determined through the ackermann geometry)

Depending on whether the tie-rod is located in front of or behind the kingpin axis, the signs of this equation can change.

If the location of the tie-rod outer hardpoint has already been computed and two values of target toe angle with their respective vertical wheel travel are provided, the procedure described can be employed to determine the location on the y-axis and z-axis of inner hardpoint of the tie-rod in such a way to match the target toe angle.

As it is possible to observe, in order to determine the the tie-rod inner given a bump steer characteristic, most of the front view kinematics of the suspension has to be already determined. Therefore, the optimal value of bump steer cannot be found before designing the rest of the suspension. As a consequence, these formulas are directly dialed in the parametric model, in a similar way to what can be done in an optimisation model.

Validation of the Alternative Model

The accuracy of the results of this model has been validated by creating a suspension completely identical to the SC22 front suspension and changing the location of the inner hardpoint of the tie-rod according to the targets in input to the *Equation 4.78*. The resulting suspension is then fully simulated in Adams' Car in order to obtain the real bump-steer characteristics.

The result of this procedure show that there is a systematic error in the process, that can be found by setting the target toe to zero and removed from the result by adapting the targets to the systematic error.

This error is related to an assumption used to solve the bi-dimensional system described. In fact, the vertical movement is considered identical for every single point of attached to the upright. This approximation can be avoided by considering a 3D representation of the suspension. Also considering the distance between the outer hardpoints of the control arms as constant may partially solve this problem, however this solution has not been tested during the choice and validation processes of the alternative model of bump steer.

4.4 Parametric Model

Assumptions and Constraints

There is one main assumption applied in the definition of the input parameters and the previous models validations. The steering angle is measured on a plane perpendicular to the kingpin axis.

Even for extreme values of KPA and ca the difference between the steering angle and its projection on a plane perpendicular to the kingpin axis is negligible.

The main constraints of the generation of a suspension is related to the inner hardpoints' plane. As a matter of fact, for the sake of simplicity, the SC22s' chassis has been designed and manufactured in such a way that the zone assigned to the application of the inserts for the inner pick-up points of the suspension is a plane.

The insert relative to the suspensions' inner hardpoints can only be located on this plane. In order to enable for the use of the same tab design for every inner pick-up point, the inner hardpoints are located on a plane parallel to the inner hardpoints' plane.

In an ideal case scenario the dimension of this zone has to be restricted to include the dimensions of the tabs and to avoid positioning part of the inserts where they would apply a stress on the honeycomb of the lower panel of the chassis. Being this panel practically perpendicular to the inner hardpoints' plane, the honeycomb in this panel is stressed in a perpendicular direction with respect to the direction where it should be stressed. Therefore, the compliance in this case rises. Furthermore, to put an insert in that zone causes the manufacturing of that zone of the chassis more complex, potentially lengthening the production times of the chassis.

In the parametric model a view of the inner hardpoints plane is plotted after calculating the new suspension hardpoints' locations. This plot is reported for the front suspension in *Figure 4.37*.

Input Parameters Definition

The results obtained during *Chapter 3* can be used to determine a combination of parameters, which can be used to create the suspension.

Camber Related Parameters

On the front axle, the suspension's kinematics parameters related to camber are:

- camber recovery (fvsa and track combination)
- KP Angle
- caster angle
- svsa

They can be fully determined through an iterative process. Despite this process can be fully automated by limiting the range of values of some parameters and giving

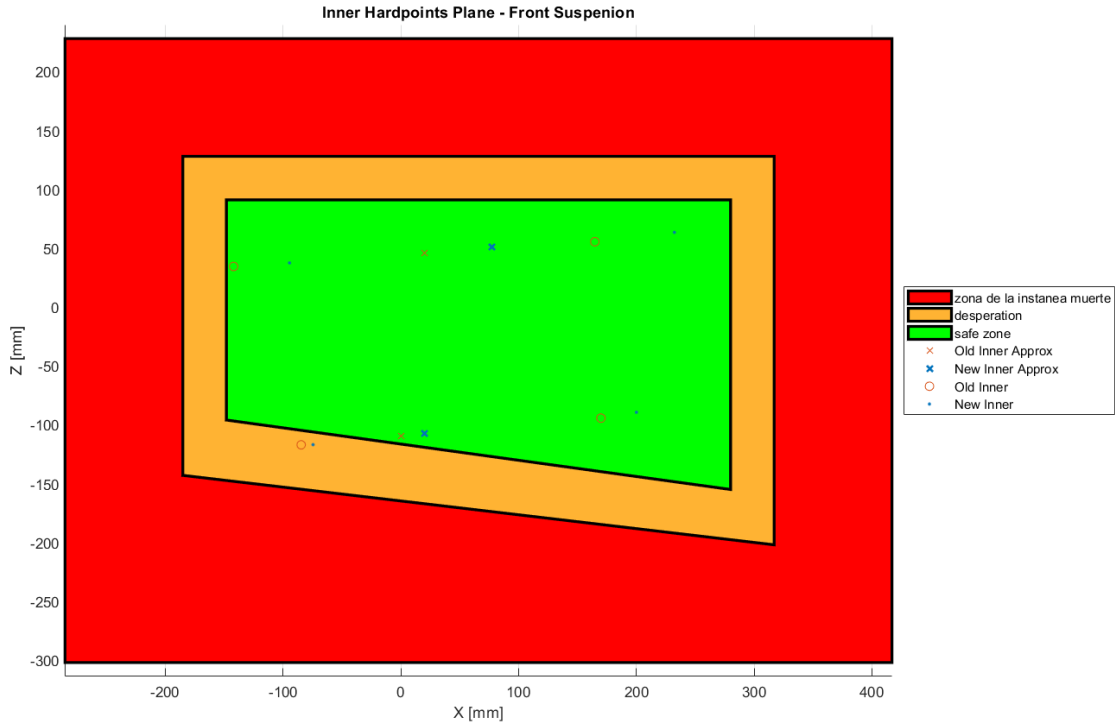


Figure 4.31: Inner Hardpoints' Plane

priority to the variation of some parameters over the others, for this analysis the tuning of these parameters is performed manually. The combination of the parameters

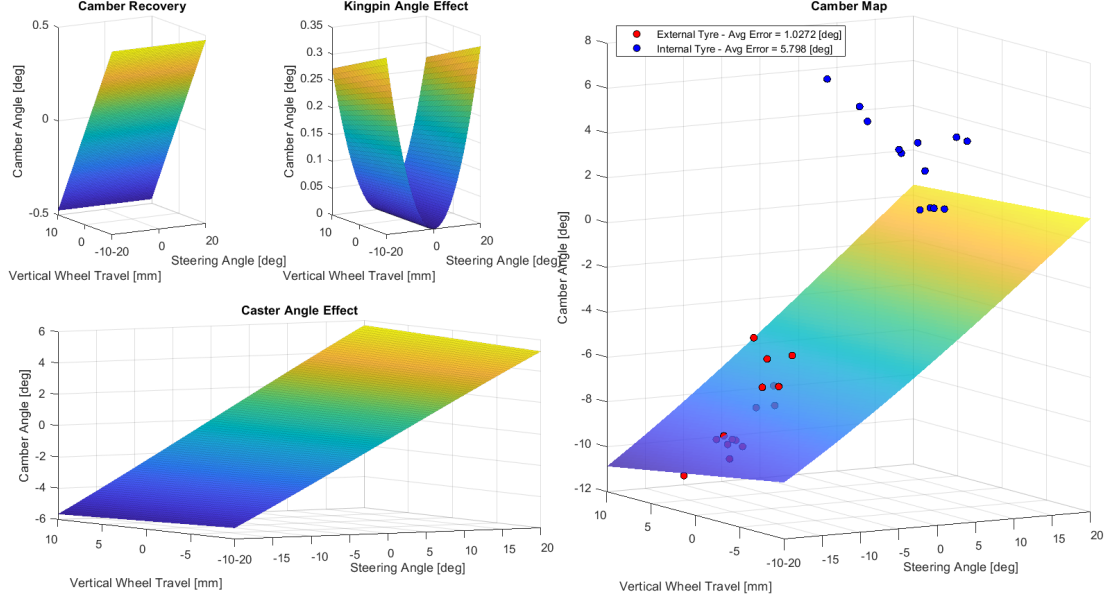


Figure 4.32: Camber Related Parameters Effect - Front Axle

listed above influence the values of camber angle as function of the vertical wheel travel and of the steering angle. The functions utilised to determine the theoretical camber map are the ones used in the previous *Section 4.3*.

As it is possible to notice from *Figure 4.32*, the effect of the kingpin angle and

of the caster angle is not only dependent on the steering angle but also on the vertical wheel travel. This is related to the caster recovery and to the camber recovery which respectively affect the caster angle and the kingpin inclination.

In *Figure 4.32* also the target values of camber found in *Section 3.3* are reported (in red for the external tyre and in blue for the internal one). The average differences between the camber map value and the target value for the internal tyre and for the external one of the axle considered are the error of in the definition of the camber related parameters.

Ideally, these two errors have to be both minimised. However, to achieve this target, the caster angle required would be too high to enable an efficient packaging of the suspension in the rim. Moreover, the vertical wheel travel of the wheel is too small during cornering to use the camber recovery to achieve the target camber values in this specific vehicle.

As a consequence what has been described above, the caster angle and camber angle recovery are maximised and then the error is only minimise on the external tyre by using static camber, whilst the camber recovery is minimised.

To only optimise the external tyre can be an effective way to obtain the large majority of the positive effect of the camber optimisation. This is related to the fact that the camber thrust is approximately directly proportional to the vertical force applied on the tyre. Due to the lateral load transfer, vertical force during cornering is much higher on the external tyre than on the internal one. Therefore, the camber angle is by far more effective on the external tyre.

A positive aspect of minimising the camber recovery and increasing the static camber is that the static camber can always be tuned to be reduced. Therefore, if the high value of static camber needed to reach the target camber impair too much the longitudinal performance of the vehicle it can always be reduced through vehicle setup.

Due to the fact that the rear axle of the vehicle cannot steer, the only camber related kinematic parameter to be tuned is the camber recovery. Therefore, also in this case high values of static camber are required to reach the target camber on the external tyre.

Toe Related Parameters

The two parameters considered to generate toe-angle are the ackermann and the bump-steer.

Given that the bump-steer cannot be computed as long as the suspension kinematics has not been defined, the toe angle targets are only considered in terms of ackermann steering geometry, which is only effective on the front axle as it is the only one that can be steered.

The consequence of this approach is that the toe related parameters can only be

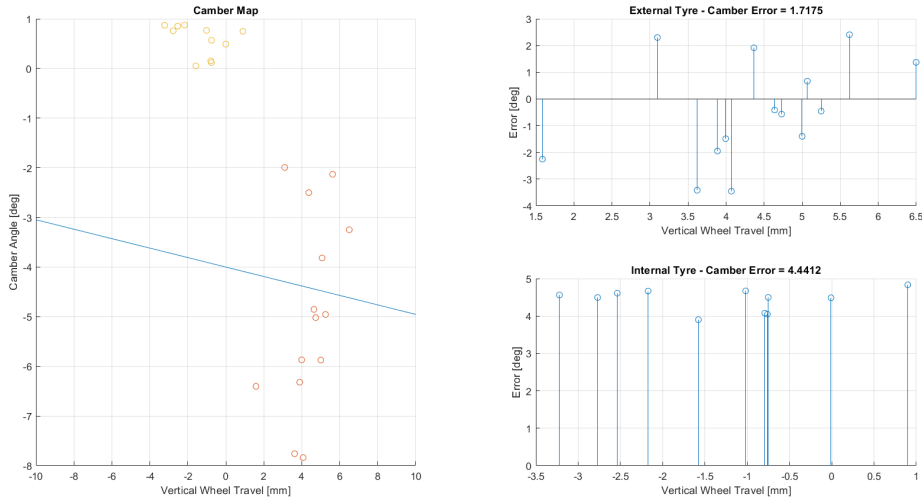


Figure 4.33: Camber Related Parameters Effect - Rear Axle

pre-determined for the front axle.

In terms of bump-steer, the approach changes depending on whether considering the front axle and the rear axle.

In the former case, the bump-steer characteristics of the vehicle can be tuned in such a way to generate toe-out during the compression of the suspension and toe-in during rebound. This characteristic aids rotation during corner entry and enables to limit the understeer during traction. Despite it can be argued that this bump-steer characteristic causes an increase of the steering angle of both wheels during turns, the magnitude of this effect is minimal when compared to the steering angle input.

On the other hand, it makes sense to tune the bump-steer characteristics of the rear axle in such a way to not provide any toe due to the vertical wheel travel or in order to have both the tyres will slightly steer towards the corner (in-phase steering).

To steer the rear tyre in-phase with the front tyres can be done in order to compensate the fact that on the rear tyres the target camber is tougher to reach than on the front axle. However, if the tyres steer in-phase with the front tyres, it means that the suspension generates toe-out in extension and toe-in during traction. In turn, this generates instability during braking and understeer during traction.

In addition to these negative effects related to an in-phase steering, the unpredictability of the vehicle behaviour due to a non-flat vertical wheel travel to toe characteristic can easily be controlled by the driver only when present on the front axle. This is related to the fact that the front axle is directly controlled by the driver through the steering.

Caster Trail and Scrub Radius

The caster trail and the scrub radius can be determined in a similar way. These two characteristics generate the a moment around the z-axis of the tyre when respectively coupled with the lateral force and the longitudinal force.

Starting from the caster trail, it should be tuned in such a way to avoid the inversion of the steering torque during cornering when the vehicle is not oversteering (*Subsection 4.3.4*).

First of all, the zones where the lateral force is high and the longitudinal force is negligible are taken into account. In these zones, the lateral force and the moment around the z-axis are extracted from the TIR file of the tyres considered.

Due to the fact that the moment around the z-axis is both due to the lateral force and to the longitudinal force, but the longitudinal force is negligible, the caster trail can be determined as the peak value of the ratio of M_z and F_y . Therefore, M_y is considered as only caused by F_y which is a conservative condition, due to the fact that the in this way the caster trail is overestimated.

During this procedure, the tyres' working condition extracted from the simulation have to be smoothed and corrected. However, these steps are not treated in this analysis.

The procedure detailed above is only used to determine the caster trail on the front axle. However, the procedure to determine the scrub radius on the front and rear axles and the caster trail on the rear axle consists in a similar procedure.

First of all, when considering the scrub radius, the cases where the longitudinal force is high and the lateral force is low have to be analysed. Lastly, instead of consider the peak value of the F_y and F_x arms, when the values of F_y and F_x are near to their peak, the average values of the arms are respectively used as caster trail and scrub radius.

Miscellaneous Parameters

There are many parameters that have to be determined based on what has been discussed in previous sections. They are listed here:

- h_{RC} = roll centre height from the ground [mm]
- t = track [mm]
- R_L = loaded radius [mm]
- $UCA_{out,z}$ = z-coordinate of the outer hardpoint upper control arm [mm]
- $LCA_{out,z}$ = z-coordinate of the outer hardpoint lower control arm [mm]
- P_1, P_2, P_3 = three points needed to determine the plane where the inner hardpoints of the control arms are located [mm]
- front brake balance (for the front suspension) [%]
- rear traction balance (for the rear suspension) [%]

- h_{CG} = centre of gravity height from the ground [mm]
- wb = wheelbase [mm]
- $UCA_{front,aperture}$ = longitudinal distance between the approximated inner hardpoint of the upper control arm and the final position of the front hardpoint of the upper control arm [mm]
- $LCA_{front,aperture}$ = longitudinal distance between the approximated inner hardpoint of the lower control arm and the final position of the front hardpoint of the lower control arm [mm]
- $UCA_{rear,aperture}$ = longitudinal distance between the approximated inner hardpoint of the upper control arm and the final position of the rear hardpoint of the upper control arm [mm]
- $LCA_{rear,aperture}$ = longitudinal distance between the approximated inner hardpoint of the lower control arm and the final position of the rear hardpoint of the lower control arm [mm]
- z_P = z-coordinate of the outer tie-rod hardpoint [mm]
- sa = steering arm = distance between the tie-rod outer and the kingpin axis [mm]
- Da = angle between the x-axis of the tyre and the line that connects the outer tie-rod hardpoint and the kingpin axis (perpendicular to the kingpin axis) [mm]
- toe_1 = toe value on the single tyre when the wheel centre moves of " z_1 " [deg] (generally the toe is the difference between the steering angles of two tyres of the same axle, hence the double of what inserted here)
- z_1 = vertical wheel travel that generates " toe_1 " through the bump steer [mm]
- toe_2 = toe value on the single tyre when the wheel centre moves of " z_2 " [deg]
- z_2 = vertical wheel travel that generates " toe_2 " through the bump steer [mm]

For each one of these variables three different methods can be applied:

- use a new value
- use the value present in the SC22 suspension
- use the value present in the SC22 suspension adding a delta in the same units of the variable chosen

Some of these values are kept the same as the SC22 suspension during this analysis, whilst others are tuned in order to avoid interference with the rim, ensure that the packaging remains in the boundaries of the chassis plane and that the forces on the control arms are minimised.

Model Description

In this section, the steps executed by the parametric model to create a suspension are reported. These steps can be divided in three macro categories:

- old suspension characterisation
- new suspension generation
- post-processing

The whole process has been performed through Matlab scripting.

Old Suspension Characterisation

First of all, in order to characterise the old suspension (SC22 spec), its hardpoints are loaded into the workspace. Then, a check of the coplanarity and collinearity of the inner hardpoints of the control arms is executed. This step is needed to determine whether the chassis' plane can be reused in the new suspension.

Once the old hardpoints have been imported and checked, the parameters of brake (or traction) distribution, h_{CG} and wb are manually defined based on the values present on the SC22.

The first step of the suspension analysis regards the front view. It consists into identifying the approximated inner hardpoint for each of the control arm. As it has already been explained at the start of this chapter, the inner hardpoint is defined as the point with the same x-coordinate of the outer hardpoint of the same control arm, but laying on the 3D line that connects the front hardpoint to the rear one.

In order to identify the inner hardpoints' locations, the x-y projection and x-z projection of the line that connects the front hardpoint to the rear one is considered. From these two projections the y-coordinate and the z-coordinate of the inner hardpoint can be found.

The values of aperture can now be determined from the inner hardpoints approximations and from the real inner hardpoints as difference of the x-coordinate between the former and the latter.

The location of the approx. inner hardpoints and the outer hardpoints enable the identification of the front view instant centre. In fact, the two lines that indicate the front view inclination of the approximated control arms (formed by the outer hardpoints and the approximated inner ones) can be calculated and their interception happens in the front view instant centre location.

The projection on the ground of the line that connects the front view instant centre to the contact patch (front view n-line) is the fvsa which can be directly employed to calculate the camber recovery ([Equation 4.4](#)).

On the other hand, the h_{RC} is computed as the height of the front view n-line interception with the mid-plane of the vehicle ($y = 0$).

Lastly, the analysis of the front view of the old suspension is characterised by the study of the kingpin axis in front view. Its line is obtained considering the y and z coordinates of the outer hardpoints of the control arms. The inclination of the line is the *KP Angle* and y-coordinate of its interception with the ground is the scrub radius.

In terms of side view of the suspension, the first step is to define the side view instant centre location. This can be done in a similar way to what has been done for the front view instant centre. In fact, it is found as the interceptions between the lines that connect the front and rear hardpoint of each control arm.

Knowing the location of the side view instant centre, the svsa and the anti-features can be computed. The svsa is defined as the longitudinal distance between the contact patch and the side view instant centre, whilst the anti-features are determined from the inclination of the side view n-line, that connects the contact patch to the side view instant centre (from *Equation 4.65* to *Equation 4.69*).

The kingpin axis can also be studied in side view. From this view it is possible to calculate the caster angle and caster trail of the suspension. In order to find the values of these parameters, the x-z projection of the kingpin axis is obtained from the outer hardpoints of the control arms. The inclination of this projection is the caster angle, whereas the longitudinal distance between its interception with the ground and the contact patch is the caster trail.

New Suspension Generation

The first step in the suspension generation is the definition of the parameters, which can either be inserted manually or as a delta from the values found in the old suspension.

Once all the new parameters' values have been defined, the coefficients of the inner hardpoints' plane are calculated.

The next step in defining the new suspension hardpoints is the definition of the new outer hardpoints. With the intention of shaping these hardpoints, the kingpin axis can be calculated. Following the reversed procedure with respect to what has been done for the analysis of the old suspension, the kingpin axis is obtained in its x-z projection from the caster trail and caster angle, while the y-z projection is defined starting from the scrub radius and the KP Angle.

The $UCA_{out,z}$ and $LCA_{out,z}$ are the vertical coordinates of the upper control arm outer hardpoint and of the lower control arm outer hardpoint respectively, which are inserted as inputs of the parametric model. Therefore, the other coordinates of these two hardpoints can be determined according to the projections of the kingpin axis calculated before.

The outer hardpoint of the tie-rod cannot be found as function of the kingpin axis, because it does not lay on kingpin axis. Therefore, the location of this hardpoint is determined as it has been detailed in *Section 4.3.9*.

The new roll centre location can be defined from the h_{RC} and from the fact that it is located in the mid-plane of the vehicle.

The new front view n-line is determined as the line passing through the contact patch and the roll center location. The front view instant centre location is calculated from the n-line, the fvsa and the track. In particular, the last two parameters allow to determine the y-coordinate of IC front ($y_{IC} = fvsa - track$) to be considered on the n-line.

In order to calculate the new inner hardpoints' approximations in front view, the

control arms' lines that connect the front view instant centre to the outer hardpoints of the control arms are defined in 3D as parametric equation ($t = \text{parameter}$). The values of t that correspond to the inner hardpoints are the ones where these lines intercept the inner hardpoints' plane. By substituting the parameters found to the respective control arms' lines.

With the aim of identifying the position of the real inner hardpoints, the side view kinematics of the suspension has to be taken into account.

The side view n-line is the line that connects the side view instant centre to the contact patch. Therefore, by considering the anti-features, the wb and the throttle/brake distribution, the inclination of side view n-line is calculated. In addition, the location of the contact patch can be used to determine the constant term of the line.

The side view instant centre is identified as the point of the of the side view n-line at a longitudinal distance between the contact patch and the side view instant centre equal to the svsa.

The lines that connect the side view instant centre to the control arms approximated inner hardpoints are used to determine the real inner hardpoint. In fact, by considering the control arm apertures, the front and rear hardpoints for the upper control arm and for the lower control arm are computed.

Lastly, by using the target toe angles and the formulas in [Section 4.3.10](#), the tie-rod inner hardpoint can be determined.

Post-Processing

The post-processing consists in a series of representation that enable to speed up the process of analyse the results and debug the parametric model.

First of all, the old suspension hardpoints, the new ones and their variation is displayed on a table. The order of the hardpoint in the table is the same that is used in Adams' Car (in fact, a provisional push-rod outer hardpoint has been added to the table). In this way, the hardpoints can be copied and pasted in Adams' Car in order to make the iterative process of defining the lower part of suspension between Matlab and Adams' Car quicker. As it is possible to notice from the table above, in

		X-New	Y-New	Z-New	X-Old	Y-Old	Z-Old	X-Delta	Y-Delta	Z-Delta
1	LCA F FRONT	-74.4026	-223.6146	-116.9334	-84.5490	-233.1090	-117.0870	10.1464	9.4944	0.1536
2	LCA O FRONT	20.4464	-527.2912	-85.7000	0.3000	-563.3000	-95.7000	20.1464	36.0088	10
3	LCA R FRONT	200.0504	-239.8527	-89.4248	169.9040	-247.8560	-94.3900	30.1464	8.0033	4.9652
4	provisional PROD OUTBOARD FRO...	77.3764	-464.2517	120.6000	77.3764	-464.2517	120.6000	0	0	0
5	TIE I FRONT	56.5000	-209	-118	46.5000	-219	-128	10	10	10
6	TIE O FRONT	56.5000	-553	-110.4000	46.5000	-563	-120.4000	10	10	10
7	UCA F FRONT	-94.4106	-239.5790	37.4522	-141.8870	-246.9620	34.4510	47.4764	7.3830	3.0012
8	UCA O FRONT	77.3764	-464.2517	120.6000	19.9000	-538	110.6000	57.4764	73.7483	10
9	UCA R FRONT	232.2544	-258.1615	63.4022	164.7780	-264.0370	55.4330	67.4764	5.8755	7.9692

Figure 4.34: Lower Suspension Hardpoints - Front Axle

order to adapt the results to the hardpoint table in Adams' Car, a provisional outer

hardpoint is added to the table.

This table is coupled with a series of plots representing:

- inner hardpoints plane representation *Figure 4.37*
- side view of the lower part of the suspension *Figure 4.36*
- front view of the lower part of the suspension *Figure 4.35*
- total view of the lower part of the suspension *Figure 4.38*

In particular, *Figure 4.37* is needed to efficiently iterate the process when the inner hardpoints are either in a sub-optimal position or in a zone where they cannot be placed.

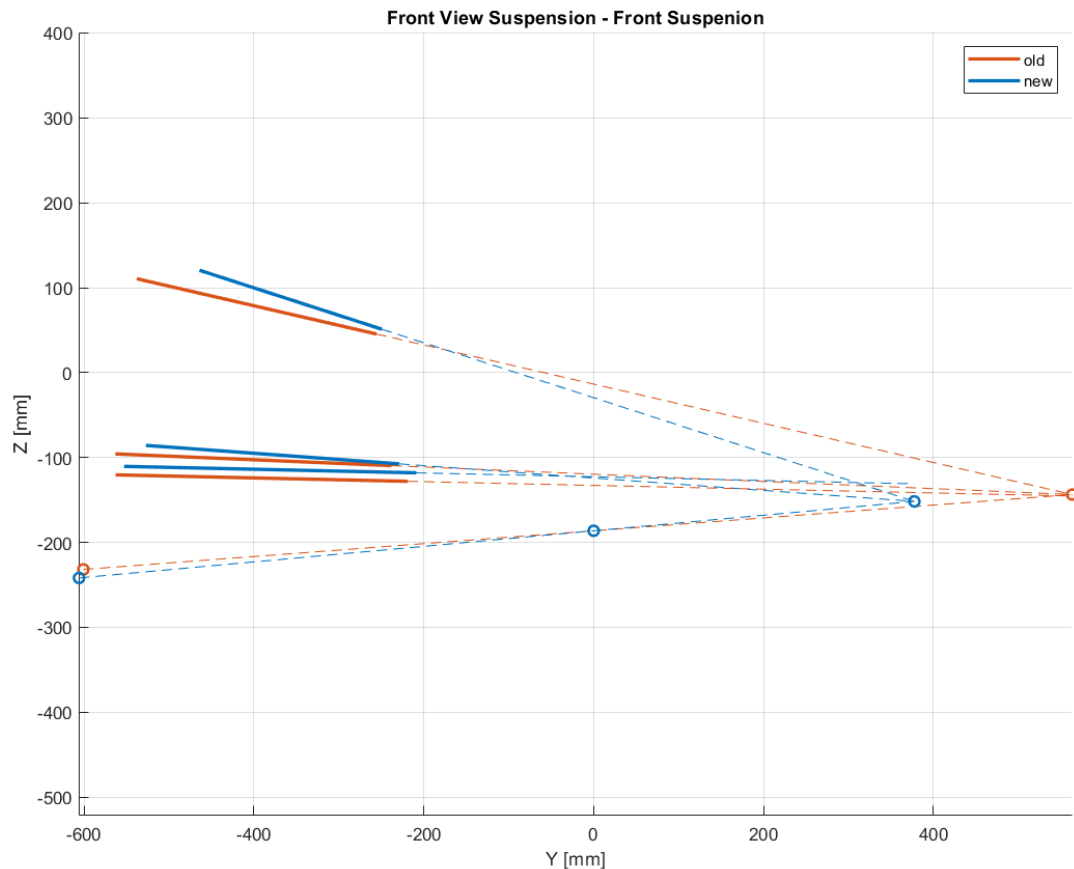


Figure 4.35: Front View of the Lower Part of the Suspension - Front Axle

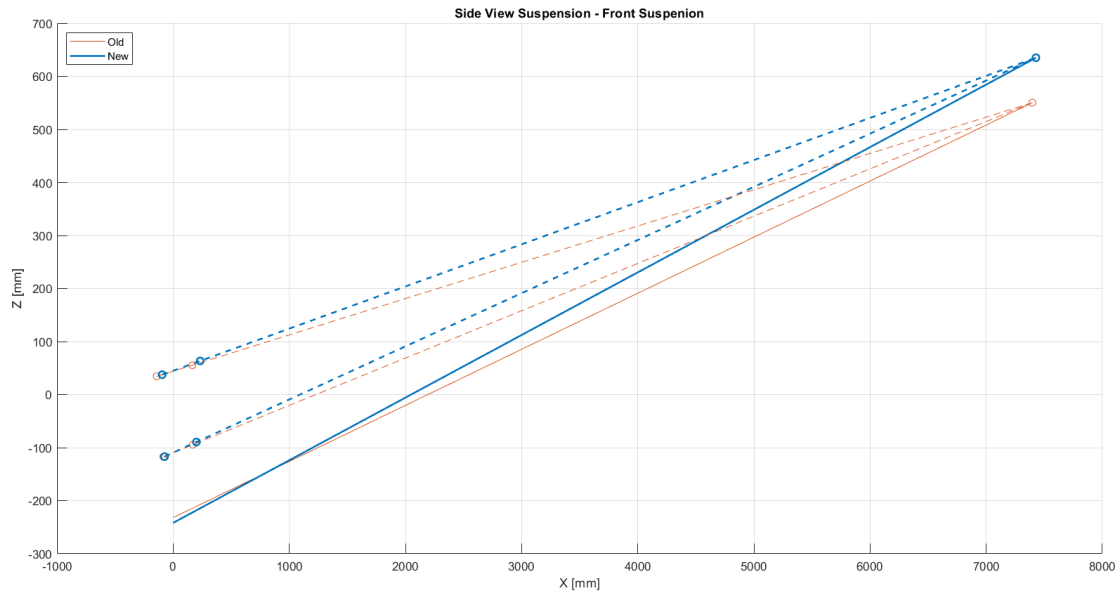


Figure 4.36: Side View of the Lower Part of the Suspension - Front Axle

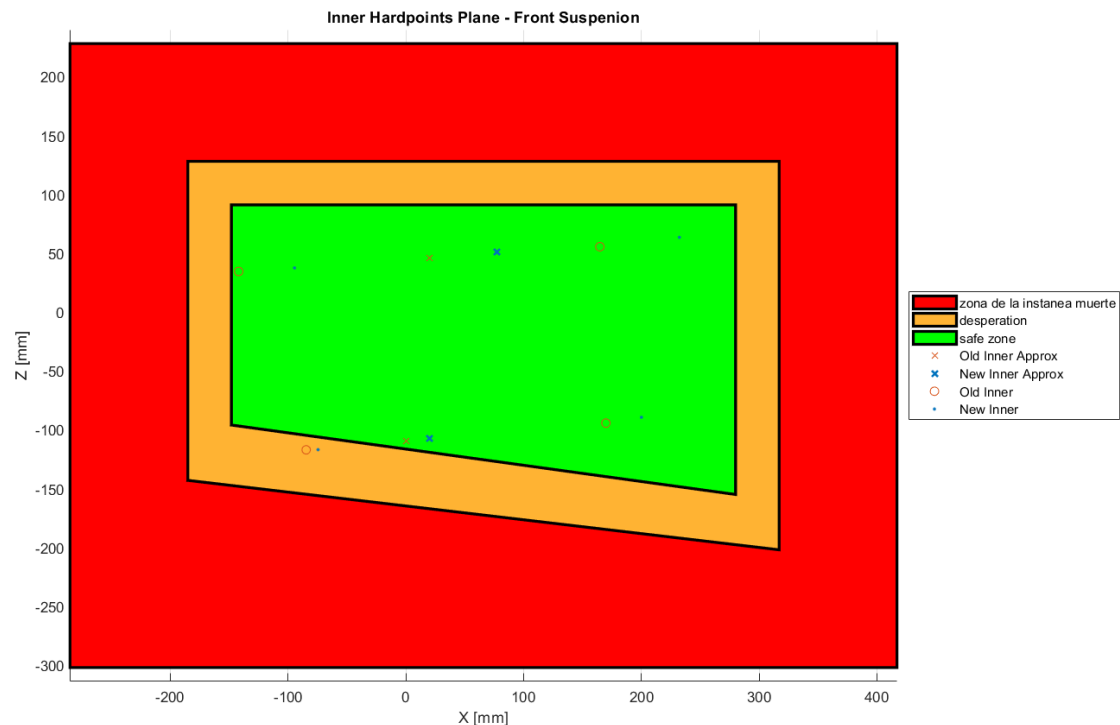


Figure 4.37: Inner Hardpoints Plane - Front Axle

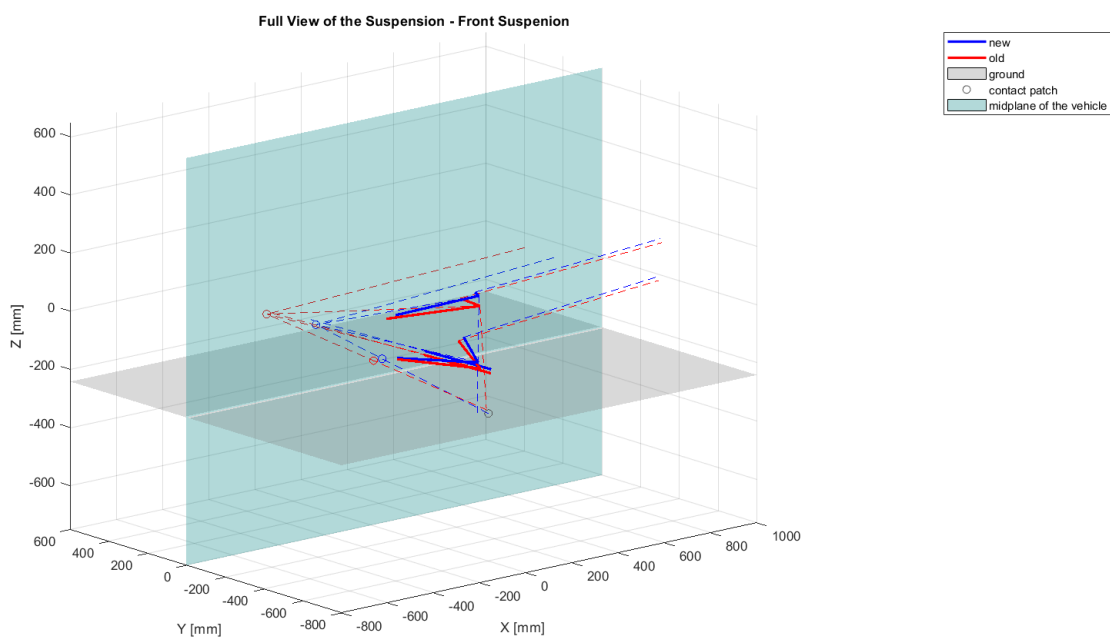


Figure 4.38: Complete View of the Lower Part of the Suspension - Front Axle